Non-Conventional Thermoelectric Generation Potential in Bangladesh

A Thesis

Submitted to the Department of Electrical & Electronics Engineering, BRAC University

By

Ishmam Ahmed Chowdhury 13121142

Shadman Sakib Islam 13121128

Mufazzol Hussain 13121112

Ismam Bin Hasnat 13121134

Supervised by

Dr. Abdul Hasib Chowdhury

Associate Professor, Department of EEE, BUET

In Partial Fulfillment of the Requirements for the Bachelor of Science degree in Electrical & Electronics Engineering

Spring 2017

DECLARATION

This is to declare that this thesis titled "Non-conventional thermoelectric generation potential in Bangladesh" is submitted to the department of Electrical and Electronics Engineering of BRAC University for the partial fulfillment of the degree of Bachelor of Science in Electrical and Electronics Engineering. We hereby affirm that the theoretical research and result was conducted solely by us and has not been presented previously elsewhere for assessment. Materials of the study and work found by other researchers have been properly referred and acknowledged.

Submission Date: 18th April, 2017

Ismam Bin Hasnat
Student ID: 13121134

Shadman Sakib Islam
Student ID: 13121128

Ishmam Ahmed Chowdhury
Student ID: 13121142

MD. Mufazzol Hussain
Student ID: 13121112

Thesis Supervisor

Dr. Abdul Hasib Chowdhury
Associate Professor
Department of EEE,
Bangladesh University of Engineering and Technology

ABSTRACT

Non-Conventional thermoelectric generation includes electricity generation from the heat salvaged from engines exhaust, municipal solid wastes based power generation, stirling engine in solar thermal power generation, solar-thermal hybrid system etc. This thesis estimates non-conventional thermoelectric generation potential in Bangladesh. Due to inefficiency of the combustion engines, lots of heat is wasted and dumped in the environment. There are options to salvage the heat and convert it into electrical energy. Even a small percentage of salvaged heat will have a significant impact. Considering several sectors where massive amount of heat is wasted, the study intends to perform how the waste heat can be of great use. The potential for energy harvesting from sunlight using Stirling engine and solar thermal hybrid system will be assessed. Also, the municipal solid waste based power generation will be investigated. This paper provides a framework with abundant ideas of major works related to the study, the chronological research conducted by some scientists as well as the development in technology all along the period.

ACKNOWLEDGEMENTS

First and foremost we are thankful to our God for providing us with the patience and strength to go on and complete this thesis.

We are grateful to our supervisor Dr. Abdul Hasib Chowdhury, Associate professor of Bangladesh University of Engineering and Technology (BUET) for his utmost support as well as critical comments and extensive guidelines. His invaluable guidance, excellent research attitude and knowledge about the field of study always encouraged us.

Lastly we offer our regards and gratitude towards all of those who supported us in any aspect during the completion of this thesis.

.

Table of Contents

List of Abbreviations

a-Si	Amorphous Silicon
ASU	Air Separation Unit
Bi_2Te_3	Bismuth Telluride
CHP	Combined Heat and Power
c-Si	Crystalline Silicon
CSP	Concentrated Solar Power
DCC	Dhaka City Corporation
DIR	Direct Insolation Receiver
DPDC	Dhaka Power Distribution Company
DSC	Dye Sensitized Solar Cell
eKW	Electrical Kilo-Watt
EPA	Environmental Protection Agency
EPRI	Electric Power Research Institute
EPV	Energy Photovoltaics
GCV	Gross Calorific Value
GenSet	Generator Set
GHG	Green House Gas
HRSG	Heat Recovery Steam Generator
HT	High Temperature
I_{MP}	Current at the Maximum Powerpoint

IPGCC	Integrated Plasma Gasification Combined Cycle
I_{SC}	Short Circuit Current
LEC	Levelized Energy Cost
LFG	Land Fill Gas
LHV	Low Heating Value
LT	Low Temperature
MDAC	McDonnell Douglas Aerospace Corporation
MSW	Municipal Solid Waste
O&M	Operation and Maintenance
PCB	Polychlorinated Biphenyls
PCDD	Polychlorinated Dibenzodioxins
PCU	Power Conversion Unit
P_{max}	Maximum Power Output
PSA	Plataforma Solar de Almeria
PV	Photovoltaic
PVC	Polyvinyl Chloride
QW	Quantum Well
RDF	Refuse Derived Fuel
SBP	Schlaich-Bergermann und Partner
SCE	Southern California Edison
SCR	Selective Catalytic Reduction
SES	Stirling Energy System
$Si_{0.7}Ge_{0.3}$	Silicon Germanium Based Thermoelectric Module

SOTA	State of The Art
STC	Silicon Thin film Solar Cell
SWM	Solid Waste Management
TCL	Toxicity Characteristic Leaching Procedure
TEG	Thermoelectric Generator
TEM	Thermoelectric Module
V_{MP}	Voltage at the Maximum Powerpoint
V_{OC}	Open Circuit Voltage
WESP	Wet Electrostatic Precipitator
WPC	Westinghouse Plasma Corporation
WTE	Waste to Energy

List of Figures

List of Tables

Chapter 1

Introduction

Over the last two decades, the demand for electrical energy has increased significantly. Since fossil fuels are non-renewable and require finite resources which are declining because of environmentally damaging retrieval technique, there are needs for nonconventional methods to reduce ongoing energy crisis. Due to such concern, developing countries like Bangladesh are facing setbacks in sustainable development.

Research shows that about 42% of the population of Bangladesh have no access to electricity. Rest of the 58% people has maximum demand of 10,390MW per day in which day peak demand and evening peak demand are 5,515 MW and 6,987 MW respectively. But the total capacity of electricity generation is about 8,709 MW which accounts for a deficit of 2081 MW. [**1**] Despite of having such huge deficits only 3.3 % of electricity is being generated by renewable sources. **[2]**

In order to improve the efficiency of power generation from wasted heat, this study has come up with futuristic capable technologies and proposals involving Thermoelectric Energy Harvest from Internal Combustion Engines, Thermal Plasma Gasification from Municipal Solid Wastes, Dish-Stirling Systems and Photovoltaic-Thermoelectric Generator Hybrid System depending upon its worldwide acceptance. These nonconventional methods will not only help resolve deficits considerably over the conventional ones but will also cover access to remote regions both on aspects from Bangladesh and globally.

1.1 Objective

The aim of this thesis is to investigate fundamental science and technological aspects of generating electricity via non-conventional methods. Some key focuses are:

- Introducing renewable energy as an alternative solution for power generation.
- Improving conventional systems efficiency using TEG/TEM.
- Utilizing plasma assisted gasification as an alternative to land filling.
- Using concentrated solar power (CSP) for energy harvesting.
- Investigating combined PV/TEG system over single PV panel for efficiency evaluation.

1.2 Present State of Art

Among other non-conventional methods of power generation, thermo-electric process is a thriving one. Because of the usage nano-technology for building the thermo-electric modules, the figure of merit is increased, so does the efficiency. [**3**] Those are mostly used in case of vehicular engine's wasted heat system. [**4**] A commercial generator has been developed by "Alphabet Energy" that uses exhaust waste heat to electricity using TEG. [**5**]

Plasma Gasification Process is currently at different stages of commercialization. Various companies are adopting this method and with some modifications in process it is on its way to become more mature. Besides "Alter NRG" companies like "Europlasma", "Plasco Energy Group" and "InEn Tec" have currently been conducting several pilot experiments but have no commercial unit in operations unlike Westinghouse which has full scale facility and multiple projects completed and under construction in Japan, UK, and China. [**6**]

For using the solar energy at an efficient manner, Dish-Stirling system can be an option. Previous works on this system was mostly prototypes. At present, Schlaich Bergermann und Partner (SPB) and Stirling Engine System (SES), these two companies are working on commercializing the Dish-Stirling system. In this process, an experimental 1.5 MW rated power plant, using this system was established by SES in 2010 at Arizona, USA. [**7**]

The Bangladeshi government is working towards universal electricity access by 2021 with the Solar Home System (SHS) program projected to cover 6 million households by 2017. Besides several power plant projects of BPDB is going on. For example:

- 650 KW_p (400 kW load) Solar Mini Grid Power Plant at remote Haor area of Sullah upazila in Sunamgonj district under Climate Change Trust Fund (CCTF) on turnkey basis.
- 8 MWp Grid Connected Solar PV Power Plant at Kaptai Hydro Power Station,at Rangamati on turnkey basis.
- Solar Street Lighting Projects in seven City Corporations of the country. [**8**]

But PV/TEG hybrid system is yet to be implemented on commercial basis.

1.3 Thesis Organization

Chapter 1

This introductory chapter provides background information about several non-conventional ways of generating electricity. It also includes background to the present research work, describes the objectives and outline of the thesis.

Chapter 2

This second chapter gives an overview of the thermoelectric energy harvesting process from ICE engines wasted heat. Heat dissipated from the radiator and the exhaust system were mainly utilized to feed the thermoelectric generator/ module (TEG/TEM). Using nano-wired TEG the overall efficiency of the system was increased considerably.

Chapter 3

The third chapter outlines the use of MSW as feedstock to reactor for plasma assisted gasification using plasma arc torches to increase temperature inside the chamber and generate syngas to convert into power efficiently through steam turbine and generator.

Chapter 4

This chapter explains the generation procedure of electricity via Dish-Stirling system. A theoretical design has been proposed in the context of Bangladesh. A background study has also been done to form an economically comprehensive model.

Chapter 5

In this chapter, Photovoltaic/TEG designs are introduced and the methods of integration are described. The construction of the model based on energy balance equation is explained, followed by calculating the parameters for both the PV cell and the TEG.

Chapter 6

This chapter summarises the non-conventional methods that has been studied in the earlier chapters and also describes some ideas about future progression.

Chapter 2

Thermo-Electric Energy Harvest from ICE Engine's Wasted Heat

2.1 Introduction

Among the different approaches for producing electricity, diesel generators and gas generators serve a large portion of electricity supply in developing countries such as Bangladesh. But due to limited efficiency of diesel and gas generators, a lot of thermal energy is wasted in this process. The amount of wasted heat, if salvaged, can offer us a promising amount of recovered electric energy. In this chapter, it is discussed to convert this wasted heat into electricity using a direct conversion method as an energy salvaging process.

TE generators are direct convertors of heat to electricity. Their conversion process is done due to the principle of TE Seebeck effect, which was discovered in 1821. At first, thermocouples were used to measure temperature only. But discovering materials with more TE efficiency made the TE materials useful for refrigeration (TE cooler) and also electricity generation. [**9**]

In Bangladesh, among the electricity generations, 7.83% is HSD (High Speed Diesel) based, 21% is HFO (Heavy Fuel Oil) based and 62% is Gas dependent. Among the installed capacity 35.21% power is generated by reciprocating engines (gas/diesel). [**10**]

This chapter discusses about, using thermoelectric modules with optimum parameters and design, about 7.62% of the thermal waste energy can be recovered. If calculated, about 483 MW power can be recovered in total.

2.2 Literature Review

Thermoelectric generators (TEGs) can harvest electrical energy when a temperature difference is applied across the two ends of the device. [**11**] It was first discovered by Thomas Johann Seebeck in 1821. According to his discovery, the phenomenon of generating electricity gradient of a conductor due to a temperature gradient across it in open circuit condition is called the Seebeck effect. Peltier effect is the opposite of Seebeck effect that absorbs or evolves heat when current is passed through the junction. The basic schematics of a thermocouple is shown in figure 2.1.

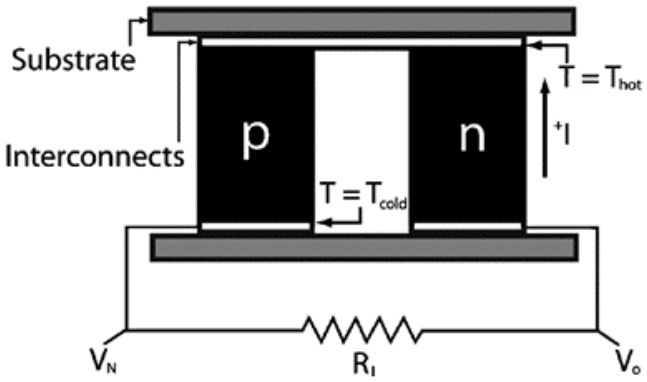

Figure 2.1 Schematic of a single thermocouple TEM operating in generation mode.

A set of thermo-couples are joined together to make a thermoelectric module. (See figure 2.2)

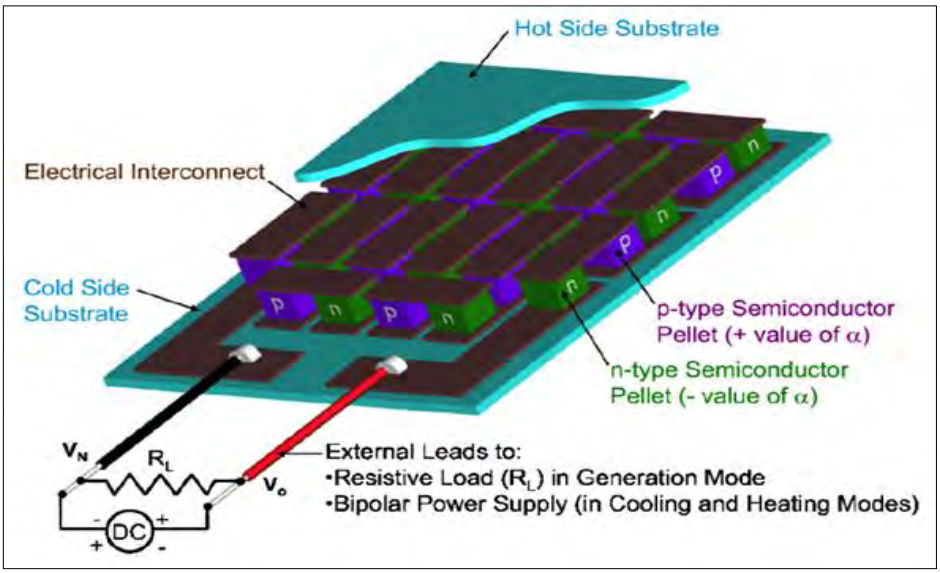

Figure 2.2 Cut-away view of a TEM. [**12**]

The performance of the device, determined by properties of the junction materials, is typically quoted using a figure of merit, ZT, a dimensionless parameter. Yang [**13**] gives a timeline of advances in thermoelectric materials and their figures of merit. Bulk materials, such as bismuth telluride and lead telluride, identified in the 1960s and 1970s have ZT in the range of 0.5 to 1.0. These materials are most common in present-day applications, including demonstration vehicle waste heat recovery programs. Equation for calculating figure of merit ZT,

$$ZT = \frac{\alpha^2 \sigma T}{\kappa}$$

Here,

α = material seebeck coefficient

σ = material electric conductivity

T = Temperature of the hot side of TEM

κ = Thermal conductivity

More recently discovered thin film materials silicon carbon and boron carbon, operating on a quantum well principle, have demonstrated ZT of 4 to 5 in the laboratory, but have yet to be scaled up to practical systems. In addition to higher efficiency, these thin film designs offer the potential for much lower cost compared to bulk designs because less junction material is required. [**14**]

2.3 Present State of Art

New and more-efficient nanostructured thermoelectric materials have been developed. These new materials called quantum wells (QW), are composed of alternating layers of 10 nm thick silicon and SiGe films and with such confinement, all of the thermoelectric properties are improved to increase the thermoelectric Figure of Merit, ZT. QW ZTs greater than 3 lead to conversion efficiencies greater than 20% for QW materials which allows for much wider commercial applications, particularly in applications such as the waste-heat recovery from truck engines, refrigeration, and air conditioning, where SOTA bulk thermoelectric modules were shown to be technically feasible but economically unviable due to low conversion efficiencies. **[3]**

For over 35 years, the ZT stayed close to the value of 1. However, breakthroughs have occurred in the Figure of Merit by using the recent QW alternatives to bulk material, with the QW material reaching the remarkable ZT value of 4.1 in performance tests at Hi-Z Technology, Inc. (Hi-Z). [**3**]

2.3.1 Alphabet Energy E1

Alphabet Energy has designed a generator that uses no fuel. Instead, it uses racks of thermoelectric modules to convert the waste heat from industrial machines into electricity. [**5**] The Hayward-California based startup introduced the E1, claiming that it is the first large-scale commercial thermoelectric generator on the market (see figure 2.3). The company is already taking orders from mining companies that have large amounts of waste heat and no use for it.

To set it up, a mining company needs to connect a flexible tube to direct exhaust from an engine into Alphabet Energy's generator, which is packaged in a shipping container. The gases flow through 32 racks of thermoelectric modules that produce a direct current, which is inverted to alternating current and fed to the site's breaker. A radiator cools the modules because they need a difference in temperature to produce current.

Figure 2.3: Alphabet Energy E1 thermoelectric generator

Alphabet's generator can produce 25 KW from the waste heat given off from an engine that generates 1000 KW of electricity from fuel, such as diesel. The solid-state modules are designed to work for ten years and can be replaced as better materials are developed. The company plans to target other industries with copious amounts of waste heat, including oil and gas as well as steel and glass manufacturing.

Alphabet energy originally set out to use a silicon nanowire material licensed from Lawrence Berkeley National Laboratory as the core material for its thermoelectric modules because it promised higher conversion efficiency than conventional materials, such as bismuth telluride. In recent years, it licensed a different class of materials called tetrahedrite from Michigan State University. It is an abundant, naturally occurring mineral, which the company expects will work well over a broad set of temperatures. [**5**]

2.4 Design

Thermoelectric generator/module design is a quite complex process. Although, some parameters in the physical and mathematical aspects can be considered for desired performance of the TEM.

2.4.1 Physical Design

A TEM consists of an array of n and p-type pallets connected electrically in series and thermally in parallel between ceramic substrates. The Hot side and cold side substrates are placed accordingly, then electricity is harnessed from the series connected P-N junctions as shown in figure (2.4). A heat sink is placed at the cold side of the TEG to enhance the efficiency. [**12**]

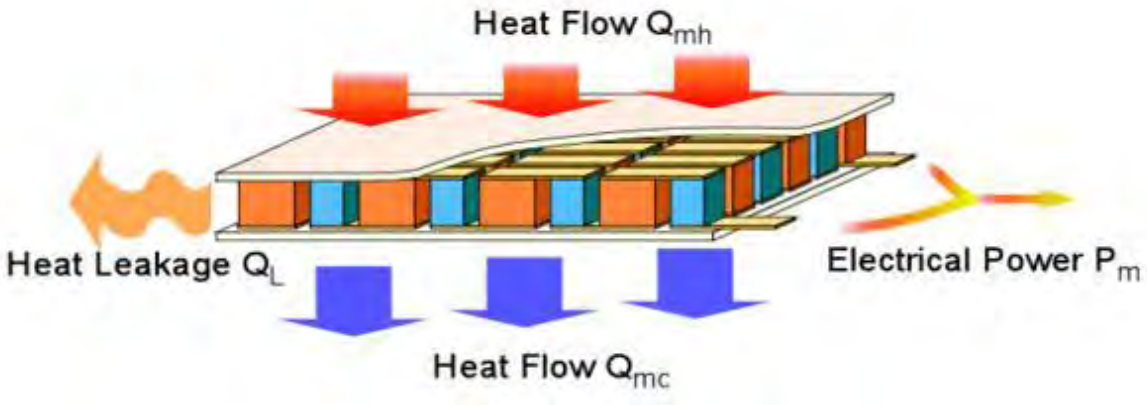

Figure 2.4: Configuration of a TEM [**15**]

2.4.2 Mathematical Design: *B. TE Generator Equations*

Figure of merit, on which the thermoelectric efficiency mostly depends on, ZT of the TEG is calculated as follows: **[9]**

$$ZT = \frac{\alpha^2 \sigma T}{\kappa} \tag{2.1}$$

Where α (V/K) is the material seebeck coefficient, σ (S/m) electrical conductivity and κ (W.m-1.K-1) is thermal conductivity.

Electrical resistivity of the material ρ (Ωm) can be obtained from electrical conductivity:

$$\rho = 1/\sigma \tag{2.2}$$

The thermal conductivity is sum of the component carrier (electron) and phonon which are respectively, κ_{electron} and κ_{phonon} :

$$\kappa = \kappa_{\text{electron}} + \kappa_{\text{phonon}} \tag{2.3}$$

According to The Wiedmann-Franz law the carrier thermal conductivity is given as:

$$\kappa_{electron} = L.\sigma.T \quad (2.4)$$

Where, L is the Lorenz number (2.445×10^{-8} $WS^{-1}K^{-2}$). [**16**]

There are several methods to calculate the TE generator performance parameters. The basic equations of them are explained here. [16]

The temperature difference between the hot and cold side of the TE generator is:

$$\Delta T = T_H - T_C \quad (2.5)$$

Where, TH is the hot side and TC is the cold side temperature in Kelvin.

The open circuit output voltage is:

$$V_{OC} = \alpha.\ \Delta T \quad (2.6)$$

So the output current is calculated as follows:

$$I = V_{OC} / (R + R_L) \quad (2.7)$$

Where R is the TE generator internal resistance and calculated as:

$$R = \rho l / A \quad (2.8)$$

Where l is the length and A is the cross sectional area of the TE pallet.

R_L is the load resistance which is set 1.323393R, for optimum efficiency. [**16**]

The output power is:

$$P = I_2.R_L \quad (2.9)$$

The input heat to the TE generator is calculated as follows:

$$Q_H = \alpha.I.T_H - 0.5R.I_2 + K.\ \Delta T \quad (2.10)$$

Where K is:

$$K = \kappa A / l \quad (2.11)$$

So the TE pallet waste heat is:

$$Q_C = Q_H - P \quad (2.12)$$

And the TE pallet efficiency is: **[3]**

$$\eta = P / Q_H \quad (2.13)$$

2.5 MATLAB Calculation

A MATLAB code is developed in order to carry out these calculations for specific temperature differences and TEM parameters. In this case, parameters for the TEG pallets are given below. In this paper, nanowire (6×6×1) mm bismuth telluride (Bi2Te3) pallet is used for the TE generator of the car coolant system. Its Seebeck coefficient is 287 μV/K at 327 K (54ºC). It has high electrical conductivity of 1.1×10^5 S/m and very low lattice thermal conductivity of 1.20 $W.m^{-1}.K^{-1}$. Its melting point is about 858 K (585ºC) and it's useful in temperature about 350 K (77ºC). [**17**] [**18**]

To design the TE generator for the exhaust system, the $Si_{0.7}Ge_{0.3}$ -1at%P (99.999999999% purity) with 10 mm in diameter and 0.3 mm thick, is selected seebeck coefficient is. Its 326.6 μV/K at 1000 K (727ºC). It has the electrical conductivity of 49079.75 S/m and the lattice thermal conductivity of 4.4 $W.m^{-1}.K^{-1}$. The melting point is about 1563 K (1290ºC) and it's useful in temperature about 1000 K (727ºC). [**19**]

For our calculation, we have chosen W18V32 generator [**20**], Wartsila (origin in Finland), a very similar type of generator (W20V32) that is used in Meghnaghat powerplant of Orion group, Bangladesh. [**24**]

Bi_2Te_3 was use at the radiator side of the Generator where temperature of the high side is of the water jacket/ radiator, 96ºC (369K) and room temperature 27ºC (300K) is considered as cold side temperature [**20**].

2.5.1 Efficiency Calculation of Bi_2Te_3

From the Matlab code (**Appendix 1**) designed for calculating the efficiency of the Bi2Te3 TEM, the result obtained is illustrated in figure 2.5 in a graphical form, where the change of efficiency with the corresponding temperature and the optimum operational zone is indicated.

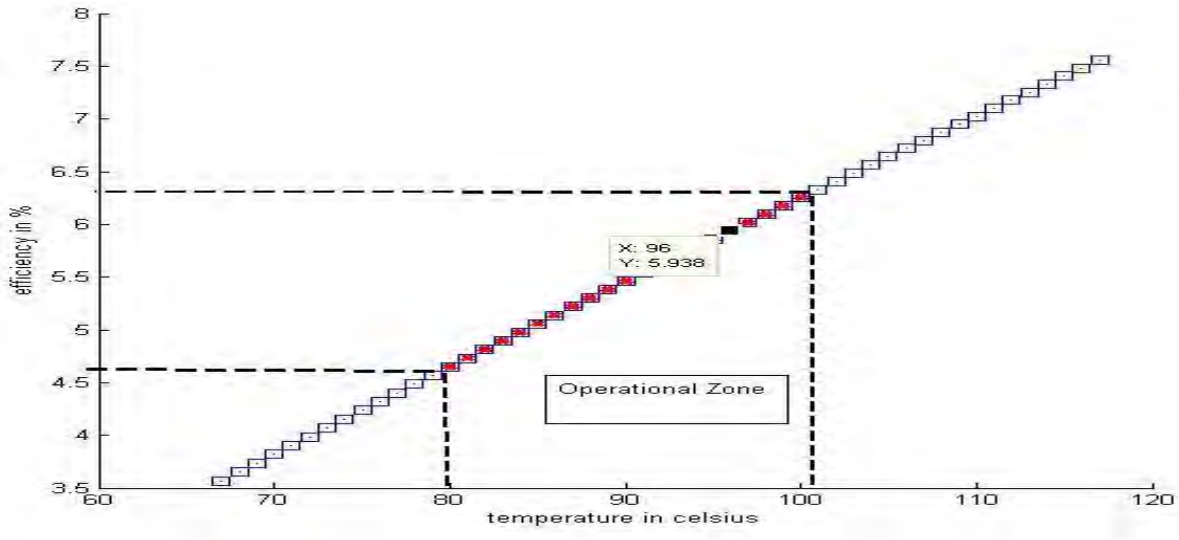

Figure 2.5: Bi_2Te_3 efficiency curve

The Calculated Efficiency was 5.936% for a temperature difference 69°C and power calculated for each pallet was 0.3807 W.

The thermal energy dissipated at the water jacket/radiator along with the charged air circuit (High temperature (HT) and Low Temperature (LT)) was (1512 + 1440 + 1193) KW = 4145 KW. [**20**]

With 5.936% efficiency, (4145 × 5.936%) KW = 246.04 KW electricity can be produced form the coolant waste heat.

The number of the TEG pallets required,

$$\frac{Total\ Power\ dissipated}{power\ produced\ by\ each\ TEG\ pallet} = \frac{4145}{0.3807} = 10887.8 \approx 10888$$

For each pallet being 6x6x1 mm, the dimension of the TEM containing 10888 TEG pallets will be,

$$\{10888 \times (.006 \times .006)\ m^2\} = 0.392\ m^2$$

According to the dimension of the radiator/ cooling water jacket, the number of the pallets may increase or decrease as well as the dimension. Noticeable that, the whole TEM is of height 1mm, hence it was ignored during the dimension calculation. [**9**]

At the Exhaust side, due to higher temperature gradient, $Si_{0.7}Ge_{0.3}$ TEG was used because of its higher melting point [**19**]. The Exhaust gas temperature after the turbocharger of the

generator at 100% load is 379ºC (652K), is considered as the high temperature side and room temperature 27ºC (300K) is considered as low temperature side.

$Si_{0.7}Ge_{0.3}$ is used at the exhaust side for its better performance at higher temperature. Low side temperature is considered as the room temperature, 27ºC (300K) and high side temperature is 379ºC (652K). [**20**]

2.5.2 Efficiency Calculation of $Si_{0.7}Ge_{0.3}$

A similar type of Matlab code (Appendix 2) for efficiency calculation of $Si_{0.7}Ge_{0.3}$, illustrates to temperature versus efficiency curve and indicates the optimum operational zone in figure 2.6.

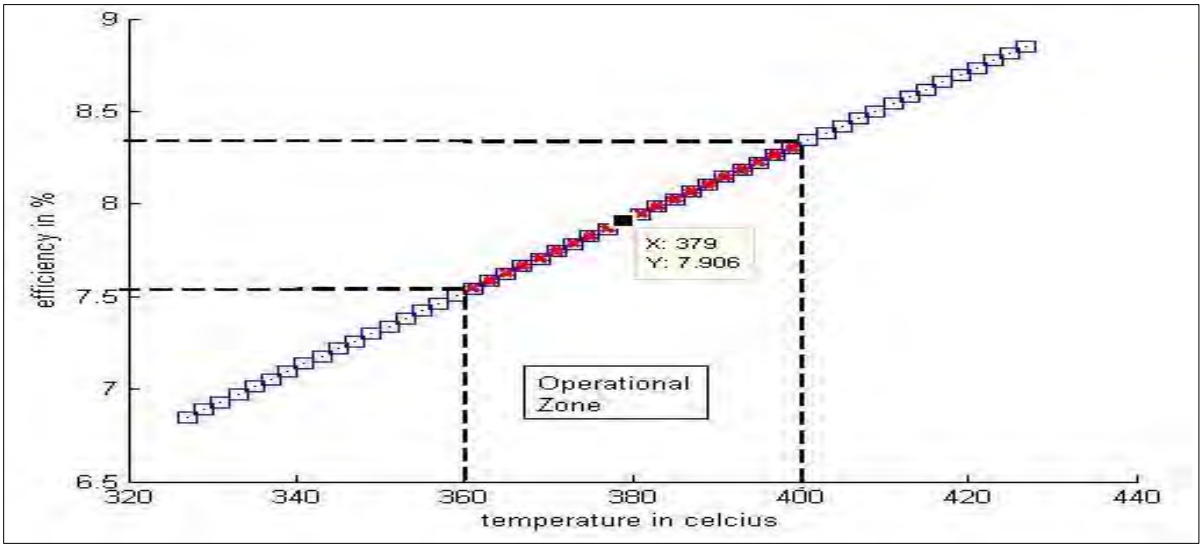

Figure 2.6 $Si_{0.7}Ge_{0.3}$ efficiency curve

The calculation shows the 7.906% efficiency at 379ºC (652K), and power produced from each pallet is 41.48 W.

Heat rejection at the exhaust is calculated from the percentage of heat distribution of the engine. The engine is of 45% thermal efficiency (excluding auxiliary losses) [**21**], which provides 9000KW power. Hence, 45% = 9000 KW, that concludes 100% = 20000KW thermal power. Heat balance at the water cooler, charged air, friction and radiation comprises of (1512 + 1440 + 1193 + 1091 + 206) KW = 5442 KW [**20**], that is 27.21% of the total thermal energy. Hence the thermal energy dissipated at the exhaust is

[100 – (45+27.21)] % = 27.79% of the total thermal energy

= 5558 KW

With 7.906% efficiency, (5558 x 7.906%) KW = 439.41 KW electricity can be produced. And since each pallet can produce 41.48 W of electricity,

$$439410/41.48 = 10593.29 \approx 10594 \text{ pallets required.}$$

Dimension of each pallet is 10mm diameter, 0.3 mm thick (height), and those will be mounted on the exhaust system at in an octagonal form, at the 8 sides of the wall of the octagonal structure; as shown in figure (2.7) [**4**]

The dimension of the thermo-electric module will be,

$$[10594 \times 3.14 \times (.01/2)^2] \text{ m}^2 = 0.831629 \text{ m}^2$$

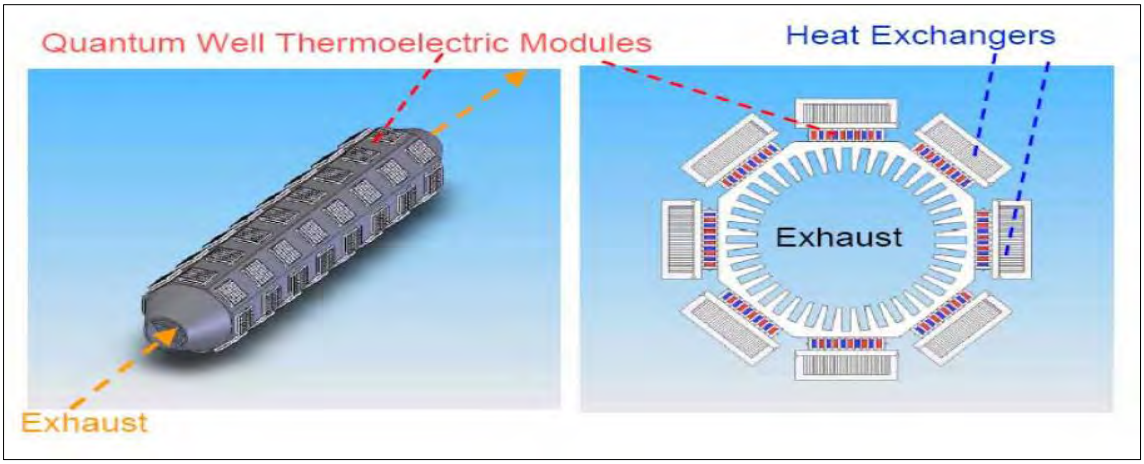

Figure 2.7 TEG pallets design at exhaust system [**4**]

Although the TEG pallets are of circle shape, each pallet will require a square area 10mm side. Considering that, the required area for TEM appears,

$$[10594 \times (0.01)^2] = 1.0594 \text{ m}^2$$

Each wall of the octagonal structure will be of (1.0594/8) m^2= 0.1324 m^2 and contain (10594/8) ≈ 1325 pallets

Hence, the total electrical energy harvested from the coolant and exhaust system is:

(246.04 + 439.41) KW = 685.45 KW

This is 7.62% of the engine output (9000 KW) and 3.43% of the total thermal energy. Considering this harvested electricity, the total efficiency of the generator becomes (45+ 3.43) % = 48.43%.

2.6 Comparison of Diesel and Gas Engine Generators

Diesel engines have relatively higher efficiency (about 38%) [**4**] than gas engines (32%) [**22**]. Due to the lower efficiency of the gas engine, its coolant and exhaust contains higher waste heat. Comparing a Caterpillar diesel generator of rating 1088 eKW with a Caterpillar gas engine generator of 1030 eKW this is the result observed in figure (2.8) and (2.9).

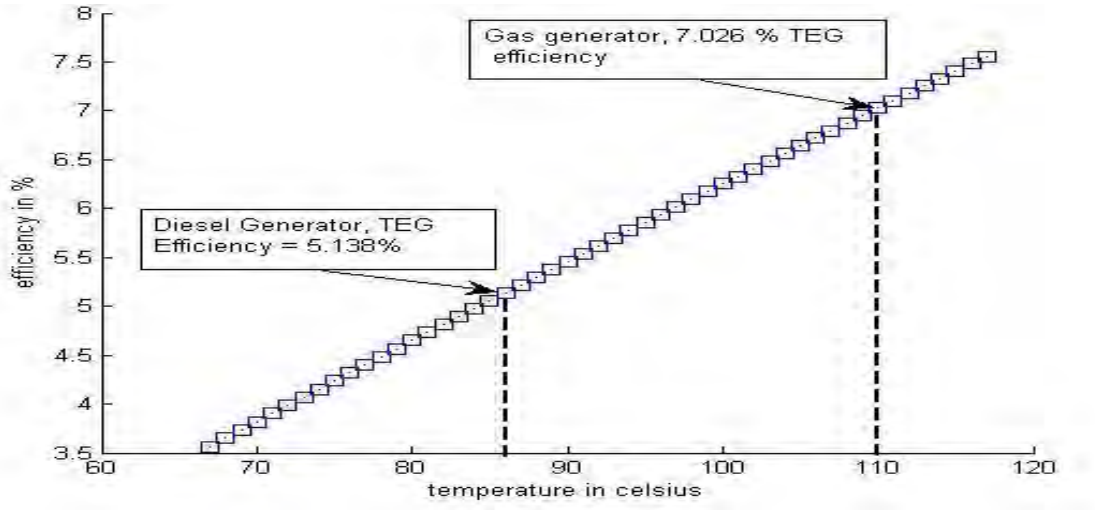

Figure 2.8: Comparison of Diesel generator and Gas generator coolant temperature vs TEG (Bi_2Te_3) efficiency

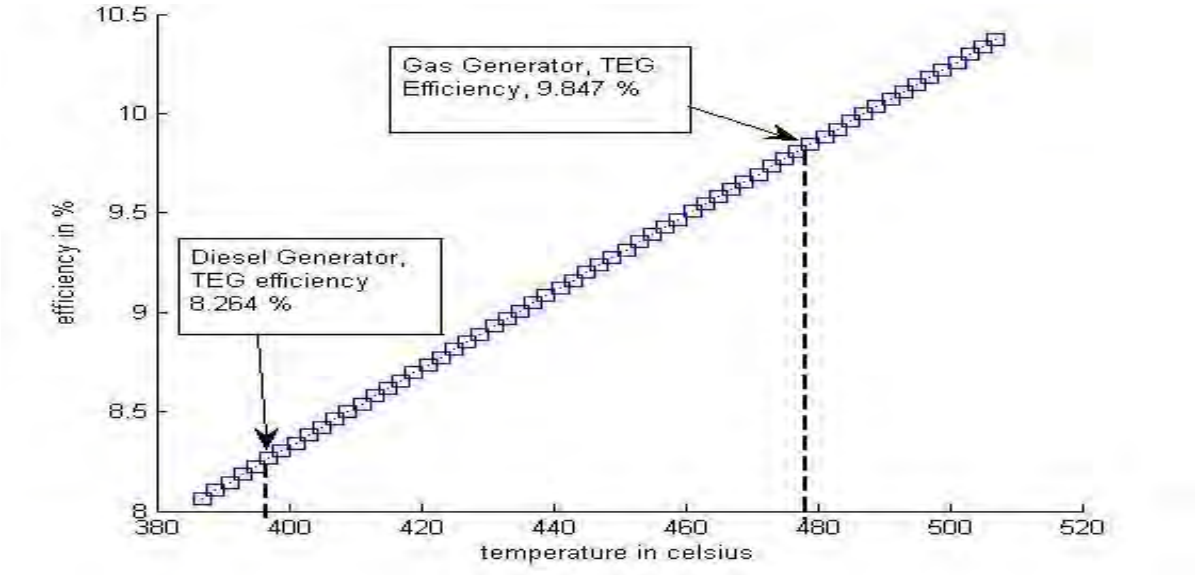

Figure 2.9: Comparison of Diesel generator and Gas generator exhaust temperature vs TEG ($Si_{0.7}Ge_{0.3}$) efficiency

2.6.1 Comparing the Generators According to Their Technical Data

Two Caterpillar generators (1 diesel generator, 1 gas generator) were chosen for the assessment. From their data sheet, the heat wasted at the coolant and the exhaust was calculated (see table 2.1) and hence compared the overall efficiency of the TEG modeled previously.

Table 2.1 Overall efficiency comparison of equivalent Diesel and Gas generators [**22] [23]**

	Diesel Generator	**Gas generator**
Generator model	CAT 3512B-1500	CAT® G3516 LEAN BURN GAS ENGINE
Rated electrical output (ekw)	1088	1030
Electrical Efficiency	38%	32%
Temperature at coolant/ radiator (℃)	86 (359 K)	110 (383 K)
TEG Efficiency (Bi_2Te_3)	5.138 %	7.026 %
Heat rejection to coolant	472 KW	817 KW
Recoverable waste heat electricity	24.25 KW	57.40 KW
Exhaust temperature (℃)	397.4	479
TEG Efficiency ($Si_{0.7}Ge_{0.3}$)	8.246 %	9.847 %
Heat Rejection to exhaust	1057 Kw	929 KW
Recoverable electricity from waste heat	87.16 KW	91.47 KW
Total recovered electricity	111.41 KW	148.87 KW
Percentage of electrical output	10.23 % (1)	14.45 % (1)
Overall electrical output	1199.06 KW (2)	1178.8 KW (2)
Improved Efficiency	41.88 % (3)	36.59 % (3)

Notes

1. For Diesel generator, total electrical output is 1088 eKW and recovered electricity from waste heat is 111.41 KW, which is 10.23% of the electrical output 1088 eKW. Similarly, 148.8 KW electricity produced from the waste heat of the gas generator of rating 1030 eKW, which is 14.45% of its electrical output.
2. Overall electrical output for the diesel generator is (1088+111.41) KW = 1199.06 KW. For Gas generator, the total electrical output is (1030 + 148.8) KW = 1178.8 KW.
3. Improved efficiency can be calculated according to the derived data. For diesel engine, 1088 eKW refers to 38% efficiency. Hence, 1199.06 eKW refers to $\left[\frac{1199}{1088} \times 38\%\right] = 41.88\%$. Similarly, for gas engine generator, the current efficiency is 32% and the improved efficiency is 36.59%.

Hence, the overall efficiency of both the diesel and the gas generator can be improved using Bi_2Te_3 and $Si_{0.7}Ge_{0.3}$ thermo-electric modules. However, the electricity produced from these TEM is DC current. This can be directly used to feed the auxiliaries or as AC output using high performance inverters.

2.7 Potential Waste Heat Recovery and Usage

The Orion Power Meghnaghat power plant with a capacity of 100MW consists of 12 engines, each one of capacity 8.924 MW. Model of the engine is W20V32, origin in Wartsila, Finland. [**24**]

With the TEM design shown, 7.62% of the total electric capacity can be recovered. Hence, from 100 MW power plant of Meghnaghat, 7.62 MW of electricity can be produced from the waste heat.

35.99 % of total electricity produced from reciprocating engines. Maximum demand served on 30-06-2016 is 9036 MW [**10**]. Hence, 3252.05 MW produced from the reciprocating engines. If 7.62% of the waste heat from the reciprocating engines can be recovered, then (3252.05× 7.62%) MW = 247.81 MW electricity is expected to be produced from waste heat.

Since the electricity produced from TEG is DC and maximum auxiliary powers for the generators are DC powered, the recovered electricity can be effectively used for feeding the

auxiliaries. The auxiliary power requirements is the 5-10% of the gross power generation. [**25**] For 100 MW power plant in Meghnaghat, 6-7% auxiliary power is required. Hence, the recovered waste heat electricity can cover up for the auxiliary power requirement for 100 MW or more capacity power plants.

2.8 TEM Pallet Optimization

TEM are compact, rugged, acoustically silent and scalable (from mm scale footprint device to meter-scale footprint arrays). It is versatile as it can be used for heating, cooling and electricity generation.

For generation mode, the optimization of pallet geometry is more complex since the optimal pallet geometry depends on the electrical resistance of the load of the TEM.

In this case, elementary criteria of a single material, constant property pallets with optimized geometry (number and height) is considered for maximum performance (output power) or maximizing efficiency for a specific performance. This is accomplished for a specific resistive load and effective footprint (sum of the cross sectional area of its pallets).

The efficiency of the TEM can be optimized by considering the optimum parameter for the Height (H), Effective Foot-print/Area (A_e) and the number of thermocouples in a TEM 'N'. This efficiency is termed as relative efficiency η_r.

Where,

$$\eta_r = \frac{optimum\ efficiency}{theoritical\ efficiency} = \frac{\eta_o}{\eta}$$

Here, optimum efficiency is the practical efficiency found by experimental procedures.

The relative efficiency η_r of the TEM increases with the decrease of the height (H) of the pallets and with the increase of effective area/ footprint (A_e)

Governing equations for maximum efficiency extraction, [**12**]

$$H(\eta_{max}) = \frac{\gamma A_e \alpha^2 \Theta^2}{4\rho W_g (1+\gamma)^2} \quad (2.14)$$

$$N(\eta_{max}) = \frac{\sqrt{(R_L W_g)}(1+\gamma)}{\Theta \alpha \gamma} \quad (2.15)$$

$$A_e = \frac{4\rho H W_g + 8 R_{ec-\rho} W_g (1+\gamma)^2}{\alpha^2 \Theta^2} \quad (2.16)$$

Here,

$\alpha = seebeck\ coefficient$

$\Theta =$ temperature difference

$R_{ec-\rho} = electrical\ contact\ resistance\ (negligible)$

$\gamma = \sqrt{(1 + ZT_M)}; [T_M = (T_{Hot} + T_{Cold})/2]$

Figure (2.10), (2.11) and (2.12) shows that, how a design of the TEM can be optimized by considering three major geometrical factors Height (H), Number of Thermocouples (N) and effective Footprint (A_e). [**12**]

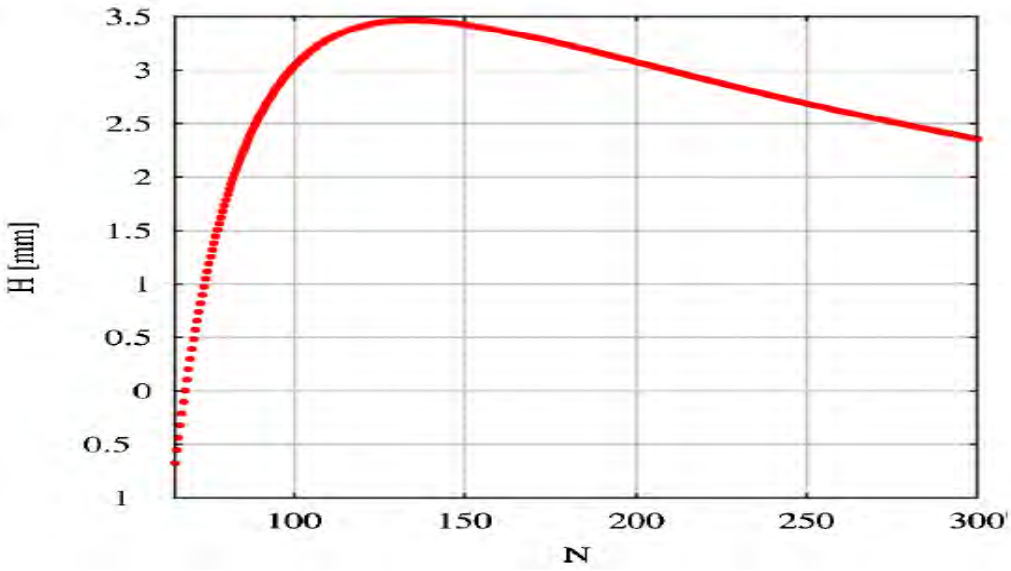

Figure 2.10: Optimum height, H of the pallet according to the thermocouples, N [**12**]

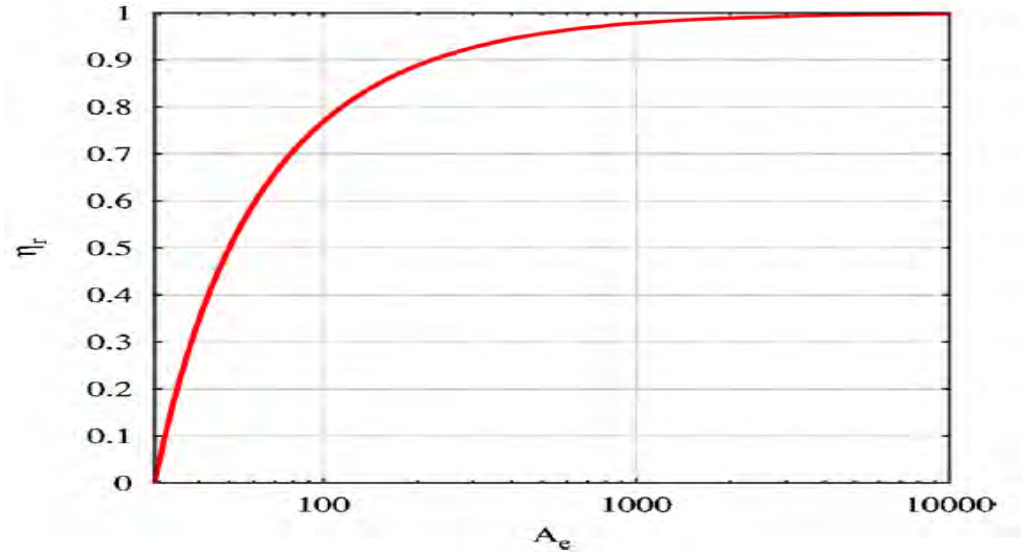

Figure 2.11: Relative efficiency, η_r vs the effective footprint A_e [**12**]

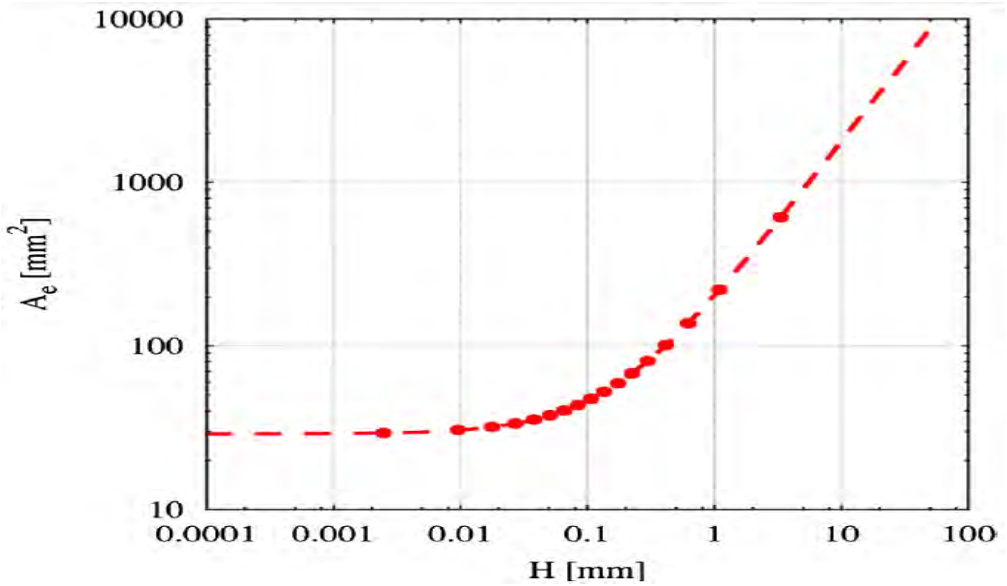

Figure 2.12: Effective footprint, A_e with respect to height of the thermocouple, H **[12]**

Relative efficiency may be made arbitrarily close to unity by sufficient increases in H and Ae as per Fig. 2.12. For example, doubling Ae such that it equals 1223.57 mm^2 results in N, H and η_r values of 118, 6.81 mm and 98.2% respectively. [**12**]

That renders the efficiency of previous calculation (7.62× 98.2%) = **7.48 %.**

2.9 Conclusion

Thermoelectric generators have a huge potential for compensating the energy losses of the reciprocating engines. As long as the efficiency of the reciprocating engines reach higher and close to unity, the use of TEMs will be very effective for wasted heat recovery system. In near future, it is expected the thermoelectric efficiency of the TEMs to be improved significantly so that those can be used in low temperature gradient thermoelectric generations.

Renewable energy is highly desired and thermoelectric generators/modules have the major role in extracting electricity from thermal energy in a more convenient and eco-friendly way. Researches should be done to improve efficiency of the TEG/TEMs significantly in order to make the best out of it.

CHAPTER 3

Thermal Plasma Gasification

3.1 Background

Overpopulation, consumerism, urban and industrial development have prompted to a significant increase of municipal solid waste (MSW) generation. These factors are constantly leading an exponential increase in rate of solid wastes to such an extent that it poses serious threat to the natural environment and putting stress on national resources. Lack of proper disposal and inefficiency of waste management has now become a global concern which must be addressed effective immediately.

Dumping wastes openly and uncontrollably near sites without proper supervision blocks the entire urban drainage system thereby stagnating water and hampers the contamination of water supply. This poses threat to the health of residents of major city corporations of developing nations and third world countries including Bangladesh.

Dhaka, the capital city of Bangladesh, has become a center of trade and commerce in recent years. The population growth here is currently at a rate of around 6 percent annually [**26**]. The greater Dhaka has a population of around 18 million as of 2016, while the city itself has an estimated population of around 8.5 million. The Dhaka City Corporation (DCC) covers an area of around 131 km^2 and population density exceeds 92000 per km^2 [**27**]. Inadequate technology, manpower and public awareness in the community are the major limitations of this city.

The information base regarding the types, quantity and characteristics of waste along with collection, operation, storage, management plan and disposal are below par that it needs work to a sustainable management system which requires educational, institutional, economic, financial and environmental sustainability.

With growing demands of electricity for households, factories, offices throughout the city and beyond major cities in Bangladesh there is an opportunity using the wastes to generate considerable amounts of electricity by means of incineration and thermal plasma arc gasification which don’t deserve to be taken for granted. Due to scarcity and increasing costs of fuels and natural gas this process can be an alternative and viable option to resolve the problem momentarily and eventually for future [**28**].

3.2 Objective

The purpose of this research is to find new ways and alternatives of proper disposal of waste collection in bulk and managing them for power generation efficiently. This study will eventually help in decision making processes as to adopt the following methods or not. This study involves dealing with amount of waste generation, characteristics, management systems and possible remedies of different city corporations in context to Bangladesh along with the associated environmental impacts. The parameters used for this study are:

- Estimation of the density of waste generated in different parts across the country.
- Estimation of power output using MSW (Municipal Solid Wastes) as an input.
- Estimation of the by-products generated that can be recycled for other purposes and develop methods to counteract environmental effects of it if any.

3.3 An Overview of WTE (Waste to Energy) Technology

There are various ways of waste to energy conversion technologies available amongst more traditional and conventional approach of direct combustion or incineration of solid wastes. Since 1970's [**29**] advanced thermo-chemical approaches including pyrolysis, gasification and plasma arc gasification have been developed and experimentally applied to selected waste streams on a small scale in a specially designed closed chamber with temperatures and pressures used as control parameters. Each technology uses different set of requirements for the input operating in different equipment configurations in different modes to generate a wide variety of products and on a different scale.

The following sections discuss the thermo chemical conversion technologies for calorific waste (RDF) treatment and a summary of conditions outlined in the table 3.1.

- Incineration-full oxidative combustion
- Pyrolyis-thermal degradation of organic material in oxygen deficient conditions
- Gasification-partial oxidation
- Plasma Arc-Gasification-combination of (plasma-assisted) pyrolysis/gasification of the organic fraction and vitrification of the inorganic fraction of the waste feed.

Table 3.1 Typical reaction conditions and products from various thermos-chemical approaches (based on Kolb and Seifert)

	Pyrolyis	**Gasification**	**Combustion**	**Plasma Treatment**
Temperature [℃]	250-900	500-1800	800-1450	1200-2000
Pressure [bar]	1	1-45	1	1
Atmosphere	Inert/Nitrogen	Gasification Agent:O_2 , H_2O	Air	Gasification Agent:O_2, H_2O Plasma Gas:O_2, N_2, Ar
Stoichiometric Ratio	0	<1	>1	<1
Products From The Process				
Gas Phase	H_2, CO, H_2O, N_2, hydrocarbons	H_2, CO, CO_2, CH_4, H_2O, N_2	CO_2, H_2O, O_2, N_2	H_2, CO, CO_2, CH_4, H_2O, N_2
Solid Phase	Ash,Coke	Slag,Ash	Slag,Ash	Slag,Ash
Liquid Phase	Pyrolysis oil and water	N/A	N/A	N/A

3.4 Literature Review

3.4.1 What is Solid Waste?

The term solid waste is used to refer municipal waste and falls under the following categories: residential (household or domestic waste), commercial, institutional, street sweeping, construction, sanitation and industrial [**30**]. Likewise, municipal solid waste refers to solid wastes from houses, streets and public places, shops, offices, and hospitals, which are more often the responsibility of municipal or other governmental authorities. Solid waste from industrial processes is generally not considered as municipal. However, since this waste finally ends up in the municipal waste stream, it should be taken into account when dealing with solid waste. Synonymous to solid waste are terms such as “garbage”, “trash”, “refuse” especially in parts of North America. [**31**]

3.4.2 Basic Operational Elements of Solid Waste Management (SWM) System

The activities related to management of SWM from the point of generation to proper disposal are grouped into some basic functional elements [**32**]:

- Waste generation
- Waste handling, sorting, storage and processing at the source
- Collection
- Processing and transformation
- Transfer and transport
- Disposal

Functional elements are closely interconnected but they are not necessarily presented in all municipal solid waste management system.

In many underdeveloped or developing countries the system is limited to

- Waste generation
- Handling at the source
- Collection
- Disposal at landfills

While in most developed countries almost every functional elements are found within the system.

3.5 Process, Power-plant Design and Construction

This section provides detailed information about the background, development and working principle of standard thermal plasma gasification power plant.

3.5.1 History of Thermal Plasma Gasification Process

One of the first industrial thermo chemical processes was gasification. Towards the end of the nineteenth century during the industrialization of Europe this technology was discovered, mostly for producing oil and gas from coal. But soon after World War II ended, the use of gasifiers reduced for petroleum was now readily more available. Between mid-1970s and 80s, the use of gasification for producing synthetic fuels began. Till now, this application has been

the biggest use of gasification. In the 1980s, U.S.A, Europe and Japan has focused on the development of gasification for the treatment of solid wastes. At present, there are about more than 150 industrial gasifiers across the world. These are mainly used to process biomass and coal. The use of gasification for MSW has been mostly applied in Japan, where their lack of space forced them to find alternatives to landfilling. Japan has also the only commercial plasma arc facility that treats MSW, in Utashinai, operated by Hitachi metals and Alter NRG. The thermoselect process was built in Germany but due to some technical difficulties it was later closed. Siemens faced similar issues with waste gasification at their Fürth plant which led to a serious accident, resulting in plug of waste formed in the pyrolysis chamber which created an overpressure and escape of pyrolysis gas. Apparently, this issue was the consequence of processing unshredded mattresses and this problem was eliminated in later versions of the gasifier. However Germany is not considering using it in near future (ref. to Dr. Michael Weltzin, Scientific Assistant of the Parliament of Germany, NAWTEC 18, 2010 Conference). Apart from Germany, gasification is generally viewed as a better alternative th1an grate combustion since it is not associated with the old and polluting incinerators. Therefore, there can be a market for gasification in competition to grate combustion. Gasification is the breakdown of the organic part of the waste into synthesis gas or syngas, which is a mixture of CO and H_2, by carefully control and monitor of the amount of oxygen present. The key difference from combustion is that the product will only be partially oxidized and the substoichiometric amount of oxidant allows keeping CO and H_2 as final products instead of the fully oxidized CO_2 and H_2O.[**6**]

3.5.2 Introduction to Plasma Arc Gasification Operation & Basic Principles

Plasma Arc Gasification is a high-temperature intensive pyrolysis process whereby the organics of waste solids are converted into syngas and inorganic materials and minerals of the waste solids yields a rock alike glass by-product called vitrified slag. The syngas is mostly composed of CO and H_2. The high temperature during the whole cycle is created by an electric arc in a torch which triggers gas being converted to plasma. The process containing a reactor with a plasma torch processing organics of waste solids is called plasma arc gasification. The plasma arc gasification reactor is typically operated between 3982^0C and 6982^0C. In commercial practice, the plasma arc gasification process is operated with an injection of a carbonaceous material like coal or coke into the plasma arc gasification reactor. This material

reacts quickly with oxygen to produce heat for the pyrolysis reactions in an oxygen deficient environment. Equation (3.1) shows the carbonaceous materials as C that reacts with the oxygen to produce limited combustion but with the necessary heat required for the syngas reactions (Equations [3.2-3.6]). In addition to this, steam is added to the plasma arc gasification reactor to promote syngas reactions. The combustion reactions (exothermic reactions) supply heat with additional heat from the plasma arc torches for the pyrolysis reactions (endothermic reactions), yielding a temperature typically between 3982^0C and 6982^0C. The inorganic minerals of the waste solids (MSW) produce a rocklike by-product.

Since operating conditions are very high these minerals are converted into a vitrified slag typically comprising metals and silica glass. This vitrified slag is basically non leaching and exceeds EPA (Environmental Protection Agency) standards. Metals can be recovered from the slag and the slag can be used to produce other by-products such as rock wool, floor tiles, roof tiles, insulation, and landscaping blocks. The vitrified slag, being environmentally acceptable as a recyclable by-product, is one of the more positive attributes of plasma arc gasification process for the management of MSW compared to others.

Another positive approach of the plasma arc gasification process is that developments in the design of the reactor/chamber have improved vastly and lessened the need for pretreatment/preprocessing. [**33**]

$$C + O_2 \rightarrow CO_2;\ \text{-393kj/mol (exothermic)} \quad (3.1)$$

$$C + H_2O \leftrightarrow CO + H_2;\ \text{+131kj/mol (endothermic)} \quad (3.2)$$

$$C + 2H_2 \leftrightarrow CH_4;\ \text{+172kj/mol (endothermic)} \quad (3.3)$$

$$C + CO_2 \leftrightarrow 2CO;\ \text{-74kj/mol (exothermic)} \quad (3.4)$$

$$CO + H_2O \leftrightarrow CO_2 + H_2;\ \text{-41kj/mol (exothermic)} \quad (3.5)$$

$$C_nH_m + nH_2O \leftrightarrow nCO + (n + 1/2m)\ H_2;\ \text{-205kj/mol (exothermic)} \quad (3.6)$$

3.5.3 Comparisons among WTE Technologies

This section discusses why plasma gasification technology is viewed more as a preferable method when compared with others in terms of efficiency and economical advantage. Both figure (3.1) and (3.2) gives a clear impression that plasma gasification can generate more energy to grid and collect more earnings respectively every year unlike any other thermal treatment procedures of wastes available.

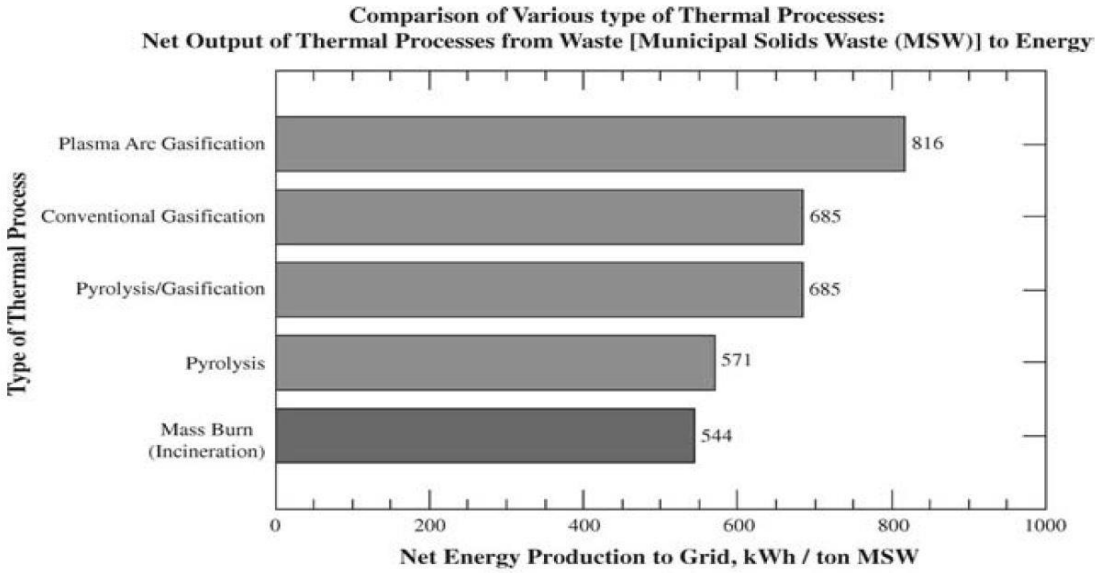

Figure 3.1 Comparisons of various thermal processes with respect to net energy production (Area electrical distribution) to grid [**33**]

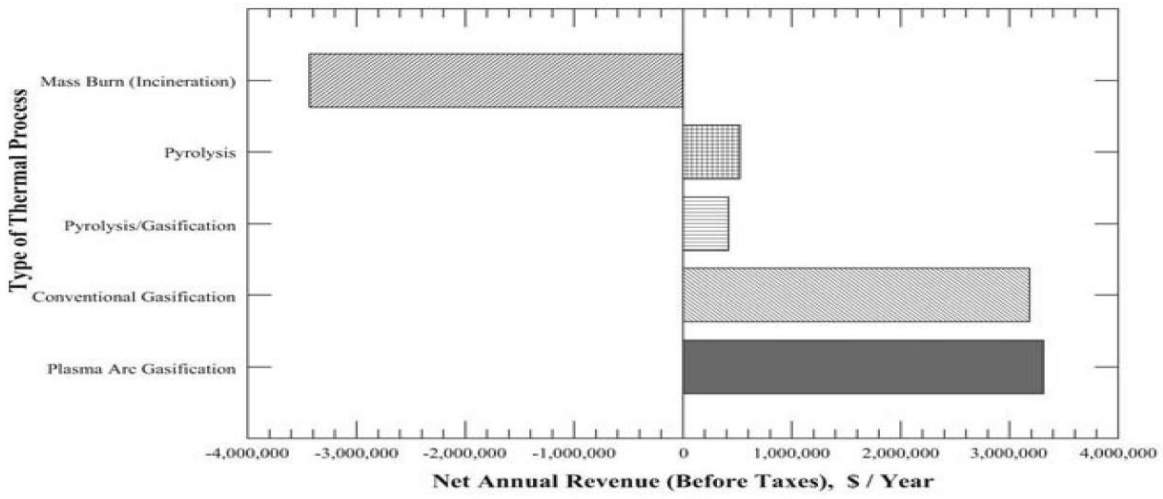

Figure 3.2 Comparison of various types of thermal processes: net annual revenue from waste to energy [**33**]

Although this technology is fairly efficient and economical one primary drawback is the constant supply of high operating temperatures when compared to other thermal procedures as shown in Table 3.2.

Table 3.2 Operating temperatures for various thermal processes [**33**]

Thermal Process Technology	Typical Range of Process Operation
Plasma Arc Gasification	3982-6982 ^{0}C
Conventional Gasification	760-1538 ^{0}C
Pyrolysis Gasification	760-1538 ^{0}C
Pyrolysis	649-1204 ^{0}C
Mass Burn (Incineration)	538-1204 ^{0}C

Since plasma arc gasification is the only process which produces non leaching vitrified slag and is environmentally friendly so Toxicity Leaching Tests were conducted on the slag produced from MSW of the plasma arc gasification reactor to compare with industrial benchmarks. Standard toxicity characteristics leaching procedure (TCLP) tests were conducted on vitrified sample materials from experiments. The results are shown in Table 3.3. [**33**]

Table 3.3 Toxicity leaching test result on vitrified slag [**33**]

Heavy Metal	Permissible Concentration(mg/l)	Measured Concentration(mg/l)
Arsenic	5.0	<0.1
Barium	100.0	0.47
Cadmium	1.0	<0.1
Chromium	5.0	<0.1
Lead	5.0	<0.1
Mercury	0.2	<0.1
Selenium	1.0	<0.1
Silver	5.0	<0.1

In general from the analysis above, it is concluded that plasma arc gasification process is more attractive for solid waste treatment due to the following characteristics:

- Thermal Efficiency
- Process different range and variety of solid wastes

- Minimal pretreatment/presorting of solid wastes
- Production of "Syngas" for conversion into a variety of energy sources such as steam, electricity, and/or liquid fuels.
- Environmentally sound, since the solid by-product, vitrified slag, can be used as a construction material such as in roads and highways.
- Environmentally sound, since the "Syngas" can be used to produce various energy products and any discharged gaseous effluents treated by currently acceptable environmental processes.
- Ability to reduce if not eliminate the need for a landfill
- Can be used to process wastes in an existing landfill and eliminate the old landfill. [**33**]

3.6 Alter NRG/Westinghouse Plasma Corporation

The following section discusses the historical background of Alter NRG/WPC, their different stages of operation of plasma gasification and specification guideline of the reactor, plasma torches.

3.6.1 History

Westinghouse Plasma Corporation's plasma technology was developed over a period greater than 30 years and with over $100 million in Westinghouse R&D funding. The WPC technology was initially developed in collaboration with NASA for use in the Apollo space program to simulate space vehicle re-entry conditions of over 5,500°C.

Between 1983 and 1990, Westinghouse and the Electric Power Research Institute (EPRI) developed a reactor using plasma for reclaiming fragmented scrap metal. Between 1988 and 1990, Westinghouse extended the plasma cupola technology for the treatment of hazardous wastes including contaminated landfill material, PCB-contaminated electrical hardware, transformers and capacitors, and steel industry wastes. In the mid-1990s WPC in cooperation with Hitachi Metals completed an R&D program and pilot testing program to confirm the capability of the plasma cupola to treat municipal solid waste (MSW) and other waste materials to produce a syngas which could be used in a power plant for the production of steam and electricity. A series of tests were completed at the WPC Plasma Center in Madison, Pennsylvania using a variety of feed materials and at varying moisture contents. The success

of these tests provided the technical basis for the design and installation of a pilot scale 24 ton/day MSW gasification plant in Yoshii, Japan.

Hitachi Metals and WPC's combined efforts culminated in the demonstration to the Japanese government that the Yoshii WTE facility was capable of using plasma energy to reliably and economically gasify waste materials for energy production. In September 2000, The Japanese Waste Research Foundation awarded a process certification of the technology and the Westinghouse Plasma Gasifier was born.

Lessons learned at Yoshii were applied to full scale facilities in Mihama-Mikata and Utashinai Japan, which both began commercial operation in 2002 and 2003 and continue operating today. The experience gained at the two Japanese facilities was used to create the next generation gasifier which was commissioned in 2009 by SMSIL in Pune, India. In 2007 Westinghouse Plasma Corporation was acquired by Alter NRG. Various projects were undertaken by the company to deal with waste management which were initially demonstrated, optimized and eventually commercialized in different parts across the world. That facility treats hazardous wastes from over 40 different industries.

More recently, Air Products purchased a plasma gasification reactor from Westinghouse for Air Products' 1000 tons per day plant to be built in Northeast England **[34].** The following figure 3.3 illustrates the commercial history of Westinghouse Plasma Corp Technology.

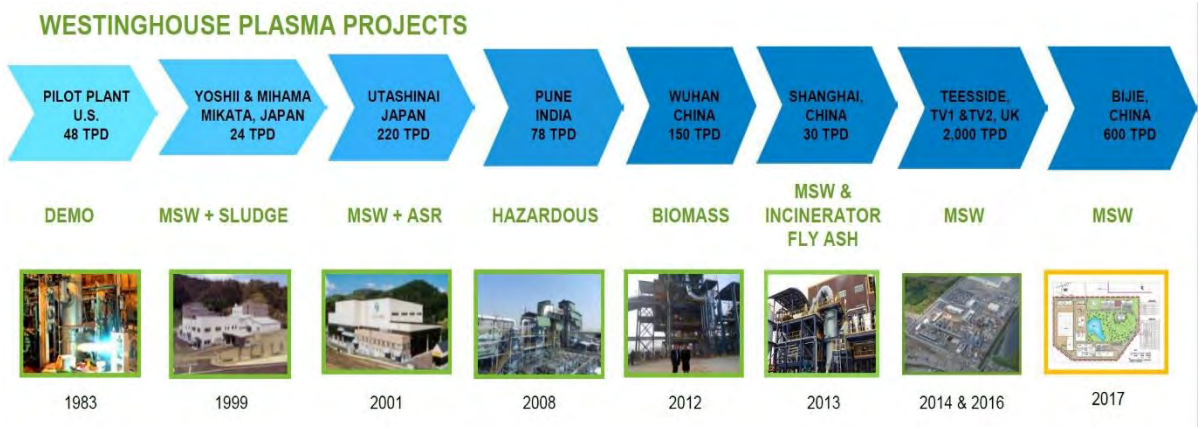

Figure 3.3 Projects operating under Westinghouse Plasma Corporation [**39**]

According to them the plasma gasification process in addition to electricity can also generate ethanol, gasoline, diesel fuel and is the best alternative available to avoid landfilling. They provide significant advantages that come with the use of this technology:

- Fuel Flexibility-uses renewable and recurring resources

- Better environmental impacts-leads to reduction in carbon footprints and overall pollution
- Commercially deployed in facilities for 10 years
- Energy self sufficiency-governments are endorsing plasma solution
- Proprietary IP, technical know-how and active patents worldwide
- Performed over 100 pilot tests on numerous feedstock at their world class plasma centre with an average of 48 tons per capacity
- Vitrified Slag- Inert/Non Leaching and can be used in construction purposes
- Scale-30 to 1000TPD per gasifier [**34**]

They have designed quite a few product line of models depending upon demand and supports distinct market verticals described in the figure 3.4 and a summary of 1000TPD IPGCC plant is shown in figure 3.5 below-

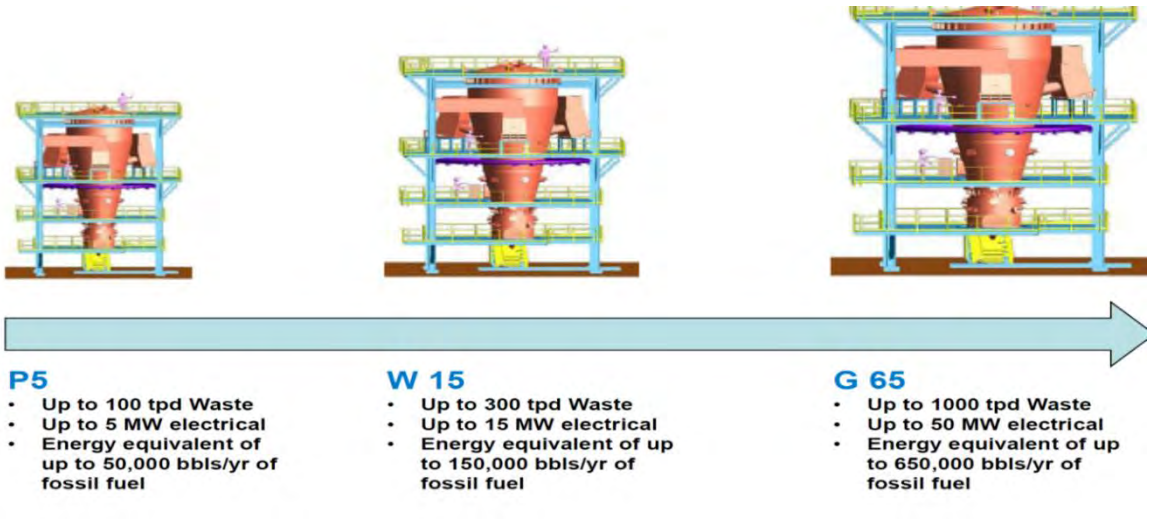

Figure 3.4: Gasifier reactor models [39]

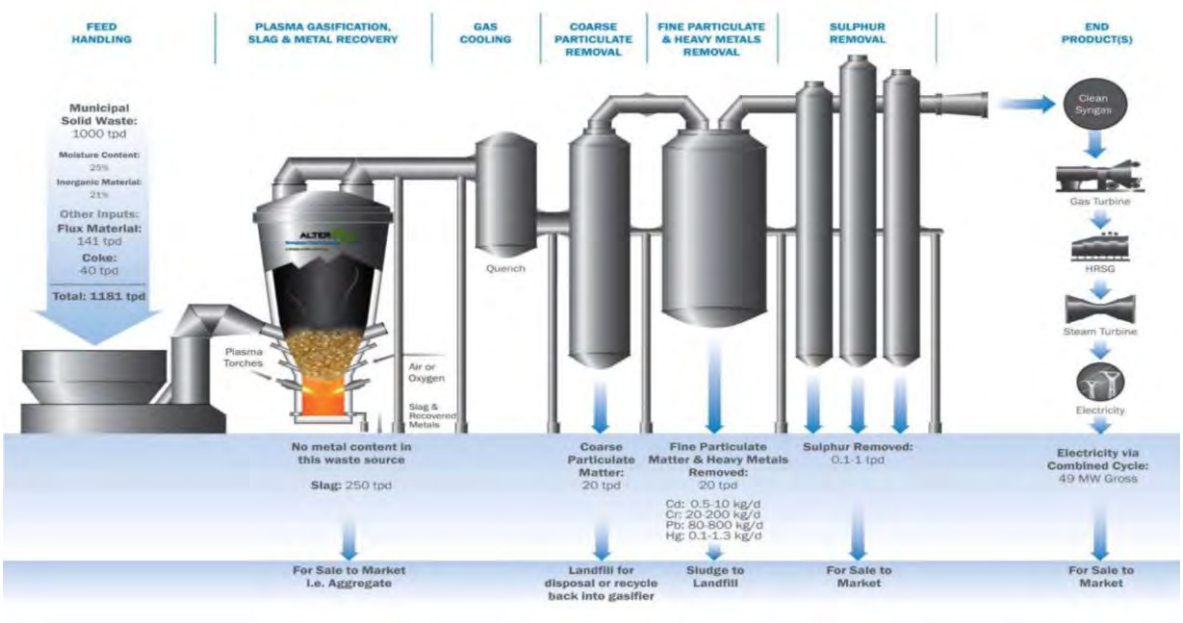

Figure 3.5 Summary of inputs & outputs for 1000TPD IPGCC plant [**34**]

The dimension of the reactor is height of 25m and width of 9m with capacity of 204 tonnes. The Syngas produced will be 3.5 million MM Btu/year. [**34**] A list of gasifier specifications are listed in the Table 3.4 below-

Table 3.4 Gasifier specifications [**39**]

		Capacity (TPD)					Dimensions (meters)			
Gasifier Model	Feedstock	Air Blown		Oxygen Blown		Syngas Produced (Nm^3/hr)	Top Diameter	Bottom Diameter	Vessel Height	Installed Height
		Low	High	Low	High					
G 65	MSW	540	620	1000	1000	65,000	9	4	24	30
	Hazardous Waste	430	720	830	1000					
W 15	MSW	120	140	240	290	15,000	6	2.5	1.5	18
	Hazardous Waste	100	160	190	300					
P 5	MSW	40	50	80	100	5000	4	2	10	13
	Hazardous Waste	30	50	60	100					

Notes

1. MSW calorific value (C.V) range -14 MJ/kg (4000-6000 Btu/lb) HHV basis.
2. Hazardous waste (C.V) range -14.0-23.3 MJ/kg (6000-10,000 Btu/lb) HHV basis.
3. Ground level to syngas exit flange. Ductwork height excluded as it is project specific.

Table 3.5 Typical energy production by gasifier model [**39**]

Gasifier Model	Capacity (TPD of MSW)	Syngas Produced (NM^3/hour)	Syngas Chemical Energy, HHV (GJ/year)	Combined Cycle Power Plant (MW gross and net)	FT Liquids BPD/BPY	Fossil Fuel Replacement (bbls/year)
G 65	1000	65000	4,100,000	58/39	785/287,000	670,000
W 15	290	15000	976,000	14/9	188/68,000	160,000
P 5	100	5000	323,000	4.5/3	62/23,000	50,000

Notes

1. Based on 14MJ/kg (6000 Btu/lb) HHV basis

The actual outputs from a WPC gasification facility will depend on the quantity of specific feedstock being used and the actual configuration of the plant. Gasifiers can be installed in parallel to create a plant with the capacity to suit any needs. The above Table 3.5 lists the quantity of syngas, gross and net power generation from different gasifier models.

The other key features of installation and operation is summarized in the following Table 3.6 [**35**]:

Table 3.6 Lists of raw materials & installation manuals [**35**]

Waste throughput	**385,000 tons/annum**	**40 tons/hour average**
Waste processed	MSW and C&I	
Number of lines	1	
Furnace technology	Plasma torch gasification	
Auxiliary Fuel	Natural Gas (10,700 kg per pre-heat period)	
Acid gas abatement	Wet	Caustic NaOH
NOx abatement	SCR	Ammonia
Reagent consumption		Emergency back-up fuel oil- Diesel 260l/h Ammonia 6650 te/annum Met Coke 12,450 te/annum Lime(flux agent) 33,450 te/annum

		Activated Carbon 15 te/annum Process Water 364,000 te/annum	
Flue gas recirculation		No	
Dioxin abatement		Activated Carbon	
Stack(Gas Turbine)		Height 26.0m	Diameter 2.5m
Flue gas(Gas Turbine)		Flow 74.7Am^3/s@96℃	Velocity 15.2m/s
Stack(Steam Turbine)		Height 26.0m	Diameter 1.5m
Flue gas(Steam Turbine)		Flow 31.9Am^3/s@110℃	Velocity 18.1m/s
Electricity generated	49.8 MWe	414,400 MWh (at 95% availability)	
Waste heat use	The facility is CHP ready-low grade heat will be exported if a user can be found if locality develops		

3.6.2 Methodology

Inside the gasification chamber the non-transferred plasma torch consists of a pair of tubular water cooled copper electrodes. The operating gas is injected through the small slots between the electrodes. Pushing the air through the electric arc will convert the air stream into a plasma plume ("ionized gas") with a temperature in excess of 5500 ℃. These torches are used to create intense heat inside the gasifier. Not only these torches boost temperatures but they provide important functions in destroying hazardous waste and vitrification of WTE ash. The thermal efficiency of WPC torches range from 60-75%. [**6]**

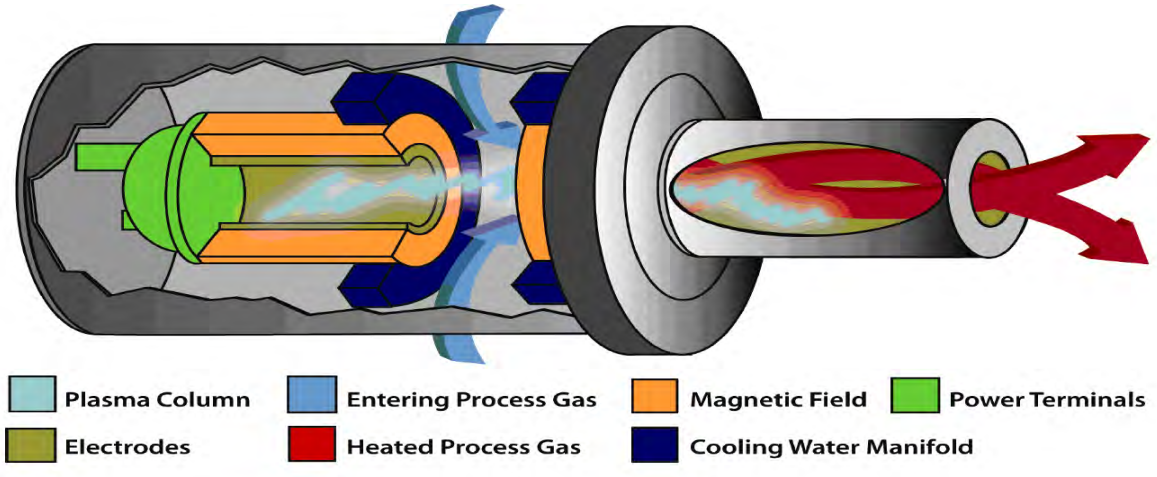

Figure 3.6 WPC plasma torch [**43**]

WPC has developed a plasma gasifier where the plasma jets are located at the bottom of the gasifier. Six plasma torches at maximum are used at the bottom of the gasifier to provide sufficient heat for the gasification to take place. A simplified diagram showing the internals of a plasma torch is being shown in figure 3.6 above. A bed coke is created within the cupola using metallurgical coke (met coke) to absorb and retain the heat energy from the plasma torches and provide a "framework" that supports the MSW feed as it descends through the gasification reactor and is converted to gas and liquid slag, this action is similar to the phenomena occurring in a blast furnace. The met coke is fed simultaneously as the MSW and is paramount for the operation of the gasifier. The actual velocity of the plasma jet coming out of the torches is about Mach2, so we need something to lower the gas velocity and allows distribution of heat evenly. The met coke has a very good structural integrity and is able to support the weight of the waste onto it. This process can handle any moisture content in the MSW since it is vaporized along with the syngas. The waste coming in should be about 10 inches in any size. The preferred design for the feeding of the waste into the gasifier is now from the top. WPC only provides for the gasification island, which includes the gasifier and the plasma torch system and the rest units are available separately.

The process is entirely controlled by the monitoring of the temperature of the output gases. The latter should be between 982º C to 1093º C, in order to prevent the tar formation and that small particles mix into the output gases. Hence, the keys for the process control are the plasma torches. More or less heat will be added through them depending on whether we want to raise or lower the syngas temperature. As the mix of waste and met coke is going down through the gasifier, the waste will start gasifying whereas the met coke will remain solid. The bed coke will slowly gasify but will remain at the bottom. The bed waste will lie on top of it. The only materials that will escape the bed coke are the slag and melted metals. They will be recuperated at the end. Metals are separated from the slag through an ultimate quick process.

Torches are running continuously, and after the process is steady, the energy supply can be modified. Each power torch is alimented separately, thus one torch can be shut down and modified without the need to shut down the whole process. As it is possible to wholly removed one of the plasma torch while the system is running, some valves are specifically designed so that the inside vessel gases do not escape while this process. The gasifier is working at slightly negative pressure to avoid gaseous leaks. The following figure 3.7 provides an illustration of the different stages of operating temperatures inside a gasifier chamber.

The vessel into which the plasma torch is inserted is actually the proprietary design of WPC shown in figure 3.8, and it is the element allowing the good operation of the gasifier. Some air has to go around the plasma torch because it is necessary that the plasma jet does not touch the walls, otherwise they would melt. [**34**]

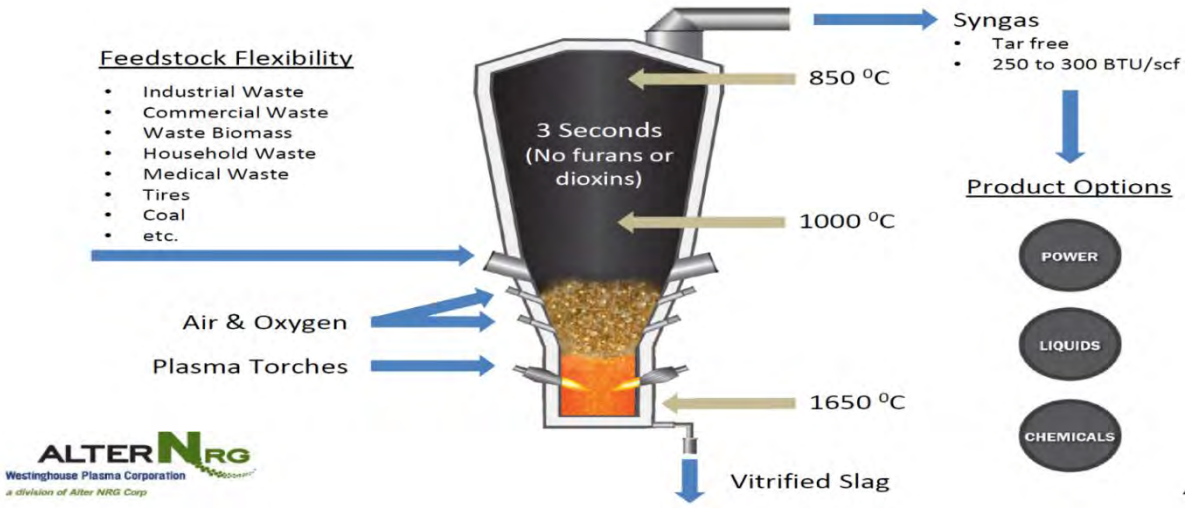

Figure 3.7 Internal structure and operating temperatures inside a gasifier [**43**]

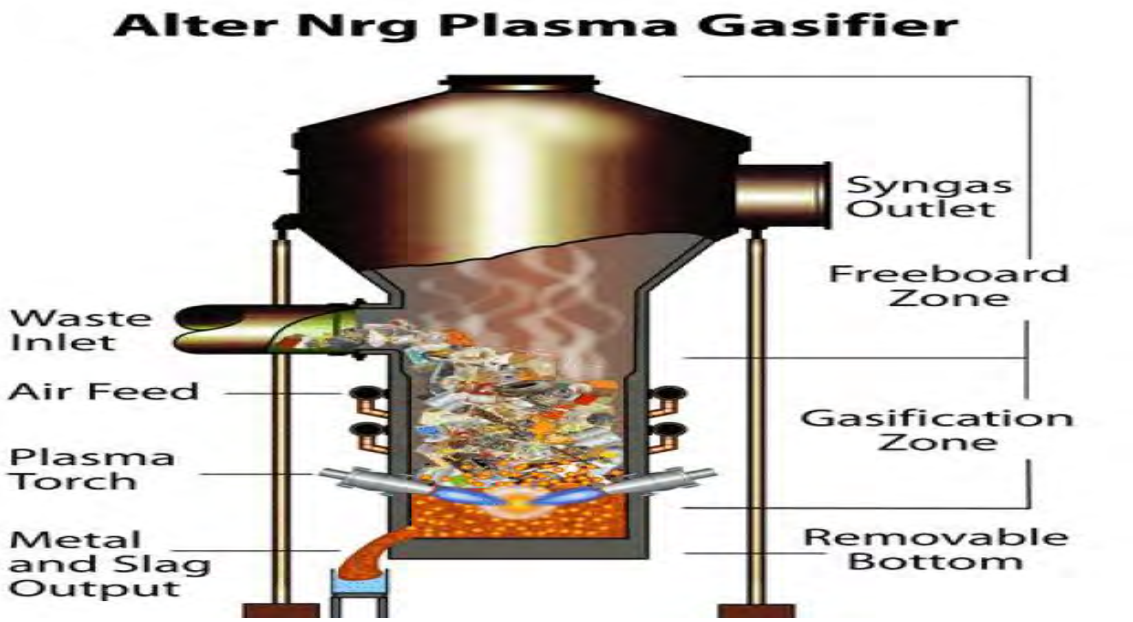

Figure 3.8 Input & output of a typical gasifier [**6**]

The inside of the vessel is walled with refractory (cement type material that provides insulation), especially at the bottom. The width and height are calculated depending on the residency time, the flow rates, adequate temperature, and heat losses.

The syngas will have at best a third of the energy content of natural gas. Hence, the turbine used has to be compatible with a lower energy gas or natural gas has to be added to make it operate properly. WPC currently has a partnership with Solar Turbines to study the use of their turbine that is compatible with the low energy content of the WPC syngas (can work on 100% syngas). The purpose is to sell to clients both the gasifier and the turbine of solar turbine. However, if the client rather chooses to add natural gas, WPC will work with them to choose another system. In this review, we are interested in the Integrated Plasma Gasification Combined Cycle (IPGCC) where MSW is gasified with addition of metallurgical coke (4% by weight) to produce syngas and then electricity via a gas turbine. Met coke is added to the heterogeneous feed in order to raise the calorific value of the feed. This IPGCC design is the ultimate goal of Alter NRG, along with a 100% feed of MSW. The main difference between the classic steam cycle and the combined cycle is the presence of turbines that compress the syngas instead of combusting it all in a steam boiler. In both cases, the waste heat is combusted through a steam boiler to recover more energy. The figure 3.10 reflects the addition of turbines in a typical IGCC block diagram unlike Conventional Steam Cycle in figure 3.9 which does not.

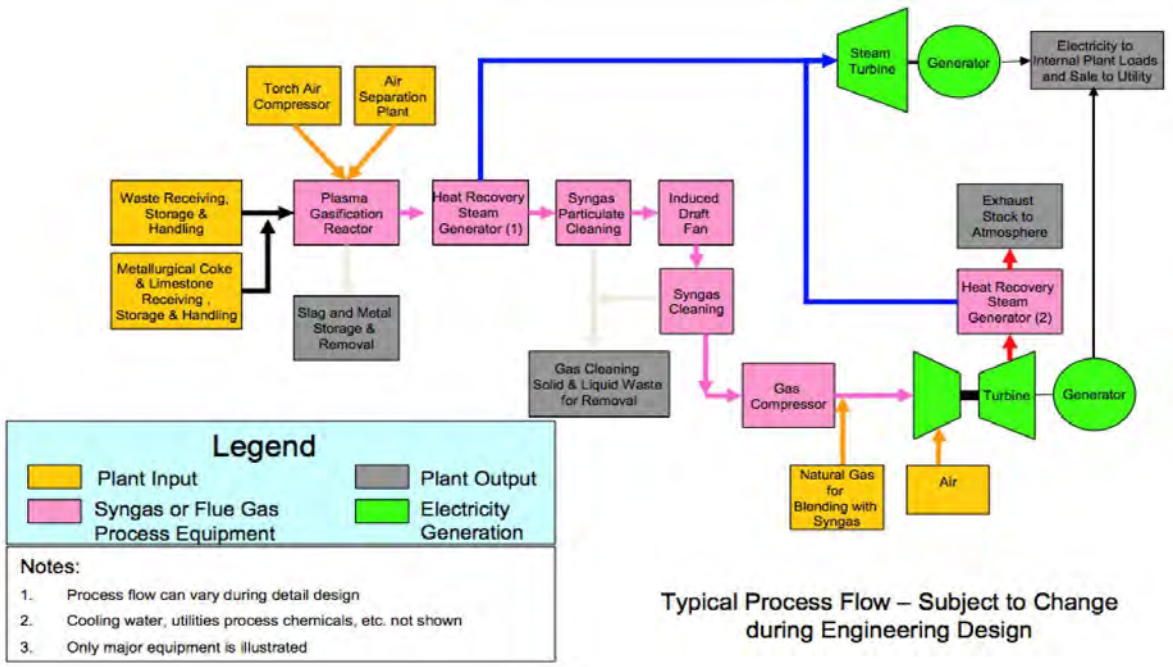

Figure 3.9 Steam cycle (alter NRG) **[6]**

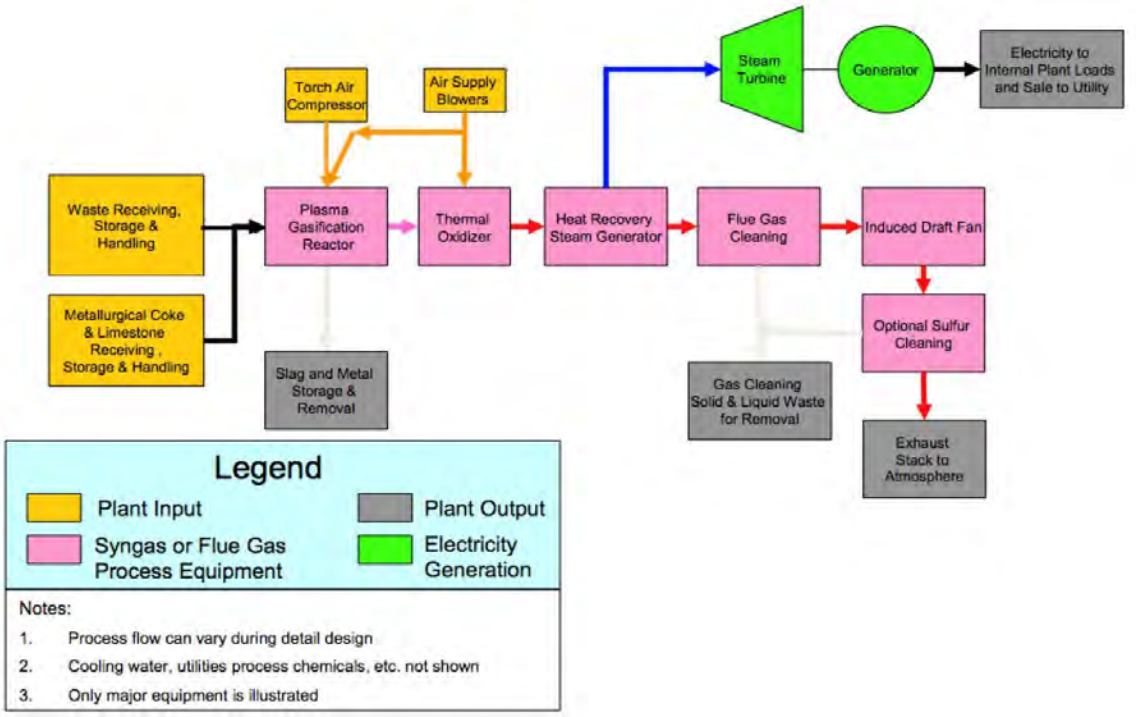

Figure 3.10 Integrated gasification combined cycle (IGCC) [**6**]

The Air Product Tees Valley Renewable Energy Facility located in United Kingdom is a project which is configured as an IPGCC. Plasma gasification can be used to produce syngas which can be conditioned and then converted to liquid fuels or power through technology platforms like fuel cells or reciprocating engines. For all of those applications, the majority of the plant, that portion that is dedicated to processing waste and making clean syngas, will be almost similar. [**34**]

3.6.3 An IGPCC Plant Process Summary

MSW is delivered to the plant receiving facility which will have several days of storage capacity. The other two materials, coke and flux, which are fed into the gasifier concurrently with the MSW are also delivered to the facility. The flux material is typically crushed limestone and its purpose is to promote proper slag flow within the gasifier. The coke forms a bed within the reactor. Coke usage is typically 1:25 on a mass basis versus the MSW. The amount of flux necessary can vary between 0:25 and 2:25 on a mass basis.

The three materials are metered onto a common charge conveyor which transports the feedstock to the gasifier. Depending on the size of the MSW, it may have to be shredded on site to a size less than approximately 15 cm before being put onto the conveyor.

Within the gasifier, the organic portion of the MSW is converted into syngas. The syngas is partially quenched with atomized water at the top of the gasifier prior to exiting the gasifier at a temperature of approximately 850 ℃ through two nozzles. The metallic and ash content of the MSW forms molten slag, which flows through the tap holes at the bottom of the gasifier. The slag is then quenched and granulated upon exiting the gasifier. The resulting vitreous granules are conveyed and loaded onto trucks for export to customers off-site. The gasifier is equipped with Westinghouse plasma torch systems to ensure the internal temperatures in the reactor are sufficient to guarantee complete conversion or inorganic material to syngas and to melt all the inorganic material.

Syngas is cooled through a caustic venturi quench and scrubber system and then proceeds through a wet electrostatic precipitator (WESP). The primary purpose of the venturi quench and WESP is to remove the particulate matter entrained in the syngas.

The cooled and particulate free syngas proceeds through a series of syngas cleaning processes to remove chlorine, sulphur, lead, cadmium, zinc and mercury. Intermediate compression and cooling steps remove moisture from the gas.

The clean syngas is then compressed in a multi-stage compressor and fed into a gas turbine to produce electrical power. The turbine flue gas heat is recovered by a heat recovery steam generator ("HRSG"). The steam from the HRSG is combined and fed to a multi-stage steam turbine to generate power.

Alternately, the cleaned syngas can be used in reciprocating engines to make power or it can be converted to liquid fuels using a number of available conversion technologies. [**34**] Figure 3.11 provides a detailed step by step procedure for an IPGCC plant.

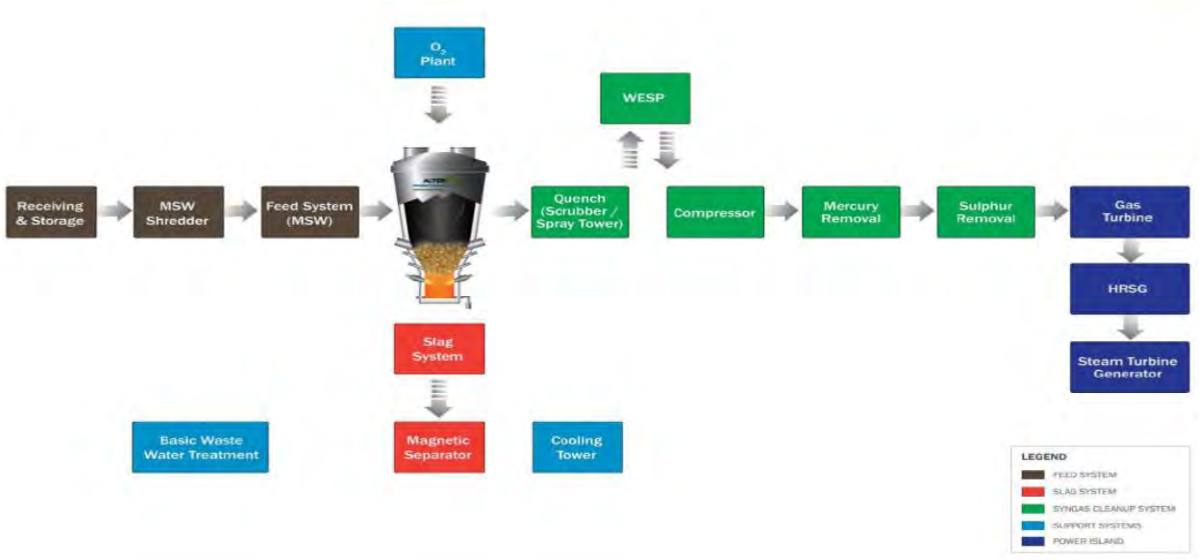

Figure 3.11 Process block flow diagrams for IPGCC plant [**39**]

3.7 Calculation

The following section calculates power that can be generated considering percentage components of different elements in solid wastes found in Dhaka City.

3.7.1 Potential and Net Electric Power Generation Calculation from MSW in DCC

Average tons of waste generated in Dhaka City (based on 2015) = 5500 TPD

= 200,750 Tons per year

Calorific Value of MSW in DCC = 8 MJ/kg

= 8000 MJ/ton

= 2222.22 KWh/ton

Specific Power Output per Ton of Waste at Thermal Efficiency[1] of 20%

= 20% Efficiency × Calorific Value of MSW

= 0.20 × 2222.22

= 445 KWh/ton

Potential of Electric Power Plant Capacity from MSW in DCC

$$= \frac{Total\ Waste\ Generated\ Annually \times Specific\ Power\ Output\ from\ Waste\ per\ Ton}{Calorific\ Value\ of\ Solid\ Fuel}$$

$$= \frac{2007500 \times 445}{8000 \times 1000}$$

$$= 112\ MW$$

Measurement of Calorific Value[2] (using Modified Dulong's Equation):

$$\text{Gross Calorific Value} = (337 \times C) + \{1428 \times (H - O/8)\} + (9 \times S) \qquad (3.7)$$

[**36], [42**] [**Note:** Since we have a large quantity of moisture component in our solid waste so far the energy context of the waste in Dhaka City the chemical component can be estimated using the above equation.]

Percentage Composition Calorific Value of Component

- Carbon 81.592 %
- Hydrogen 10.729 %
- Oxygen 5.0049 %
- Sulphur 0.241 %

Heat (KJ/kg) = (337×0.81592) + {1428 × (0.10729-0.50049/8)} + (9×0.00241)

= 338.859 KJ/kg

Steam Energy Available = 70% of GCV

= 0.70 × 338.859

= 237.201 KJ/kg

The steam energy is used to run the turbines which are coupled with generators to produce electricity

1KW = 36000 KJ/h (3.8)

From the above equation it is interpreted that if the energy conversion is 100 % efficient then to produce one unit of electricity 3600 KJ energy is required. But practically it is not possible considering the conversion efficiency of 31.6% in a power plant heat input of 3600/31.6% = 11,395 KJ/KWh is required. So to produce 1KWh electrical energy 11,395 KJ/KWh of steam energy is required.

Electric Power Generation = Steam Energy (KJ/kg)/11,395(KJ/KWh)

= 237.201/11,395

= 0.02081625 KWh/kg

In 2015 the MSW generation of DCC = 5500 x 10^3 kg/day

Total Power Generation = 0.02081625 × 5500 × 10^3

= 114.489 MWh /day

Station Service Allowance = 6% of Electric Power Generation

= 0.06 × 114.489

= 6.86934 MWh /day

Unaccounted Heat Loss = 5% of Electric Power Generation

= 0.05 × 114.489

= 5.72445 MWh /day

Net Electric Power Generation = 114.489 – (6.86934 + 5.72445)

= 101.89521 MWh/ day

≈ 102 MWh /day **[36]**

1) **Thermal Efficiency**

   In thermodynamics it is a dimensionless performance measure of a device that uses thermal energy. It indicates the extent to which energy is added by heat is then converted to network output.

2) **Calorific Value**

   The amount of heat released by unit weight or unit volume of a substance upon complete combustion.

3.8 Costs and Economic Evaluation

This section will include detailed explanations about the installation and operating costs along with revenue collection for a specified plant capacity. It will also give an estimation of land and time required to set up a standard thermal plasma power plant.

Table 3.7 Economic of scale in integrated combined cycle plasma gasification [**37**]

Plant Capacity MT/day	Heat Input MWh/ton	Gross MW	Net MW	Plant Load	MWh/MT MSW	Overall Efficiency %
500	83.3	33.7	26.7	6.93	1.28	32.1
2500	416.4	186.9	152.1	34.76	1.46	36.5
5000	832.7	393.42	323.8	69.52	1.55	38.9

The economics of a new technology are important to its development, especially in the case of the utilization of plasma as it uses electricity, the most expensive source of energy. Table 3.7 provides a list of power input, output and efficiencies for various plant capacities. The capital costs are likely to be high as the technology is not mature enough to lower the prices. The capital costs will be broken between the gasifier unit and the classic air pollution control to clean the syngas along with the power production unit. The slag will not need any more treatment and could be directly sold after vitrification. The fuel is indeed free, except for the case of Alter NRG that uses met coke. This extra cost will have to be taken into account and for the gate fees paid by the neighboring communities, the average cost was assumed for every ton of garbage processed by the plant, $65 is paid to the plant. Overall, the incomes of this plant would be the gate fees, the electricity generated by the syngas combustion, and possibly the slag that can be reused if it passes the leachability tests and also the recovered metals that are present in the MSW can also be sold separately.

3.8.1 Alter NRG/Westinghouse Plasma Corporation Cost Calculation

Economic costs of Westinghouse Plasma Corporation were given in a public presentation for a traditional and average 750 TPD plant with the two different configurations-the steam cycle that is currently applied in all the commercial plants and the IGCC one that is the goal for the upcoming plants.

So we consider a plant of capacity 750 TPD of feedstock, operating on air, in a combined cycle power. Alter NRG gave the capital costs. According to Alter NRG, labor skills needed for the

plasma-assisted WTE plant are not much different than the ones needed for classic grate combustion. The operating costs should be investigated especially since they will be using met coke in bulk quantities, which is very expensive.

Capital costs for a 750 TPD plant are $200.99 million (price communicated by Alter NRG). This price includes the ASU (Air Separation Unit) and all the units needed to achieve the air pollution standards. The shutdown times are on average 4 weeks a year, up to 35 days a year. The start-up year may include more down times than this average, but for the simplicity of this analysis, it was not taken into consideration. Taking into 10% of capital paid each year, the capital costs represent $81/ton. In comparison, to the steam cycle the capital cost is $156 million for a 750 TPD plant. Table 3.9 shows a brief comparison of the costs summary between a steam cycle and an IGCC 750TPD capacity power-plant. If we do calculations of both per annual ton, we have the following:

- Capital costs of $63/annual ton of MSW for the steam cycle
- Capital costs of $110/annual ton of MSW for the IGCC

It can be concluded that the steam cycle is as costly as the classic grate combustion plant.

- The operating costs includes maintenance, electrode replacements, metallurgical coke
- Maintenance Cost is assumed to be $43/ton MSW
- The classic maintenance of the plant is 6 million USD
- The electrode maintenance can be estimated at a cost of $120,000/year.

The met coke is added 4% by weight of the MSW feedstock, so for a 750 TPD plant annually there is 9,900 tons of coke processed.

- Labor Costs is approximately $10/ton MSW
- The price for met coke is about $180/ton, so a total cost of $1.80 million per year.
- The total operating costs are $7.92 million per year. Hence, the operating costs represent $32/ton. [**6**] Table 3.8 gives an idea about per ton of operating costs when being operated in different gasifier models.

Table 3.8 Operating cost (net of tipping fees) [**39]**

Scale	$60/t	$80/t	$100/t
1000 TPD G-65	$0	$2.40	$4.75
200 TPD W-15	$3.60	$1.10	$1.40

Table 3.9 Cost data summery for a 750TPD WTE project [**6**]

	WTE IGCC	**WTE Steam Cycle**
Total Capital Cost ($M) [1]	276	156
Net Production Capacity (MW)	52	25
Gross Annual ($M)	38	25
Cash Flow/MWh	84	112
Capital Cost/MWh	21	43
Pre Tax ROE (%) [2]	18	13

Notes:

1. 20% Tax Contingency
2. After Tax

The revenues based on the material balance are the following-

The Gross Energy Production for the 750 TPD plant is 929 kWh/ton of MSW processed. However, the net output is decreased by the internal energy of the plant and eventually, the net energy produced by the plant is 617 kWh/ton, based on MSW feedstock of LHV of 10.6 MJ/kg. The sale of this electricity brings $61.7/ton of MSW. Electricity sales revenue is taken from the residential tariff rate ($0.13/KWh) of Dhaka Power Distribution Company Limited (DPDC), because the generated electricity is assumed to consume at the residential sector. [**38**] The slag is non leachable and can be sold as an aggregate for road construction, at a price of $1/ton. A 750 TPD plant produces a stream of metals and slag of 8,212 kg/hr. Annually it creates 65,039 tons of slag and metals. Assuming the metals recuperation was the same as that for a WTE plant then 11,137 tons of metals ($50/short ton) recovered and thus 53,900 tons of slag produced. The sale of both will be then $610,800 per year, or $2.47/ton.

- The gate fees are $65/ton.
- A renewable credit of $1 per MWh was assumed. Hence $0.55/ton MSW is obtained. [**6**]
- Table 3.10 gives an overview of the comparison between expenses and revenue summarized by Alter NRG.
- Figure 3.12 shows a graphical representation of the construction costs against plant capacity in different countries.

Table 3.10 Comparison of expenses and revenue collection per ton of MSW

Alter NRG Expenses $/ton		Alter NRG Revenues $/ton	
Personnel	10	**Gate Fee**	65
Other Operating Costs	32	**Electricity To Grid**	61.7
Total Operating Costs	42	**Metal Recovery**	2.47
Capital Charges	81	**Renewable Credit**	0.55
Total Costs	123	**Total Revenues At Start Up**	129.72

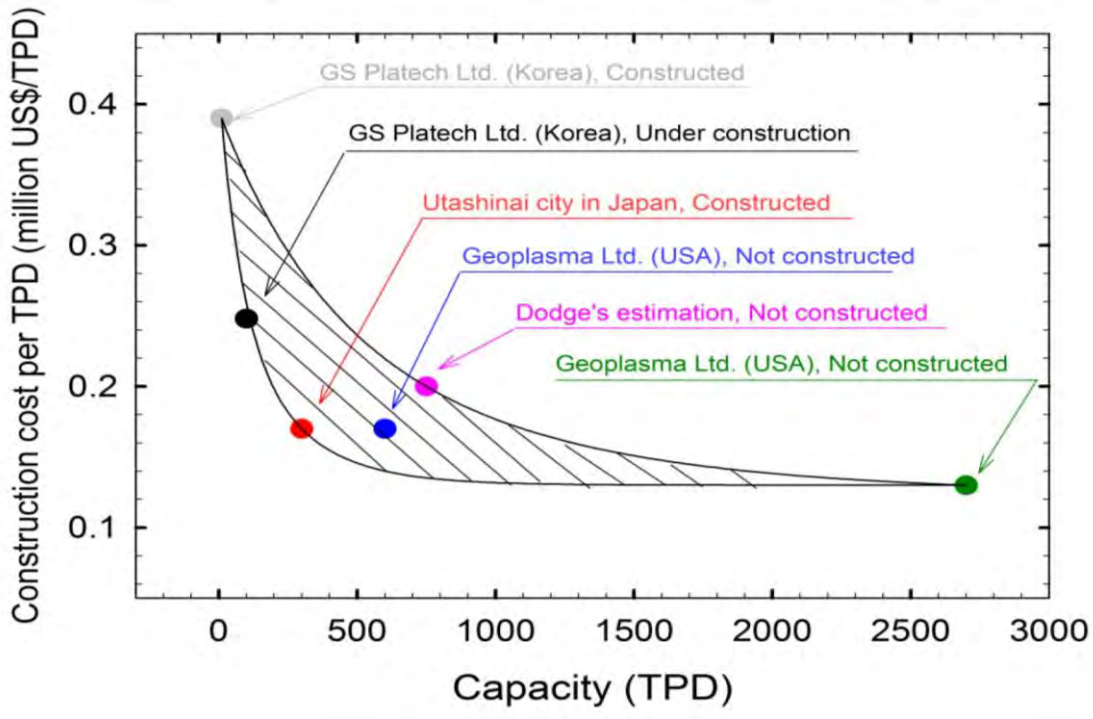

Figure 3.12 Construction cost (million US$) of thermal plasma treatment plants according to treatment capacity (TPD) [**40**]

3.8.2 Land Requirement

As per the provisions of Municipal Solid Waste (Management and Handling) Rules, 2000, the landfill site shall be large enough to last for 20-25 years. In general the land requirement for development of the MSW landfill site is around 0.2 ha/MT of MSW generation per day with minimum requirement of 2.0 ha land area. The projected minimum land requirement for Plasma Gasification Process (PGP) is dependent on the processing capacity of the plant and ancillary processes that maybe included in the overall plant design. However, a standard IGCC configured plant having a capacity of 1000 M.T per day would require about 2.02 Hectares

(5Acres) of land. Increasing the capacity of the plant to 3000 M.T. per day would increase land requirement to about 4.04 Hectares (10 Acres). **[37]**

In Dhaka City the North Zone comprises of 36 wards while the South Zone comprises of 55 wards. Wastes from 55 wards in Dhaka City are dumped in Matuail and 36 wards wastes are dumped in Amin Bazar the only two sanitary landfills in the city. Amin Bazar covers 50 acres of land while Matuail landfill covers about 52 acres of low lying agricultural land acquired by DCC in 1986. Out of this 13 acres have been developed for parking/platforms and the rest 39 acres used for landfilling. Land requirement was calculated as follows:

$$Volume\ Disposed\ at\ landfill = \frac{[Projected\ Waste\ Generation \times Collection\ Efficiency]}{Compacted\ Waste\ Density} \quad (3.9)$$

$$Landfilling\ Area\ required = \frac{Volume\ Disposed\ at\ Landfill}{Dumping\ Height} \quad (3.10)$$

Assumptions

Dumping Height = 6m

Compacted Waste Density 1.1 ton/m^3

Collection Efficiency of 50% to 75%

Thus solid waste will demand an area of 206.31 acre for disposal on the year 2020 if 50% collection efficiency is assumed. If 75% collection efficiency is assumed, the area requirement will reach 309.46 acre. This is likely to create a serious crisis in the years to come and since plasma arc gasification technology covers less area it is more of a suitable approach to avoid conventional landfilling. [**41**]

3.8.3 Power plant Design Timeline

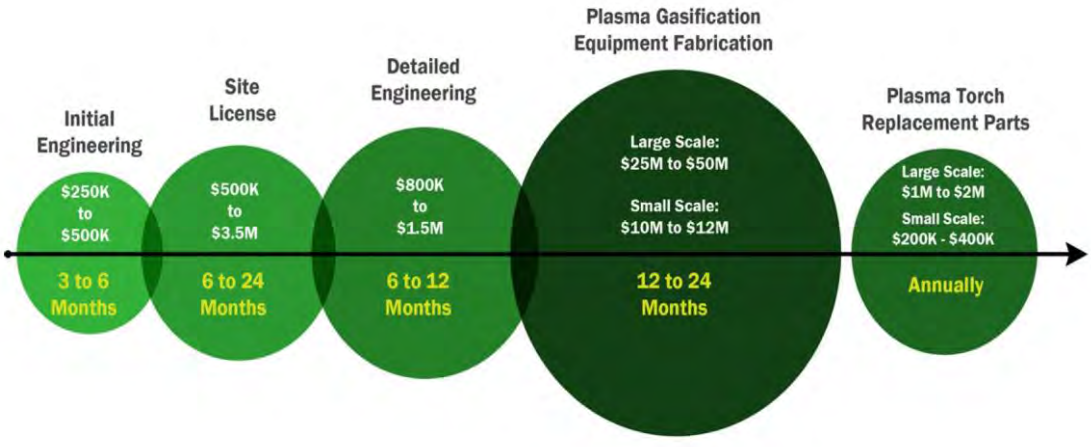

Figure 3.13 Representation of duration for fabrication of Plasma power plant [**39**]

Figure 3.13 gives an estimation of the overall installation charges, licensing fees and annual maintenance costs along with time taken to build a fully functioning plasma gasification power plant.

3.9 Environmental Impacts

The first noticeable difference of Plasma Arc Gasification process from classic WTE plant is that the syngas is cleaned before combustion, which is potentially more efficient than a post-combustion cleaning and should have a lower cost than post-combustion cleaning of WTE flue gas. Thus, the final emissions of the process will depend on the level of cleaning of the syngas, with the exception of NOX that will not be formed during the gasification process. However, NOx will be formed during combustion in the power generation equipment. Dioxins and furans can be avoided due to high heat of the plasma treatment, but they can reappear during cooling of the syngas. Quenching, i.e. rapid cooling of the syngas, avoids formation of dioxins and furans, but simultaneously result in the loss of the wasted heat. Therefore, the emissions will be characteristics of the post-cleaning combustion, and selective catalytic reduction (SCR) can be applied to the engine/turbine exhaust. Emissions to water will come from the syngas clean-up processes, and will lead to the presence of chlorine into the water. They will require treatment to give a solid residue or disposal to sewer. The vitrified ash will have to pass leachability tests in order to be recycled and reused for road construction purposes. **[6]**

3.9.1 Key Pollutants to Be Controlled

Dioxins: Dioxin is a chemical compound present in all molecules of the Polychlorinated dibenzodioxins family (PCDDs). They have been found to accumulate into humans and wildlife and are known teratogens (i.e. provoking abnormalities of physiological development), mutagens and suspected human carcinogens. Dioxins bio-accumulate in living organisms, meaning that they build up primarily in fatty tissues over time, having for direct consequence that even a small exposure can be harmful. There are some polemics about the limiting dose of dioxins one can be exposed to. They appear during the combustion of substances containing chlorine, just like PVC.

TCDD: It is a polychlorinated dibenzodioxin; a molecule of the previous family. It is the most potent compound of the series. It will cause indirect damage to DNA through induction or activation of other DNA damaging compounds in the body.

PCBs: Polychlorinated Biphenyls are odorless, tasteless, viscous liquids and likely to be carcinogens. They are very tough to remove and very stable compounds. Their destruction is difficult and, with partial oxidation, they are likely to produce highly toxic dibenzodioxins and dibenzofurans. The best treatment to degrade them is very high heat or catalysis.

Hydrochloric Acid: It is highly corrosive, strong mineral acid.

Particulate Matter: Small particles that can fly with the off-gases. According to the size of the particulate matter, several techniques are employed and the main goal is to make them agglomerate to remove them more easily.

CO: It is a well-known hazard for the health, when exposed to big amounts of it. It will replace the oxygen in the blood, causing the brain to not be able to function normally, slowing provoking death.

CO_2 in an obvious manner, CO_2 emissions must be regulated and within the legal range. [**6**]

3.10 Future Works

This section covers various power plant projects that are being planned and proposed across the globe of different capacities using different types of wastes and yielding output products in the form of power, diesel, jet fuel and syngas.

Table 3.11 Lists of other projects under development

Location	Company	Capacity (TPD)	Feedstock	Output
Australia	Conf.	800	Industrial Waste	Power
China	Dongjian	30-50	Hazardous Waste	Power
China	Borun	30-50	Hazardous Waste	Power
China	Everbright	250	MSW	Power
China (5 projects)	Kaidi	1000-2000	Biomass	Diesel & Jet Fuel
China (8 projects)	GES	600-1000	MSW	Power, Steam
Eastern EU	Conf.	500	Hazardous Waste	Power
Scandinavia	Conf.	1000	Industrial Waste	Syngas
SE Asia	Conf.	1000	RDF	Power
SE Asia	Conf.	2000	RDF	Diesel & Jet Fuel

South America	Conf.	800	Industrial Waste	Power
South EU	Conf.	1000	RDF	Power
UK	W2T	300	RDF	Power
UK	Conf.	1000	RDF	Power

In addition to Table 3.11 there has been another program in which a company, Cahill Energy signed an agreement with the Barbados government to build and operate a leading edge clean energy plant on the Caribbean island. The plant will provide waste management and energy security, and utilize Westinghouse Plasma Gasification. The plant will transform up to 1000 tons of solid waste and biomass per day into clean, renewable energy. The plant is expected to provide up to 25% of Barbados's total energy needs and reduce the cost of energy substantially. **[43**]

3.11 Conclusion

Plasma Assisted Gasification is increasingly viewed as a very potential treatment and opportunity in the waste-to-energy domain even though there are public opinions which seem to be as adverse as it was for classic grate combustion. Thermal Plasma technology is a reliable and proven method for generating high temperatures at atmospheric pressure, which is not achievable by burning fuels. Firstly, it is a convenient way to provide thermal energy in a gasification process. Using a reduced atmosphere and producing a relatively smaller amount of processed gas facilitates the gas cleaning system. Secondly, controlling the amount of heat input to the process by means of the plasma arc torches allows controlling the composition of the syngas, the hydrogen to carbon monoxide ratio to be modified easily, according to the needs of the user**. [6]**Although the technical feasibility of thermal plasma gasification of MSW has been well demonstrated, it is still not clear that the process is economically viable on the global market currently because of regional variation of the costs of MSW treatment. However, it is clear that the reuse of vitrified slag and energy production from syngas will improve the commercial viability of this process, and there have been continued advances towards further development of it. [**40**]The next decade should see how Plasma Assisted Gasification of MSW evolves. The plants in construction should be in operation in a few years and hopefully the operating issues should be resolved to make this technology more reliable as ever.

.

Chapter 4

Dish-Stirling System

4.1 Introduction

In recent days, demand of power generation using solar system is increasing day by day. Dish-stirling technology is one of the solar power generation system that is targeted for application in today's power generation race.

Dish-Stirling systems use a parabolic dish solar concentrator, tracking the sun and focusing solar energy into a receiver where it is absorbed and transferred to the Stirling engine or generator. In other words it can be said that, it is one kind of solar thermal power system which is also sometimes referred to as concentrating solar power (CSP) system. This system has a concentrator, a thermal receiver and a heat engine/generator located at the focus of the dish.

Like other countries, demand for power generation in Bangladesh is increasing rapidly. At present 78% people have access to electricity in Bangladesh **[44].** To increase this percentage solar power generation system can be very useful because of the geographic location of Bangladesh. In Dhaka the average solar insolation is 4.73 kwh/m^2 and daily average sunshine hour is 7.55 hours **[45].** To use this solar energy properly Dish-Stirling system can be a good choice because of its high efficiencies, for long term and low maintenance operations. Similarly, Dish-Stirling systems are modular, so they can be assembled into plants ranging in size from few kilowatts to megawatts. So, in this chapter we are going to describe some of the background of Dish-Stirling systems and propose a design which can be useful for power generation in Bangladesh.

4.2 Background of Dish-Stirling System

Many companies in USA, Germany, Japan and Russia has built different types of Dish-Stirling System over the last 35 years which differs in size (5 KW- 50 KW). This part concentrates on the foundation of different sorts of Dish-Stirling systems.

First one is 25KW Vanguard System (see figure 4.1) which was built by ADVANCO in Southern California (1982-1985). It was one of the most efficient system in converting solar to electricity, 29.4% which was reported as world record [**46**]. This system used glass faceted

dish of 10.5m in diameter. That system had a direct insolation receiver (DIR) and a United Stirling 4-95 Mark 2 kinematic Stirling engine.

Figure 4.1: The Vanguard system. [**49**]

In 1984 Schlaich-Bergermann und Partner (SBP) built two 50 KW system (see figure 4.2) in Riyadh, Saudi Arab [**47**]. It was also operated in the same location. The system was in 17 in diameter. DIRs were the receiver for SBP dishes and United Stirling 4-275 kinematic Stirling engines were used.

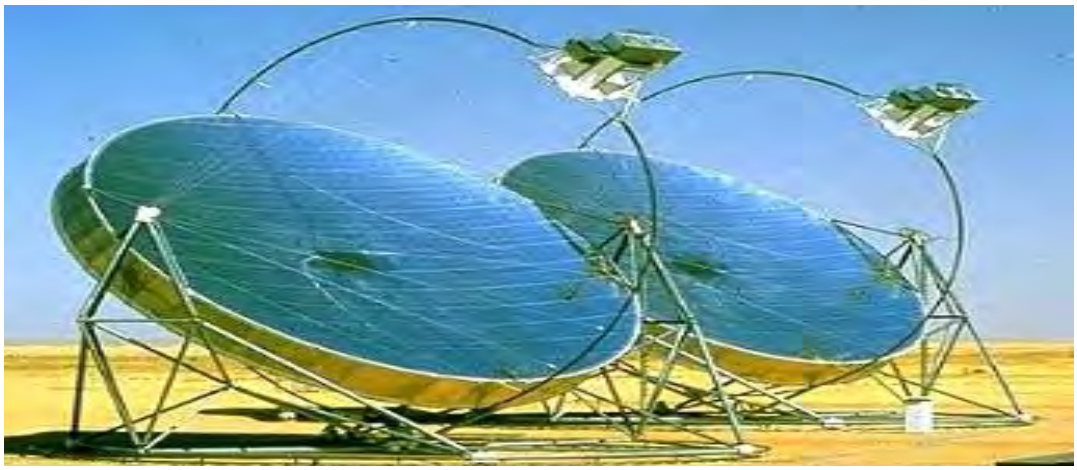

Figure 4.2: SBP 50 kW system. [**49**]

In mid- 1980's McDonnell Douglas Aerospace Corporation (MDAC) built the third system (see figure 4.3) which was acquired later by Southern California Edison (SCE) Company [**48**]. It was the first system that was designed for commercial purpose. The design of this project was same as the Vanguard Dish-Stirling system. Stirling Energy Systems of Phoenix, Arizona, procured the innovation rights and framework equipment in 1996 and had proceeded with improvement of the framework.

Figure 4.3: The MDA/SES Dish-Stirling System. [**49**]

In 1989, the Schlaich Bergermann und Partner constructed their first 7.5-m extended layer concentrator outfitted with a SOLO V160 Stirling motor [**7**]. In the first place, in polar tracking configuration and later in an azimuth/elevation tracking configuration. The frameworks worked for more than 30,000 hours on sun.

During the period from 1991-1996, Cummins Power Generation (CPG) was developing two dish-stirling projects with the U.S. Department of Energy and Sandia National Laboratories. They were developing a 7 KW system (see figure 4.4) for remote applications and a 25 KW system for grid connected power generation [**49**]. Cummins was creative in its dish-stirling frameworks, consolidating propelled advances into the plans, for example, a sun based concentrator with a polar-axis drive and polymer, extended layer features, warm pipe beneficiaries, and free-piston stirling engines.

Figure 4.4: The CGP 7 KW dish-stirling system. [**49**]

In early 2001, Schlaich Bergemann und Partner (SBP) developed two prototype of dish-stirling system systems. Each of them were capable of producing 10 KW of electricity [**50**]. This project was known as Euro-Dish project (see figure 4.5). It was located at the Plataforma Solar de Almeria (PSA), Spain. The engine used in the Euro-Dish project is SOLO Kleinmotoren 161. This system was the most tested and nearest to commercialization at that time.

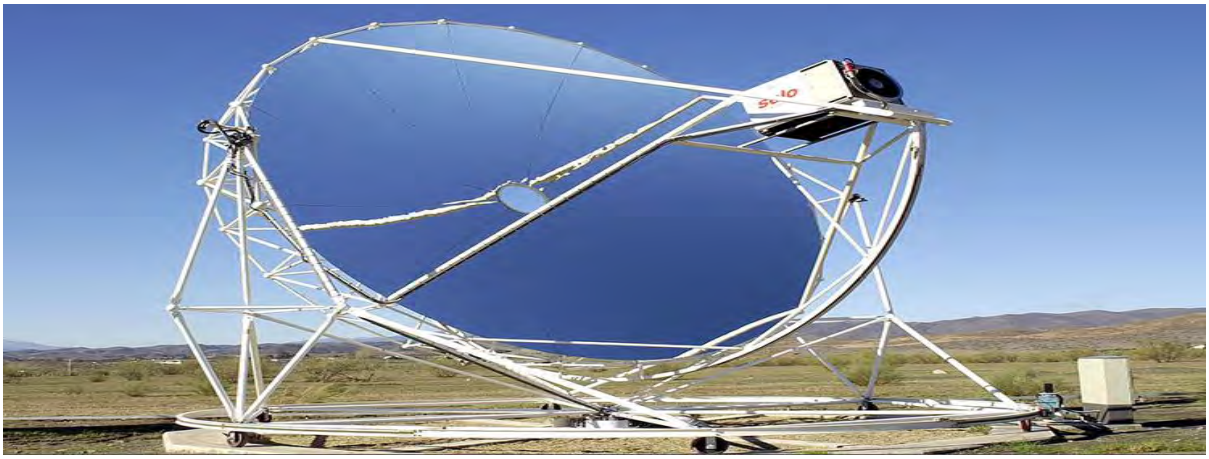

Figure 4.5: The Euro-dish project. **[7]**

The first commercial scale Dish-Stirling plant was built by Tessera Solar and Stirling Energy System (SES) in 2010. It was located in Arizona. That plant was capable of producing 1.5 MW. There were 60 dish and each could produce 25 KW [**7**]. This was also known as SunCatcher system (Figure 4.6).

Figure 4.6: The SunCatcher system. [**7**]

Dish-stirling frameworks have exhibited that they are skilled of delivering power for the framework and for remote power applications. Current endeavours are centred on setting up reliability, through break-and-repair approaches, identifying the segments that require change,

overhaul and substitution. Characteristics of different Dish-Stirling system is discussed in table 4.1.

Table 4.1: Characteristics of dish-stirling systems [**49**]

Company	Dish Area (m^2)	Engine Company	Rated System Output (kW)
Advanco Vanguard System	86.7	United Stirling	25
Schlairch Bergermann und Partner	227	United Stirling	50
McDonnell-Douglas SES System	91	United Stirling	25
Schlaich Bergermann und Partner	44	SOLO Kleinmotoren	10
Cummins Power Generation	44	Clever Fellows	7
Cummins Power Generation	145	Aisen Seiki	25
Schlaich Bergermann und Partner	56.7	SOLO Kleinmotoren	10

4.3 Literature Review

4.3.1 Stirling Engine

Stirling engine is a closed cycle regenerative heat engine operating on cyclic compression and expansion of permanently gaseous working fluid at different temperature levels. This engine basically converts thermal energy to mechanical energy through stirling cycle. Robert Stirling and his brother James invented and patented this engine in 1816. **[51]** The stirling cycle system has hot space, heater, regenerator, cold space and the cooler.

4.3.2 Why Stirling Engine?

Stirling engines are like no other energy converter, as they are capable of converting heat energy into mechanical energy in a clean climate friendly manner. Stirling engines should be used for the reasons below.

- For any available heat source stirling engine can run directly. For example: solar, biological, geothermal, nuclear source or industrial waste heat.
- Stirling engine is preferable for its high efficiency compared to steam engines.
- Stirling engine can run silently and without an air supply, for this reason it is used in the submarines.
- Stirling engine mechanisms are simpler than other engines. Stirling engines can be made by using household materials.
- If the operating pressure of the working gas is low than lightweight cylinders can be used.
- They are flexible, so that they can be used as CHP (Combined Heat and Power) in the winter and as coolers in summer.
- Stirling engines are eco-friendly and reliable.

4.3.3 Configurations

There are three major types of stirling engines which are specified by the way of movement of the air between the hot and cold areas. The diagram of those 3 types of engines are shown in figure (4.7-4.9) respectively.

1. Alpha Stirling Engine

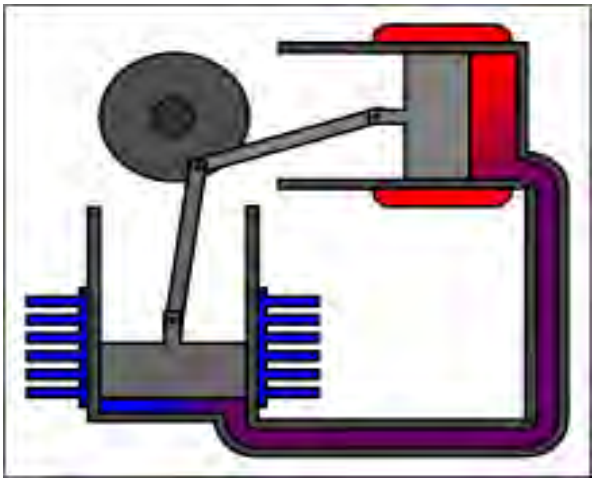

Figure 4.7: Alpha stirling engine. [52]

In the alpha configuration there is no displacer. It has two power pistons, one in a hot cylinder and one in the cold cylinder. The working gas is driven by the pistons between the two cylinders. It is typically in a V-formation [**52**].

2. Beta Stirling Engine

The beta stirling engine has a power piston and a displacer in a single cylinder with a hot end and a cold end. It is basically used with a rhombic drive to achieve the phase difference between the displacer and power pistons, but they can be joined 90 degrees out of phase on a crankshaft **[52]**.

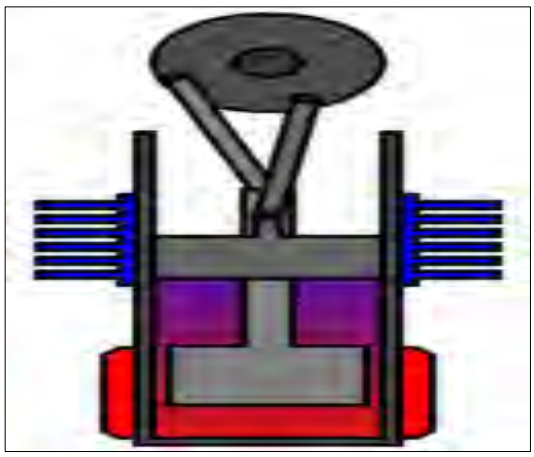

Figure 4.8: Beta Stirling Engine. [**52**]

3. Gamma Stirling Engine

It has two cylinders, one for the power piston and other containing a displacer with a hot and cold end. The pistons are in parallel and joined 90 degrees out of phase on a crankshaft [**52**].

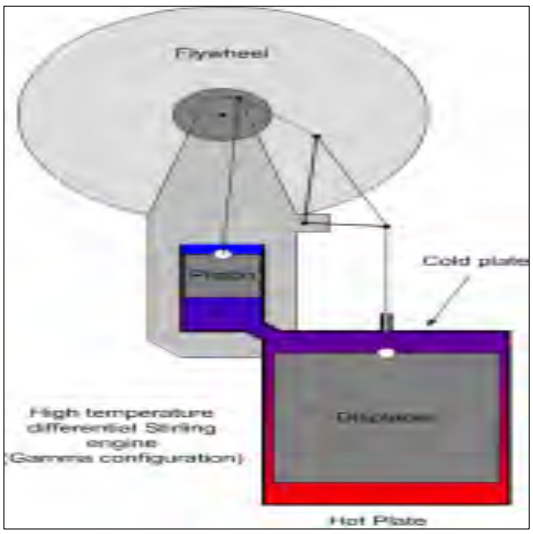

Figure 4.9: Gamma Stirling Engine. [**52**]

4.3.4 Principle of Operation

Theoretically a stirling engine is a very efficient engine. Its efficiency range is about 30-40% resulting from a temperature range of 700-800 degree celcius and operating speed is about 2000-4000 rpm [**53**]. Stirling engine works on stirling cycle. An ideal stirling cycle has three theoretical advantages. Firstly, the thermal efficiency of the stirling cycle is equal to the Carnot cycle with ideal regeneration. Secondly, the advantage is obtained by substitution of two isentropic processes with two constant-volume processes over the Carnot cycle. This results in increasing the *p–v* diagram area. The third advantage is compared with all reciprocal piston heat engines working at the same temperature limits, the same volume ratios, the same mass of ideal working fluid, the same external pressure, and mechanism of the same overall effectiveness, the ideal stirling engine has the maximum possible mechanical efficiency [**53**]. Ideal stirling cycle p-V diagram and T-s diagram is shown in figure (4.10) and (4.11) respectively.

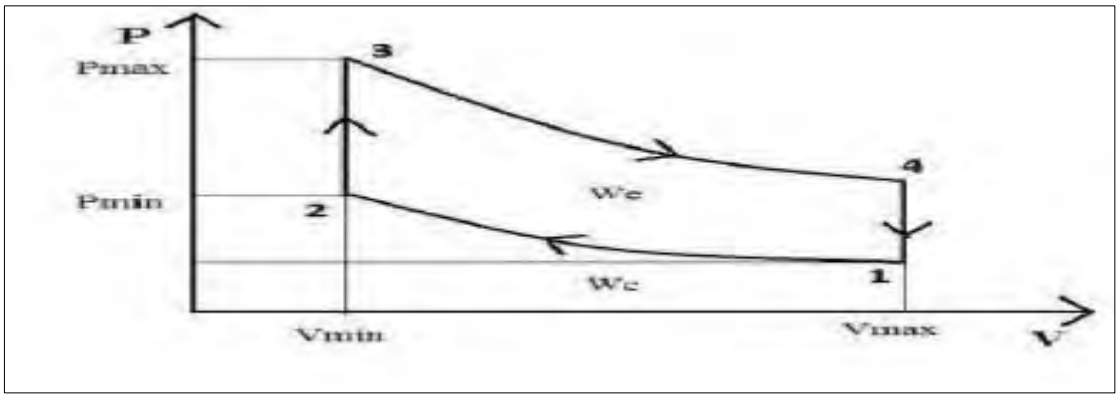

Figure 4.10: Ideal stirling cycle pressure vs volume (p-V) diagram [**51**].

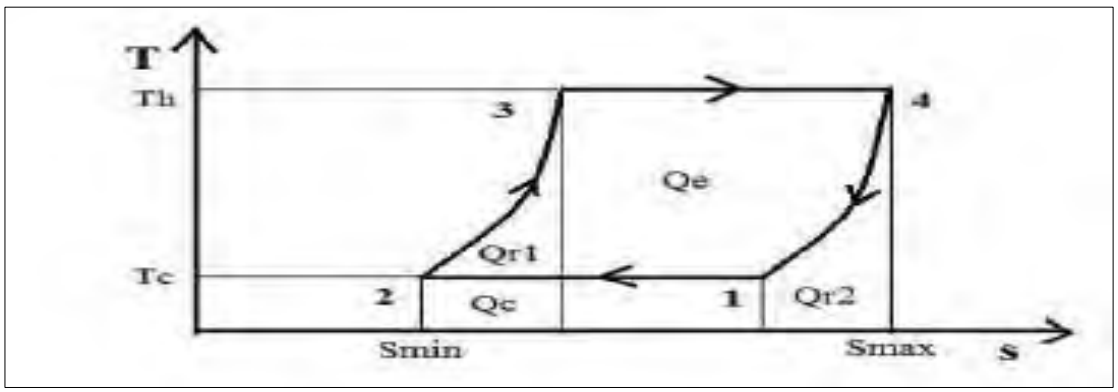

Figure 4.11: Ideal stirling cycle temperature entropy (T-s) diagram [**51**].

Stirling engine works on stirling cycle which comprises of four processes. (See figure 4.12) They are:

A. **Isothermal Compression:** At this stage, the power piston travels inwards. In this stage gas is compressed and volume is reduced which in turns raises the pressure. The area between points 1 and 2 under the p-V diagram indicates the work done to compress the gas, Wc. In this process heat is removed to the environment by the cooled cylinder and the removed heat, Qc is the area between points 1 and 2 under the T-s diagram [**51**].
B. **Isochoric Heating:** At this stage, the piston remains at its most inwards point and the volume is kept constant. Heat is added to the gas and its temperature is raised from cooling temperature, Tc to heated temperature, Th. Gas pressure reaches maximum point, pmax. The area between points 2 and 3 under the T-s diagram depicts the heat added from the regenerator, Qr1 [**51**].
C. **Isothermal Expansion:** At this stage, the expanding heated gas pushes the power piston outwards and energy transferred to the piston is We which equals the area between points 3 and 4 under the p-V diagram. In this stage heat added from the heat source to the heated cylinder is Qe and it represents the area between points 3 and 4under T-s diagram. This stage also increases the overall volume and lowers the pressure [**51**].
D. **Isochoric Cooling**: At this stage, the piston remains at its outer most point and the volume is kept constant. Heat is absorbed from the gas and its temperature is lessened from T_h to T_c. Gas pressure gets down to the minimum point p_{min}. Heat absorbed by the regenerator is Qr2 and it equals Qr1 [**51**].

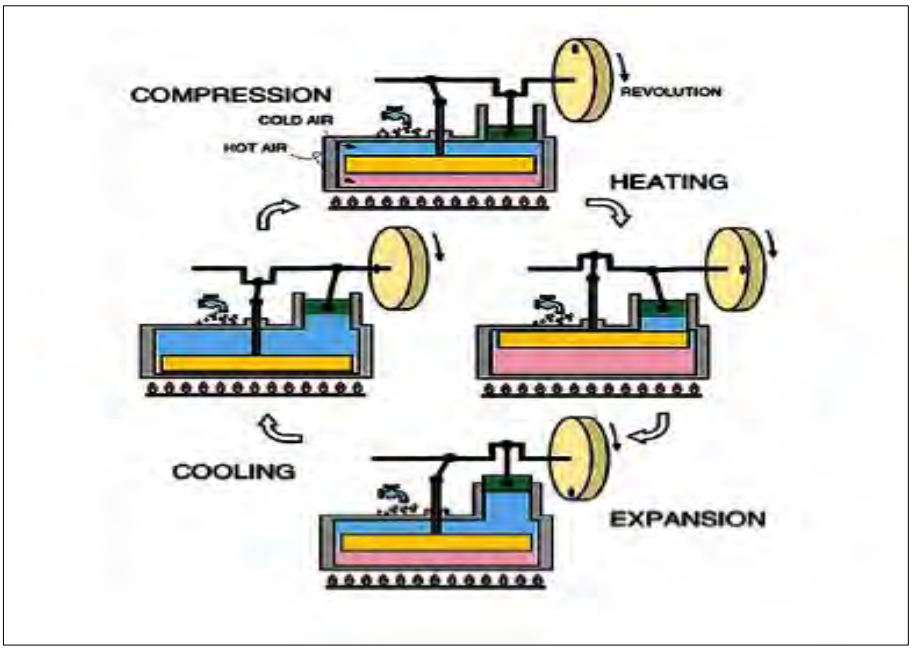

Figure 4.12: Stirling cycle **[54]**

4.3.5 Engine Power Output

Stirling engine output power can be calculated from the Beale formula. According to Baele, the power output of the stirling engine could be calculated approximately from the following equation:

$$P = \mathrm{B}.P_m.f.V_p \quad (4.1)$$

Here, P is the power output of the stirling engine, B is the Baele number which range is from 0.11 to 0.15, P_m is the mean cycle pressure in Mpa, f is the cycle frequency in Hz, V_p is the displacement of power piston in cm^3 [**53**]. This formula can be used for all types of stirling engine. Baele number is a function of both source and sink temperature.

4.4 Working Process of Dish-Stirling System

A Dish-Stirling system has three basic components. The concentrator, the receiver and the power conversion unit. (See figure 4.13)

Energy from the sun is reflected by the parabolic dish and focused onto a stirling engine, which is the high efficient power conversion unit of this system. If there is no losses occur in the concentrator, the concentration factor C will be higher. Concentration factor C is the ratio of the outgoing energy density and the incoming energy density. It can also be described by the inverse ratio of the concentrator entrance aperture area and exit aperture area [**55**].

$$C = \frac{E'}{E} = \frac{A}{A'} \quad (4.2)$$

Here, E' is the outgoing energy density, E is the incoming energy density. A is the concentrator entrance aperture area in square meter and A' is the exit aperture area in square meter.

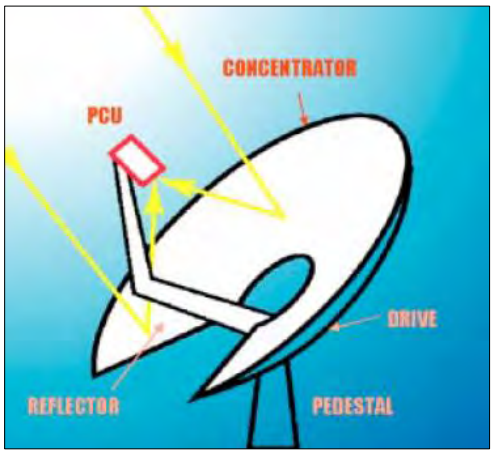

Figure 4.13: Dish-stirling system components. [**7**]

Those reflected, highly concentrated rays hit the receiver of the power conversion unit with heat. Basically receiver is the device that converts concentrated solar radiation to heat. The useful heat collected by the receiver Q can be calculated by the following equation:

$$Q = A_{AP}.\,[\alpha.\,C.\,E^{S} - \varepsilon.\,\sigma.\,(T_A)^4 - U_L\,(T_A - Ta)] \quad (4.3)$$

Here, A_{AP} is the aperture area, α is the average absorptivity of the absorber with respect to the solar spectrum, C is the concentration factor, E^S is the radiation density of the direct solar radiation, ε is the average emissivity of the absorber with respect to the black body radiation at the absorber temperature T_A, σ is the Stefan-Boltzmann constant, U_L is the heat loss coefficient due to convection and conduction and Ta is the ambient temperature **[55]**.

To transfer heat from the absorber to the working fluid a temperature difference is required. Another expression for the useful energy is:

$$Q = A_{Ab}.\,U_I.\,(T_A - T_F) \quad (4.4)$$

U_I is the inner heat transfer coefficient from the absorber to the fluid, T_F is the average temperature of the heat transfer fluid and $A_{Ab\ is}$ the absorber area **[55]**.

From these two equation, energy balance equation can be rewritten as

$$Q = A_{AP}\,[F.\alpha.C.E^{S} - F.\varepsilon.\sigma\,(T_F)^4 - F.U_L\,(T_F - T_a)] \quad (4.5)$$

Here, F is the heat removal factor [**55**].

The thermal efficiency of the receiver η_{th} is the ratio of the useful heat and the incoming solar radiation.

$$\eta_{th} = Q\,/A_{AP}.C.E^{S} \quad (4.6)$$

The variation of thermal efficiency of a receiver is shown in figure 4.14.

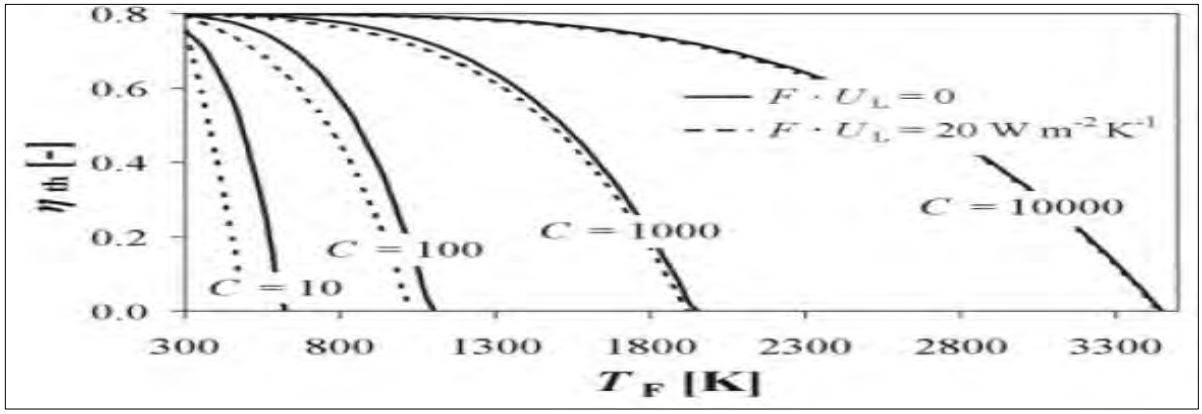

Figure 4.14: The thermal efficiency of a receiver η_{th} as a function of the fluid temperature T_F and the concentration factor C. **[55]**

When the highly concentrated rays hit the receiver 600-800 degree Celsius, it causes the working gas to expand and drive the pistons of the stirling engine. Pistons turn a generator

which produces electrical output far more efficiently than any other solar power technology. The current produced by this system is 3 phase AC and it is directly connected to the grid. The working process of the stirling engine is same as described earlier. At sunset the concentrator goes into a safe position and rotates backward to the sunrise point, ready for the next day operation.

4.5 Proposed Design

This part demonstrates a design of dish stirling system which involves the concentrator, tracking system, SOLO 161 stirling engine and the receiver.

4.5.1 The Concentrator

To construct a dish stirling system at first we need to design the concentrator. For this system, we choose a paraboloid dish, which has a diameter of 8m. So, the projected mirror area is calculated 50.3 square meter. To construct the concentrator we will use silvered glass. There are 12 facets of glass and each of them are 0.8 mm thick. In figure 4.15, a concentrator is shown with its glass facet.

Figure 4.15: Solar concentrator

The reflectivity of the concentrator is selected 0.94 and the height and width of the concentrator is selected 9m. The approximate weight will be 4000 kg. For this concentrator focal length is selected 4.5m and the intercept factor is 0.94. For this type of solar concentrator typical temperature range is 650-800 deg. Cel. [**55**]. Solar concentrator measurement is shown in table 4.2.

Table 4.2 Specification of solar concentrator **[55]**

Type	**Paraboloid**
Number of facets	12
Projected Area	50.3 square meter
Height	9 m
Width	9 m
Reflectivity	0.94
Weight	4000kg
Focal length	4.5 m

4.5.2 The Tracking System

To track the sun and operate the system correctly we need to use a tracking system. In this case we are going to use two axial tracking system. We will use six wheels and the whole structure

Figure 4.16: Tracking system

will stand on those. These six wheels will move the concentrator towards sun. The movement of the wheels will be done by a small servo motor. The whole tracking system will be controlled by a micro controller. Maximum allowable wind speed is 15m/s for this system. A model and technical data of a tracking system is presented in figure 4.16 and table 4.3 respectively.

Table 4.3 Technical data of the tracking system

Max. wind velocity	15 m/s
Drive	Servo Motor
Drive Velocity	60 deg. per min
Control System	PC, Micro controller

4.5.3 SOLO 161 Stirling Engine

In this dish stirling system we use concentrated solar power to run the stirling engine and produce electricity. For this case we have selected SOLO 161 stirling engine, which is capable of producing 3 phase alternating current. The length, depth and height of this type of engine is 1280 mm, 700 mm and 980 mm respectively [**56**]. A simple model of SOLO 161 Stirling Engine is shown in figure (4.17).

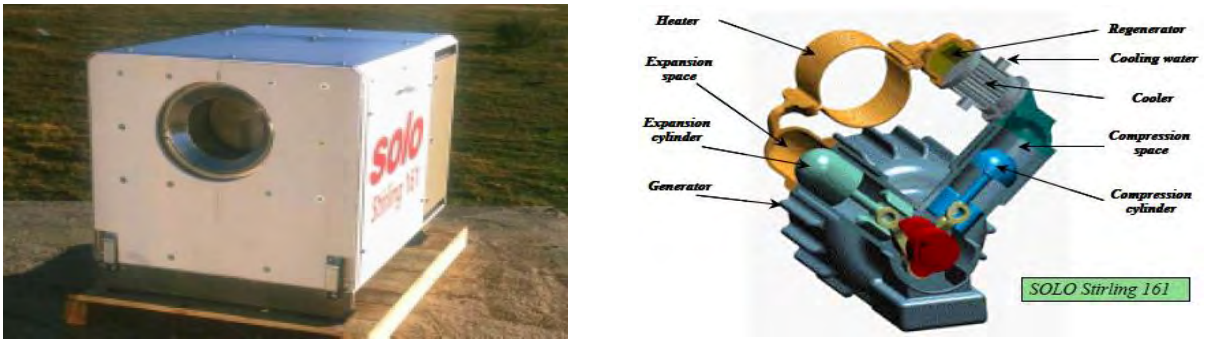

Figure 4.17: SOLO 161 stirling engine. **[56]**

This engine is rated 10 KW. It has 2 cylinders and the cylinder capacity is 160 cc. The rated speed for this engine is 1500 rpm or 25 Hz. The operating gas is helium. Helium gas is used here due to the good thermal and aerodynamic properties **[56]**. The output power can be adjusted by controlling the operating gas pressure between 50 to 200 bar and this will done by a small piston pump. This type of engine has water cooling system for the low temperature side **[56].** A specification of SOLO 161 Stirling Engine is presented in table 4.4.

Table 4.4 Specification of SOLO 161 stirling engine [**56**]

Type	SOLO 161
Swept Volume	160 cc
Rated Power Output	10 KW
Working Gas	Helium
Gas Pressure	50-200 bar
Power Control	Pressure Control

4.5.4 The Receiver

The link between the concentrator and the stirling engine is the receiver. It basically absorb solar radiation reflected onto it from the concentrator and pass this energy to the stirling engine in form of heat with least possible losses.

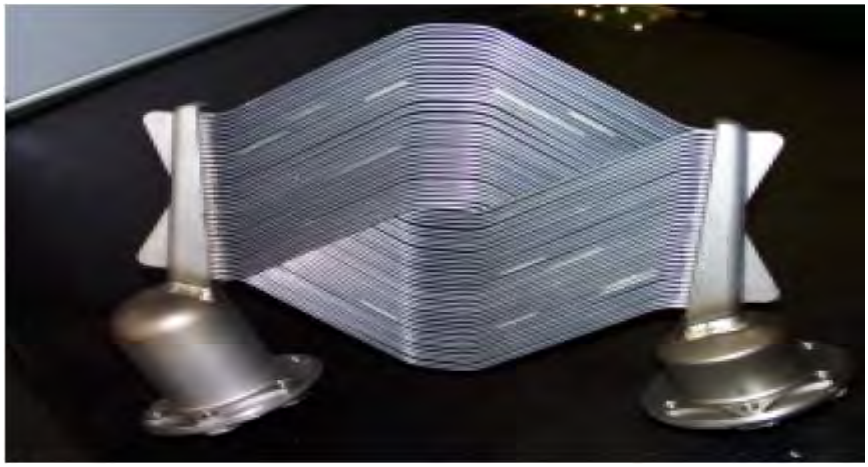

Figure 4.18: Directly illuminated tube receiver. [55]

Among two types of receiver the directly illuminated tube receiver is selected. These tubes are directly connected to the cylinder head of the stirling engine. The diameter of these tubes are 3 mm which resist very high temperature [55]. A Directly illuminated tube receiver along with a SOLO 161 stirling engine with tube receiver is shown in figure (4.18) and (4.19) respectively.

Figure 4.19: SOLO 161 stirling engine with tube receiver. [**55]**

4.6 Calculation

4.6.1 Input Power Calculation

Diameter, D = 8m

Projected Area= $\frac{\pi}{4} \times D^2$ = 50.3 m^2

Average solar irradiance in Dhaka = 700 W/m^2

Input Power = (50.3x700) W = 35210 W

4.6.2 Output Power Calculation

Displacement volume = 160 cc

Operating Speed =1500 rpm

= 25 Hz

Helium gas pressure = 50-200 bar (variable)

= 5-20 Mpa

Receiver temperature = 800 degree Celsius

= 1073 K

Beale number = 0.13

Maximum Output Power = 0.13 x 160 x 25 x 20

= 10400 W

Efficiency = $\frac{10400}{35210}$

= **29.5%**

An output power vs pressure curve is shown in fig 4.20 using MATLAB**.** The parameters were taken from Appendix 3.

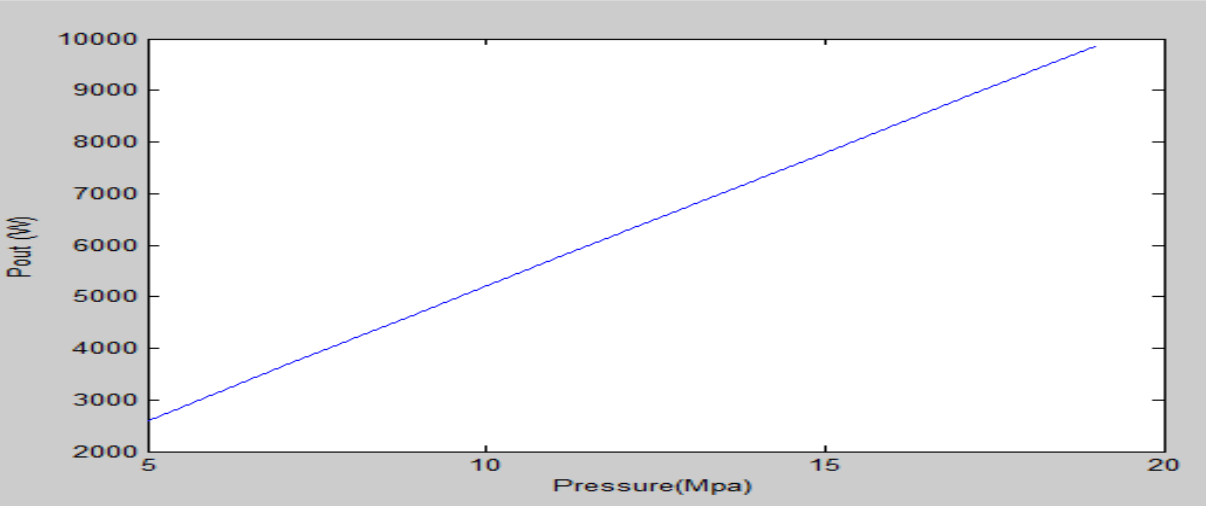

Figure 4.20: Output power of a stirling engine as a function of pressure

4.7 Proposed Design Analysis

It is important to see the effect of proposed design in the bulk power generation. To observe the effect we have decided to design a plant using Dish-Stirling system. To design the field layout we have selected 1 acre of land. Now, the most challenging part is to select the distance between two units of the proposed design. As the concentrator is tracking the sun and moving

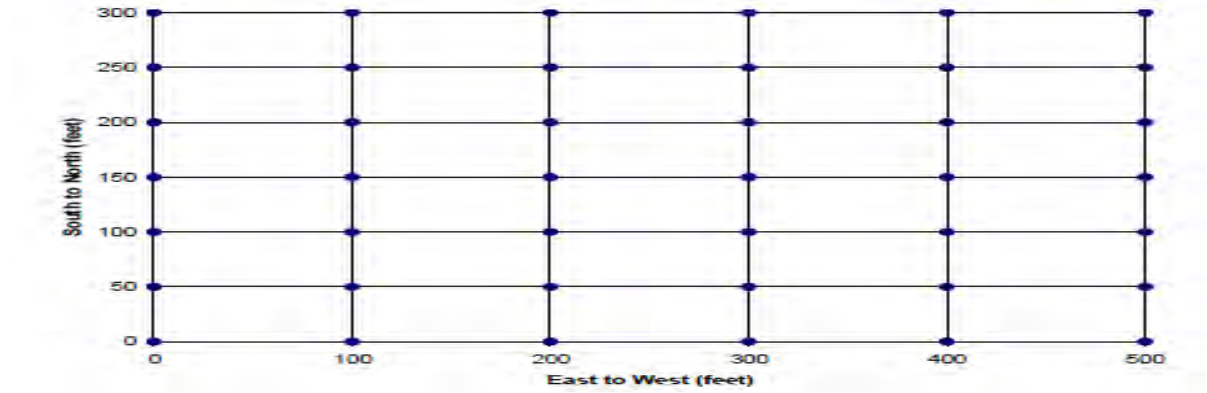

Figure 4.21: Osborn's rectangular layout model [**57**]

along with the sun the east-west distance and the north-south distance of two units will not be the same. To solve this problem we have decided to follow Osborn's rectangular layout model. (See figure 4.21)

Osborn modelled this layout based on shade interaction between round dishes and energy production [**57**]. According to his model, in east-west the gap between two units need to be 100 feet which is 30.48 meter. On the other hand, in south-north the gap needs to be 50 feet which is 15.24 meter. For selecting this distance he basically considered the shading impact, but cost also has a great impact. Increased spacing will also increase wire cost, land cost, maintenance drive times, wind impacts etc. But most importantly it will increase energy loss. By using the 15 minutes 1977 meteorological data from the Solar One Central Receiver Project, he had shown how the shading effect reduce the performance of the system. Figure 4.22 shows the impact of shading and shading degradation factor on the system performance curve.

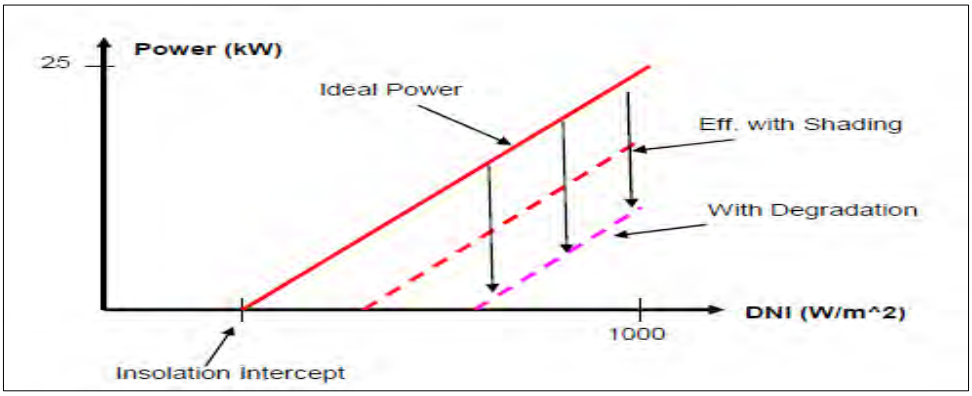

Figure 4.22: Impact of shading and shading degradation factor on the system performance curve [**57**].

To verify Osborn's model, Sandia National Laboratories modelled a field of 20,000 dishes system in Barstow, CA using the same meteorological data. In their study they have shown that Osborn's model can cause loss of energy and revenue. Then they tried to develop the model by staggering the layout. But they found that when the field is staggered there is a reduction of energy production and revenue [**57**]. All calculations were performed with the dish spaced 52 feet north to south and 104 feet east to west. In the end, they found that the optimum layout of a dish field is a rectangular grid without stagger, considering only the revenue and energy steams. Effect on Revenue and Energy production of variations in the North-South and East-West dish spacing is shown in fig 4.23.

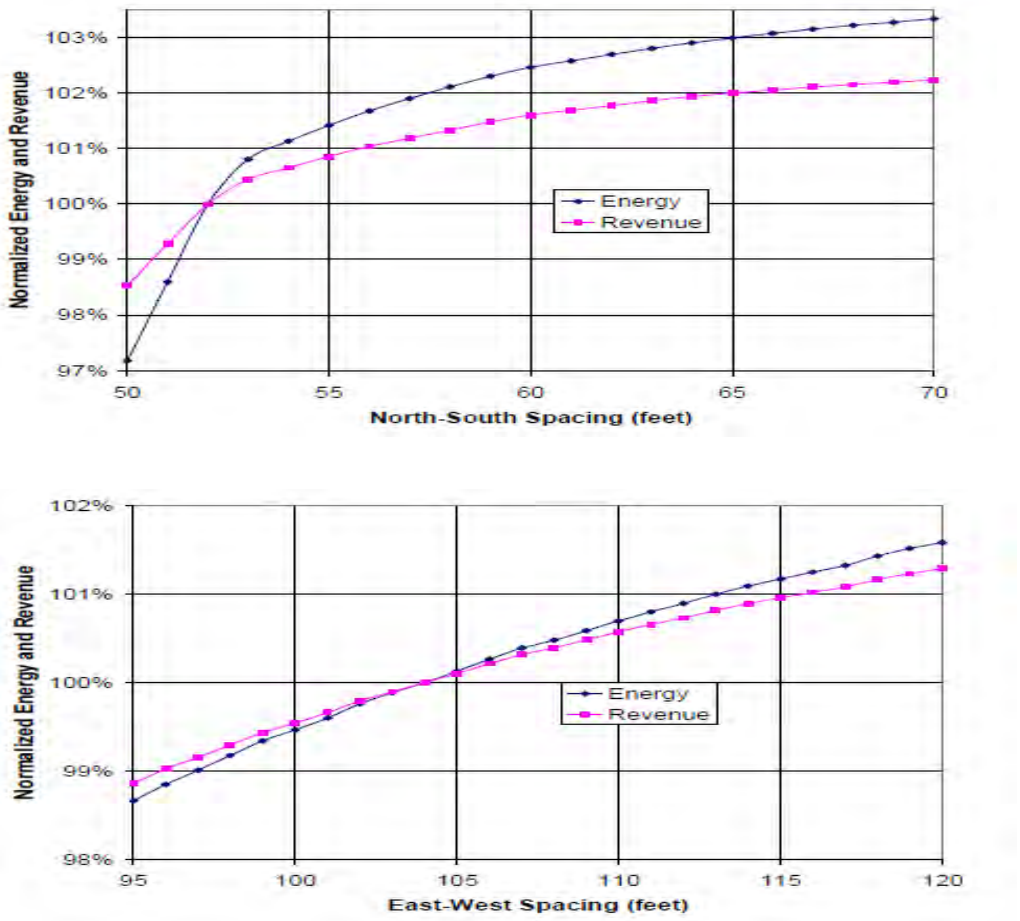

Figure 4.23: Effect on revenue and energy production of variations in the north-south and east-west dish spacing [**57**].

After reviewing these analysis we have also selected east-west dish spacing 100 feet or 30.48 meter and south-north dish spacing 50 feet or 15.24 meter. We have selected 1 acre of land, which is 4046.86 square meter = 63.61*63.61 meter. In this amount of land we can setup 15 units of dish-stirling system. We can arrange them in 5 rows and 3 columns. By installing them we can generate 150 kW. This is far more than PV panel output 78.91 kW in the same amount of area, which will be discussed in the next chapter. Field layout of proposed design on 1 acre of land is shown in figure 4.24.

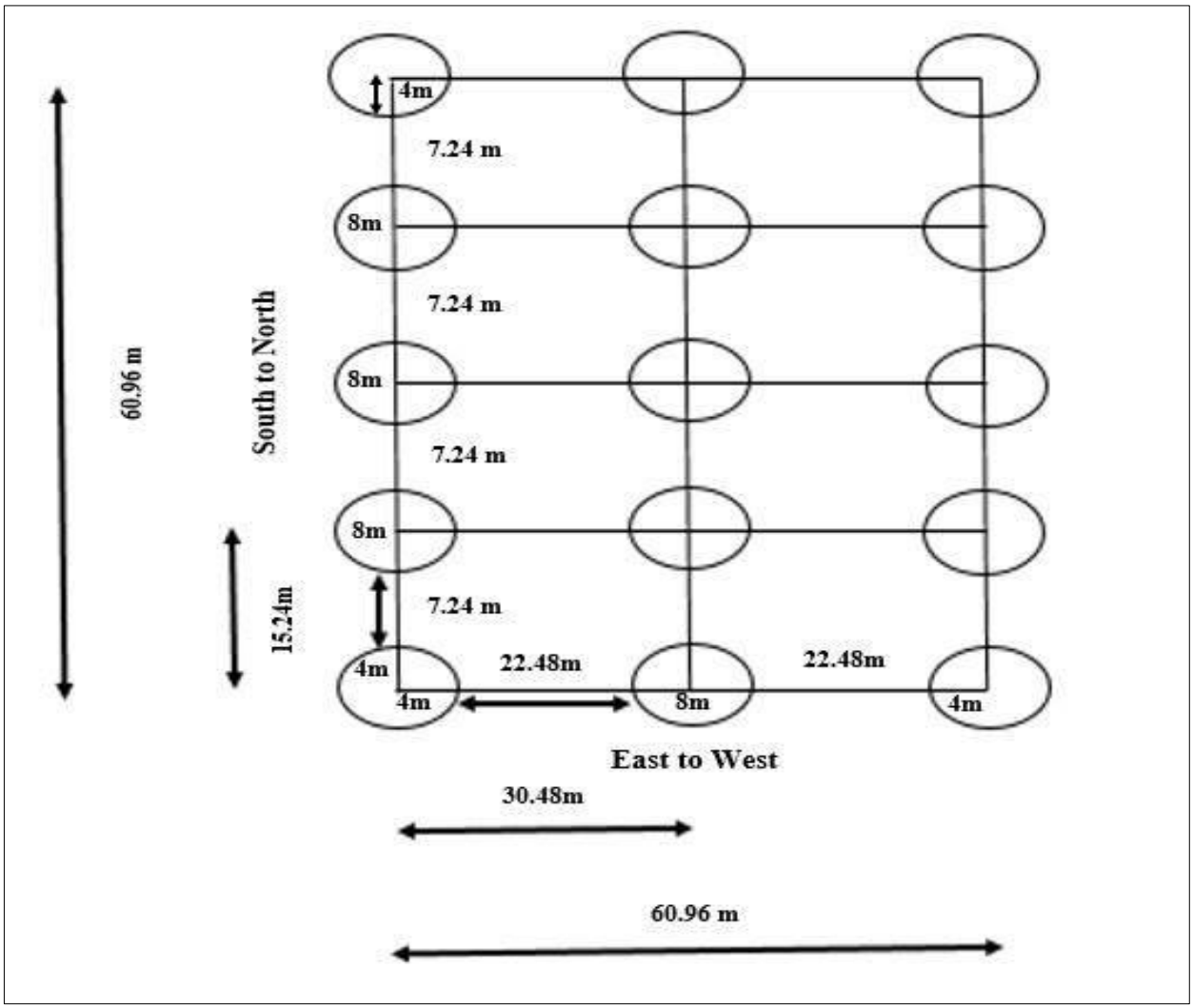

Figure 4.24: Field layout of proposed design on 1 acre of land.

4.8 Cost Analysis

Cost analysis plays a vital role in the field of bulk amount of power generation. A power generation process can be efficient, but if it is not cost effective then it cannot be used in large scale production.

The main disadvantage of dish-stirling system is its cost. This system is costly than other solar power system. We have reviewed some dish-stirling system companies cost analysis report. According to SBP and the associated Euro-Dish industry, their actual cost of the 10 KW unit is approximately $10,000 US/KW without transportation and installation cost and excluding foundation. But they have projected that if the production rate of 500 units per year is 5 MW and 5000 units per year is 50 MW, then the cost of per unit will decrease at $2,500 US/KW

and $1,500 US/KW respectively [**7**]. Similarly, installed cost for the SES dish-stirling system are high at about $10,000 US/KW. These costs are distributed with 40% in the concentrator and controls, 33% in the PCU and the remaining 27% in the balance of plant and installation of the system [**7**].

Basically, the installation cost of the Dish-Stirling system depends on the timeframe and the size of the plant. According to a study, for a 3 MW/per year production capable plant the lower capital cost for a unit is estimated $3,000 US/KW, including $300 US/square meter collector costs and $1,000 US/KW receiver/engine/generator cost. After 5 years with some improvements such as single facet stretched membrane concentrators and higher receiver temperatures and engine efficiency, a 30 MW/per year production capable plant could be more cost effective. Then the lower capital cost for a unit is estimated $2,000 US/KW, including $200 US/square meter collector costs. This time the O&M cost and LEC will be much lower. Now again after 5 years expanding the production capacity by 300 MW/per year, the estimated lower capital cost for a unit is $1,200 US/kW. Similarly, the O&M cost and LEC will decrease [**58**]. A levelized cost projection data for dish-stirling system is shown in table 4.5.

Table 4.5: Levelized energy cost projection [**58**]

Production Capacity	**3 MW/per year**	**30 MW/per year**	**300 MW/per year**
Timeframe	1995-2000	2000-2005	2005-2010
Capital Cost range $/kWe	5,000-3,000	3,500-2,000	2,000-1,250
Collector System typical cost $/square meter	500-300	300-200	200-150
Annual O&M cost range cent/kWh	5.0-2.5	3.0-2.0	2.5-1.5
Solar LEC range cent/kWh	32.8-14.6	18.6-8.8	10.6-5.5

4.9 Future Improvements

To expand the effectiveness and make it more cost effective, some research works are going on. One of its key components is the receiver. Basically the receiver converts solar radiation into heat and stirling engine use this heat to produce electricity. Some advanced receiver concepts which are currently under development is reviewed. These concepts can be useful for future developments of dish-stirling systems.

4.9.1 Heat-Pipe Receiver

This type of receivers use sodium or a sodium and potassium mixture to transfer heat to the engine heated head. In these receivers, liquid metal evaporates and vapor is transported to the engine heated head and condenses there and the liquid metal refluxes to the absorber. The liquid metal condenses at a constant temperature, which provides uniform heating to the Stirling engine. These type of receivers can improve working receiver efficiency, which can increase the system efficiency up to 20% **[7].**

4.9.2 Hybrid Heat-Pipe Receiver

This type of receivers have a gas burner along with the solar absorbing surface. By using this kind of receivers we can use dish-stirling system 24 hours and produce electricity. This type of receivers can operate during times when the sun is covered with clouds and also can operate in the dark.

Two prototypes of Hybrid heat pipe receiver have been developed by the DLR in Germany. They are also tested for the SOLO V160/161 [**59**]. They designed a receiver that can transfer 45 KW thermal power to the engine heated head at a maximum temperature of 850 degree cel. [**59**]. Sandia is also developing a 75 KWt hybrid heat pipe receiver. During this development they are also paying attention about the cost of the system [**7**]. A hybrid heat-pipe receiver model is shown in figure (4.25)

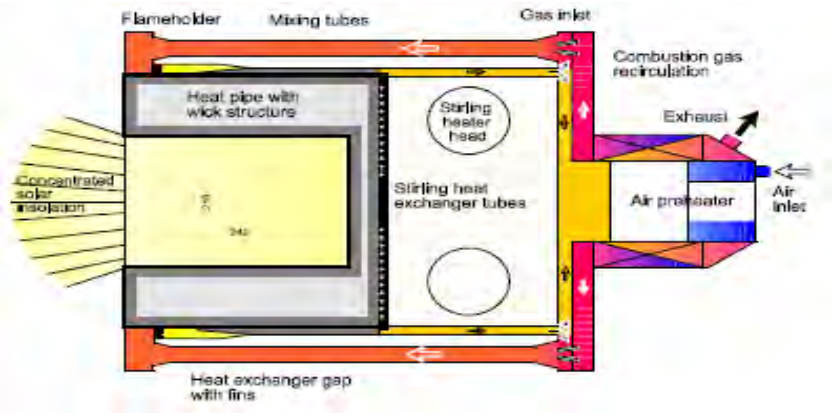

Figure 4.25 Hybrid heat pipe receiver.

4.9.3 Bio-Dish Hybrid Receiver

This type of receivers absorb solar radiation on one side and burn biogas on the backside. This project is co-funded by the European Community. This type of receivers have the same advantage like hybrid heat pipe receivers that they can operate at night. But the additional cost of adding a biomass gasifier is estimated about $3,000 US [7]. A simple diagram of a Bio-Dish Hybrid Receiver is shown in figure (4.26).

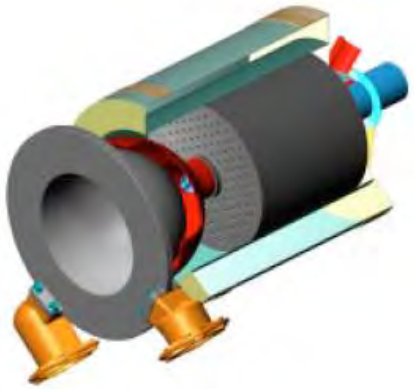

Figure 4.26: Bio-Dish Hybrid Receiver. [7]

4.10 Conclusion

This chapter illustrated the significance of Dish-Stirling system and how it can play a vital role in our power generation system. There may be some disadvantages like cost issues, but Dish-Stirling system is the most efficient solar thermal system. In our country fossil fuels are running out day by day and we are searching alternative ways to produce electricity.

We are trying to use solar energy to produce electricity by using PV panels. Similarly, if we pay attention on Dish-Stirling system then we can generate electricity more efficiently than PV panels or other solar thermal systems. On the other hand, if we can use this system in a large scale operation, then cost will not be an issue. Hence it can be said that if we use this system carefully, it could solve our electricity problem and ensure proper utilization of solar energy.

CHAPTER 5

PV-TEG Hybrid System

5.1 Introduction

For many decades, fossil fuel such as coal, oil and gas have been the primary methods for generation of electricity. However, Thanks to a global warming caused by consuming fossil powers, intensified by more prominent energy request because of enhanced expectations for everyday comforts and geopolitical strains over oil assets and nuclear energy, we are confronting a risk to the planet's prosperity. On the contrary, the usage of global energy is increasing rapidly. A prediction of global energy usage is shown in fig (2.1). To cope up with the growing demand, Photovoltaic (PV) system has turned out to be more striking for electricity generation in recent years. But then again, the frequent usage of PV systems is as of now not monetarily satisfactory due to its high cost. [**60**] Although a great deal of research has been carried out to lessen the cost of power generation using this technique.

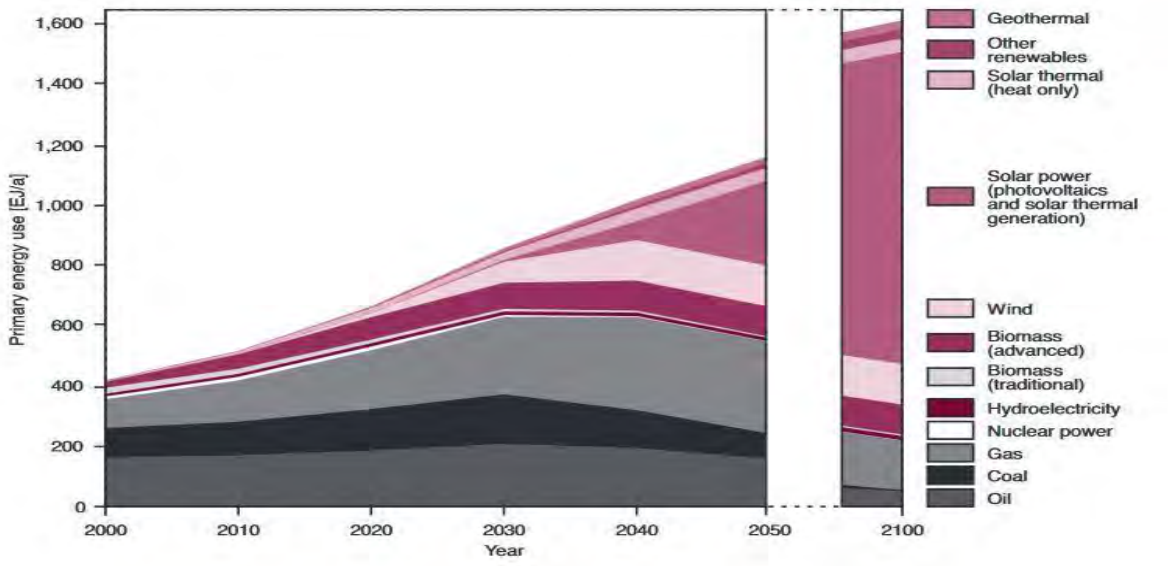

Figure 5.1: Predicted global energy usage. [**61**]

Most photovoltaic systems have been designed and built up for use in applications with low power requirements. The working principle of a Photovoltaic device is very simple. It can directly convert parts of the solar spectrum to energy, but a significant part is absorbed as heat. This results in an increase in the temperature of the PV cell and leads to a loss of power output because the power output of PV cells decreases with increasing the operating temperature. Thus efficiency of solar cells is quite low, obtaining best results in monocrystalline silicon

structures, with an efficiency of about 18% [**62**]. In order to remedy this, a number of combined photovoltaic and heat recovery systems has been proposed recently. The most simple of these convert the heat energy directly to electrical energy using a thermoelectric generator (TEG). The TEG is applied directly on the back of the PV, so that the two devices have the same temperature. This process utilizes the Seebeck effect to convert heat directly into electrical energy through the movement of charge carriers induced by a temperature span across the TEG. [**63**]

This chapter illustrates the possibility of building up a PV/TEG hybrid system that can offer preferable performance over that can be acquired from existing individual system when temperature rises.

5.2 Background

Photovoltaic (PV) system is a highly competitive technology to convert the incident solar radiation into electrical energy. This technology is developing rapidly due to its natural abundance, environmental safety, potential high performance and low manufacturing cost. Pursuing high efficiency is always the core task for PV technology. However it is still a long way from being competitive with fossil fuel based energy conversion technologies. A major issue lies in the limited efficiency of solar energy conversation. For example silicon thin film solar cell (STC) can only absorb solar light up to 800 nm which results in the difficulty of fully utilizing the solar spectrum. [**64**] Thus majority of the infrared energy is converted into waste heat and the temperature rise of the PV module leads to efficiency reduction. Therefore it is important to eliminate the waste heat and control the operating temperature.

On the other hand, Thermoelectric Generator (TEG) can directly convert thermal energy into electrical energy, so it offers a way to use solar radiation as well as waste heat. This working principle allows TEG to integrate with PV module for greater energy conversion. This section will review the basic operation of Photovoltaic (PV) cell and thermoelectric generator (TEG).

5.2.1 Photovoltaic Cell

Photovoltaic cell is a semiconductor device which converts photons into electrical energy by photovoltaic effect. The term “photo” means light and “voltaic” means electricity. When

sunlight strikes a PV cell, the photons of the absorbed sunlight dislodge the electrons from the atoms of the cell. The free electrons then move through the cell, creating and filling in holes in the cell. It is this movement of electrons and holes that generates electricity. [**65**] The physical process in which a PV cell converts sunlight into electricity is known as the photovoltaic effect. PV cells can be categorized into three main groups according to their semiconductor material.

1. **Silicon Solar Cell:** Single crystalline silicon solar cells are the most widely used solar cell. It is more energy efficient than those of polycrystalline PV cells. Commercially available silicon solar cell has the conversion efficiencies as high as 18%.
2. **III-V Group Solar Cells:** Examples include Gallium Arsenide (GaAs), Indium Phosphide (InP) etc. GaAs is popular in space applications where strong resistance against solar radiation damage and high cell efficiency are required. The disadvantage of using III-V compounds in photovoltaic devices are high manufacturing costs along with Crystal imperfections which severely reduces the device efficiencies.
3. **Thin film Solar Cells:** Amorphous silicon (a-Si) is a non-crystalline form of silicon with a significant high absorptivity. It was the first commercially produced thin film PV module and presently the only thin film technology that has an impact on the overall PV market. [**65**]

Generally, PV cells are characterised by measuring their current–voltage (I-V) curves (see figure 5.2). Using the I-V curves, the maximum power can be determined by the product of the current at the maximum power point (I_{MP}) and the voltage at the maximum power point (V_{MP}).

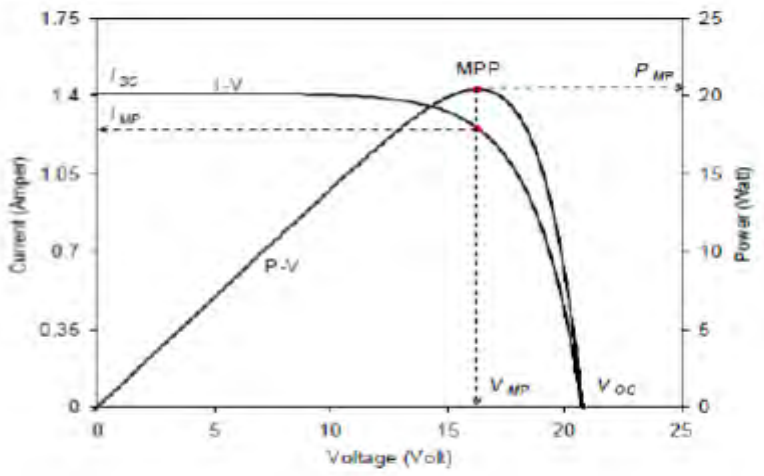

Figure 5.2: Typical I-V and P-V curves for a PV module [**66**]

Consequently, the conversion efficiency of a PV cell (η_{pv}) can be calculated by:

$$\eta_{pv} = \frac{I_{MP}V_{MP}}{GA_{PV}} \tag{5.1}$$

Here, G ($W.m^{-2}$) is the solar radiation intensity and A_{PV} (m^2) is the PV cell area.

Another useful parameter to evaluate the quality of a solar cell is the fill factor, which is defined as:

$$FF = \frac{I_{MP}V_{MP}}{I_{sc}V_{oc}} \tag{5.2}$$

Here, I_{sc} is the short circuit current and V_{oc} is the open circuit voltage. The effect of temperature on PV cells has been investigated. **[67]** It was found that the maximum power output (P_{max}) of PV cells decreases with increasing temperature (see figure 5.3). **[68]**

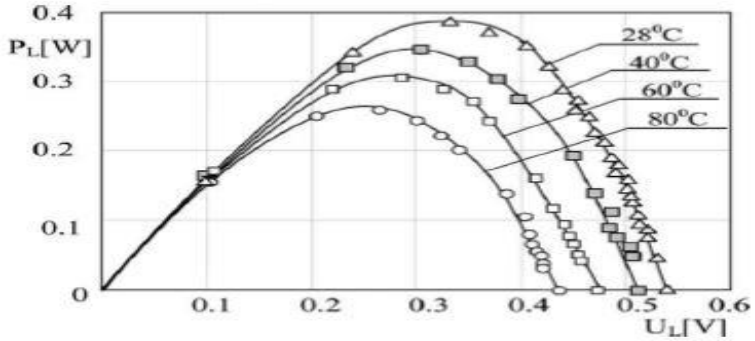

Figure 5.3: The output power as a function of temperature for a c-Si solar cell [**68**]

It has also been established that the conversion efficiency of silicon PV cells (η_{pv}) decreases linearly with increasing temperature [**69**], as shown in figure 5.4.

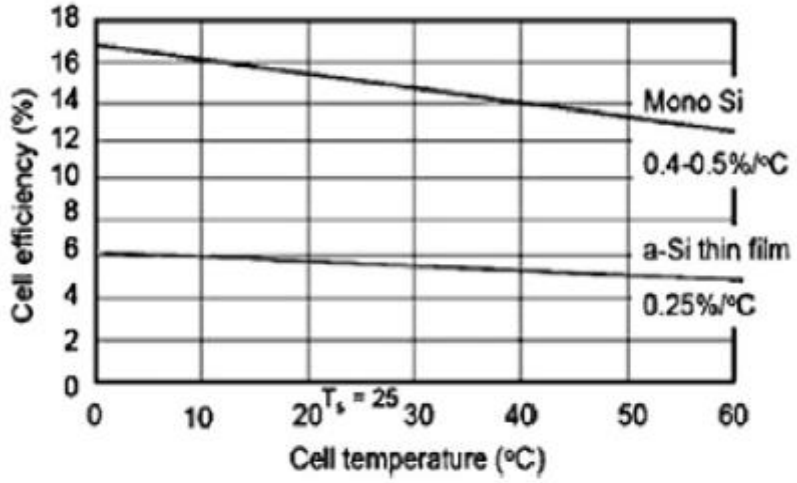

Figure 5.4: The relation between PV cell efficiency and temperature [**70**]

5.2.2 Thermoelectric Generator

A thermoelectric generator is a solid-state device that consists of a number of semiconductor elements mounted between two substrates. The elements are connected electrically in series and thermally in parallel. It converts heat flux directly into electrical energy when temperature difference arises at its two side. One side of the device creates heat while the other side absorbs heat, becoming cold. Depending on the operating temperatures and applied potential, electronic and thermal efficiency of these devices can vary. It has three effects known as the Seebeck effect, the Peltier effect and the Thomson effect [**71**].

5.2.2.1 The Seebeck Effect

The Seebeck effect is the phenomenon of producing voltage due to a temperature difference by connecting two dissimilar materials in series electrically and in parallel thermally [**72**]. The voltage generation can be calculated by:

$$V = \alpha_{ab}\Delta T \tag{5.3}$$

Where, V is the voltage generated from the TE device, α_{ab} is the difference in Seebeck coefficient of the two materials, and ΔT is the temperature difference between the hot junction (T_H) and the cold junction (T_C).

5.2.2.2 The Peltier Effect

The Peltier effect is the phenomenon of generating temperature difference across the junctions of two dissimilar semiconductors. The heat is absorbed at one junction and rejected at another junction by applying an external current [**73**]. The rate of heat removed ($\dot{Q}$) from one side to another side can be calculated as:

$$\dot{Q} = \pi_{ab} I \tag{5.4}$$

Where, π_{ab} is the Peltier coefficient and I is the electrical current.

5.2.2.3 The Thomson Effect

The Thomson effect appears in all TE devices and is the phenomenon of heat absorption or dissipation due to current flow and temperature differences [**74**].

The total rate of heat absorption (Q_T) is given as:

$$\dot{Q_T} = \beta I \Delta T \tag{5.5}$$

Where, β is the Thomson coefficient.

The three coefficients are connected by the Kelvin relationships as described in the following equations [**75**]:

$$\pi_{ab} = \alpha_{ab} T \tag{5.6}$$

$$\frac{d\pi_{ab}}{dt} = \frac{\beta_a - \beta_b}{T} \tag{5.7}$$

5.2.3 Photovoltaic – Thermoelectric Combined System

The incorporation of TEG with PV cells has been investigated in the last few years as it can recover the waste heat from PV and generate electricity in an additional stage [**76][77**]. A silicon thin film solar cell (STC) was integrated with TEG and a heat collector in a hybrid generation system (see figure 5.5). The heat collector worked by collecting the unwanted heat from the solar cells and transferring it to the hot side of the TEG.

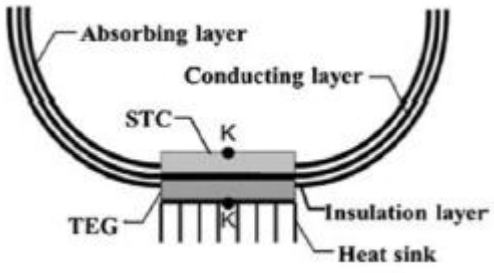

Figure 5.5: A hybrid generation system [**64**]

The total power generated from the hybrid system was 393 mW which was more than the individual system. A hybrid CPV/TEG was utilised to store the heat and use it as the heat source for the hot side of TEG. **[64]**

Recently, a study which modelled a hybrid system, including PV cells and TEG, has analysed the effect of increasing the number of elements. The effect on the power output from PV and TEG was analysed [**78**]. The number of TE modules to generate the maximum power was discussed and the power output from the TEG was calculated. The overall power generation of the hybrid PV/TEG system was investigated experimentally. The results indicate that the hybrid system is more efficient in generating electricity than using a singular system.

5.3 Selection of PV Cell for Integration

This section focuses on the identification of the PV cells that are suitable for developing PV/TEG hybrid systems. The efficiency of such PV cells should not decrease with the increase of temperature. To find the suitable PV, the performance of six types of PV cells was studied. The temperature dependence of P_{max} and η_{pv} for six types of PV cells was investigated as shown in table 5.1.

5.3.1 Sensor and Instruments

The key components for the study of different temperature dependence of PV cells are discussed.

5.3.1.1 PV Cells Comparison

The PV cells investigated in this study include 4 types of commercial products; polycrystalline silicon (p-Si), monocrystalline silicon (m-Si), copper indium selenium (CIS), amorphous silicon (a-Si). In addition the cadmium telluride cells (CdTe) and the dye-sensitised solar cells (DSCs) were used.

Table 5.1 Specifications of PV cells measured at standard test conditions

PV Cells	A_{PV} (mm^2)	Active area (mm^2)	V_{oc} (V)	I_{SC} (mA)	FF (%)	η_{pv} (%)
m-Si	900	625	0.6	180	67.1	16.46
p-Si	2000	1295	1.8	130	77.4	19.85
a-Si	1600	1600	2.6	53.9	59.4	7.5
CIS	3600	3136	4.8	69	47.3	7.17

CdTe	3000	2500	4.1	64	46.7	7.02
DSC	300	25	0.78	3.1	41.4	5.71

5.3.1.2 Peltier Module

A Peltier module was used to control the temperature for which characteristics are given in table 5.2. This device can function either as a cooler to keep the temperature of the PV cells at 25 ^{0}C or as a heater to increase the temperature of the PV cells up to 65 ^{0}C by reversing the polarity. The Peltier device was connected to a DC Power supply. By changing the voltage of the power supply, the temperature of the PV cells that is mounted on the top surface of the Peltier module can be controlled.

Table 5.2: Specification of peltier device

Total Area	40 mm X 40 mm
Number of elements	256
Cross section area of the element	1.4 mm X 1.4 mm
The length of the elements	1.2 mm

5.3.1.3 Solar Simulator and Pyranometer

A solar simulator was used as the light source to provide the light in the experiments. A calibrated pyranometer was used to measure the light intensity, which was provided by the solar simulator. The distance between the pyranometer sensor and the solar simulator was calibrated to get 1000 W/m^2.

5.3.1.4 Thermocouples

K-type thermocouples were used to measure the temperatures of the hot and cold sides of the system. Specifications are shown in table 5.3.

Table 5.3 Specifications of K type thermocouples

Characteristic	Type K
Minimum Temperature	-60 °C
Maximum Temperature	350 °C
Cable Length	1m

5.3.1.5 Heat Exchanger

A water-cooled aluminium heat exchanger (8 cm x 8 cm x 3 cm) was used to take the heat away from the Peltier device by connecting it to tap water. A uniform layer of heat sink compound with a thermal conductivity of 2.9 W/m.K was used between the heat exchanger and the Peltier device.

5.3.2 Experimental Procedure

The PV cell absorbs the light from the solar simulator. Part of the light is converted into heat in the PV cell, which can result in an increase in the operating temperature of the PV cell. In order to maintain the temperature of the PV unchanged, a temperature control system is employed which consists of a Peltier module and water heat exchanger. Two K-type thermocouples were used to measure the temperature of the PV cell. The top thermocouple was attached to the surface of the solar cell, or placed inside the glass electrode by drilling a hole from the side when possible. Another thermocouple was fixed inside a copper plate, which acted as a thermal conductor.

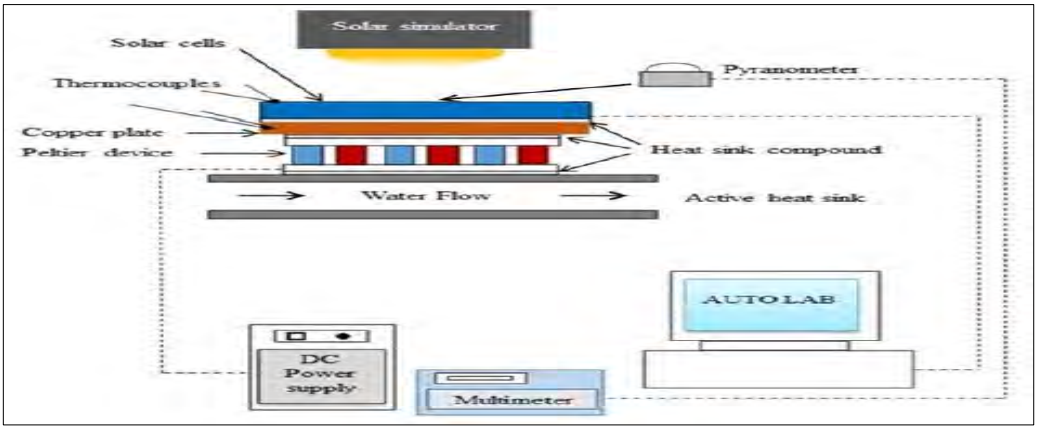

Figure 5.6: Experimental set up of the solar cell assembled with the Peltier cooling device

A thin uniform layer of heat sink compound was applied between the copper sheet and the rear of the PV cell to provide a good thermal contact. A Peltier device was placed between the copper plate and the heat sink using the same heat sink compound. The I-V and P-V curves were obtained at stable PV cell temperatures of 25°C, 35°C, 45°C, 55°C and 65°C using AUTO LAB System. A schematic diagram of the experimental setup is shown in figure 5.6.

5.3.3 Results and Discussion

The I-V curves for the 6 different types of PV cells are shown in Figure 5.7. It can be observed that increasing the operational temperature from 25°C to 65°C leads to a significant decrease in V_{OC} for all types and a slight increase in short circuit current (I_{SC}) except for DSC and a-Si where, the I_{SC} was almost constant when the operational temperature increased from 25°C to 45°C.

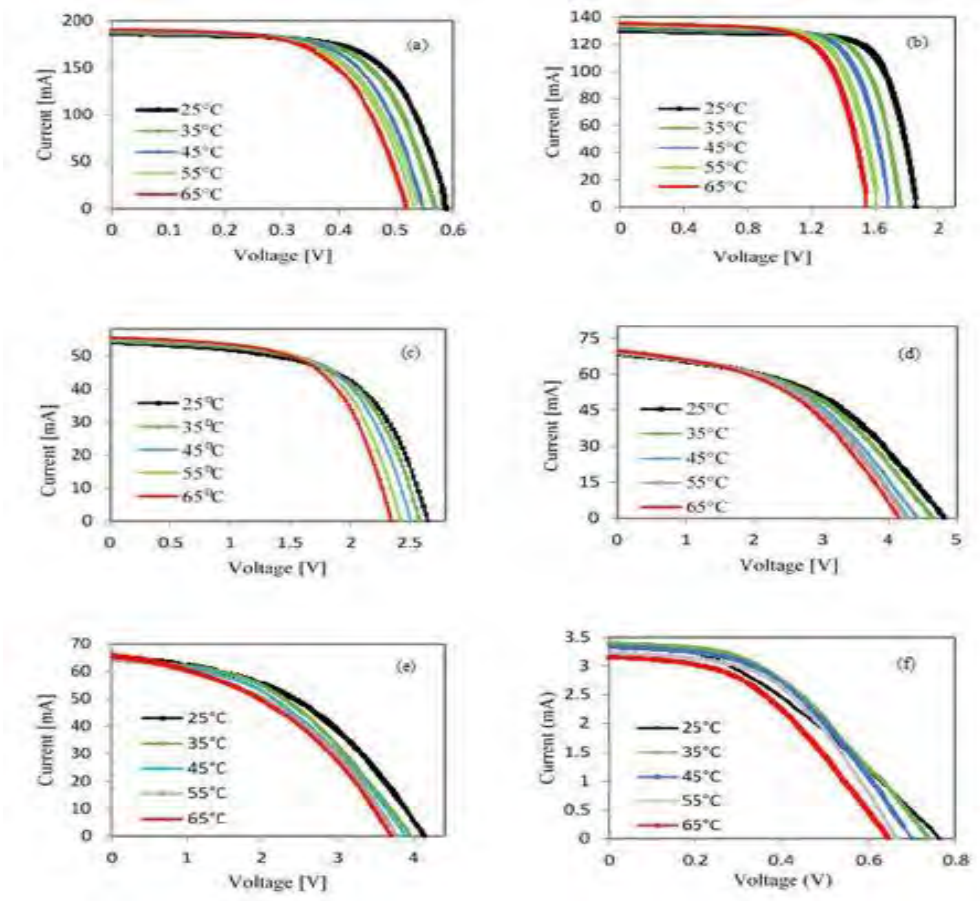

Fig 5.7: Current vs voltage curves for (a) m-Si (b) p-Si (c) a-Si (d) CIS (e) CdTe and (f) DSC

The decrease in V_{OC} results in a net reduction in P_{max} for all of the devices tested except for a-Si and DSC, as shown in Figure 5.8.

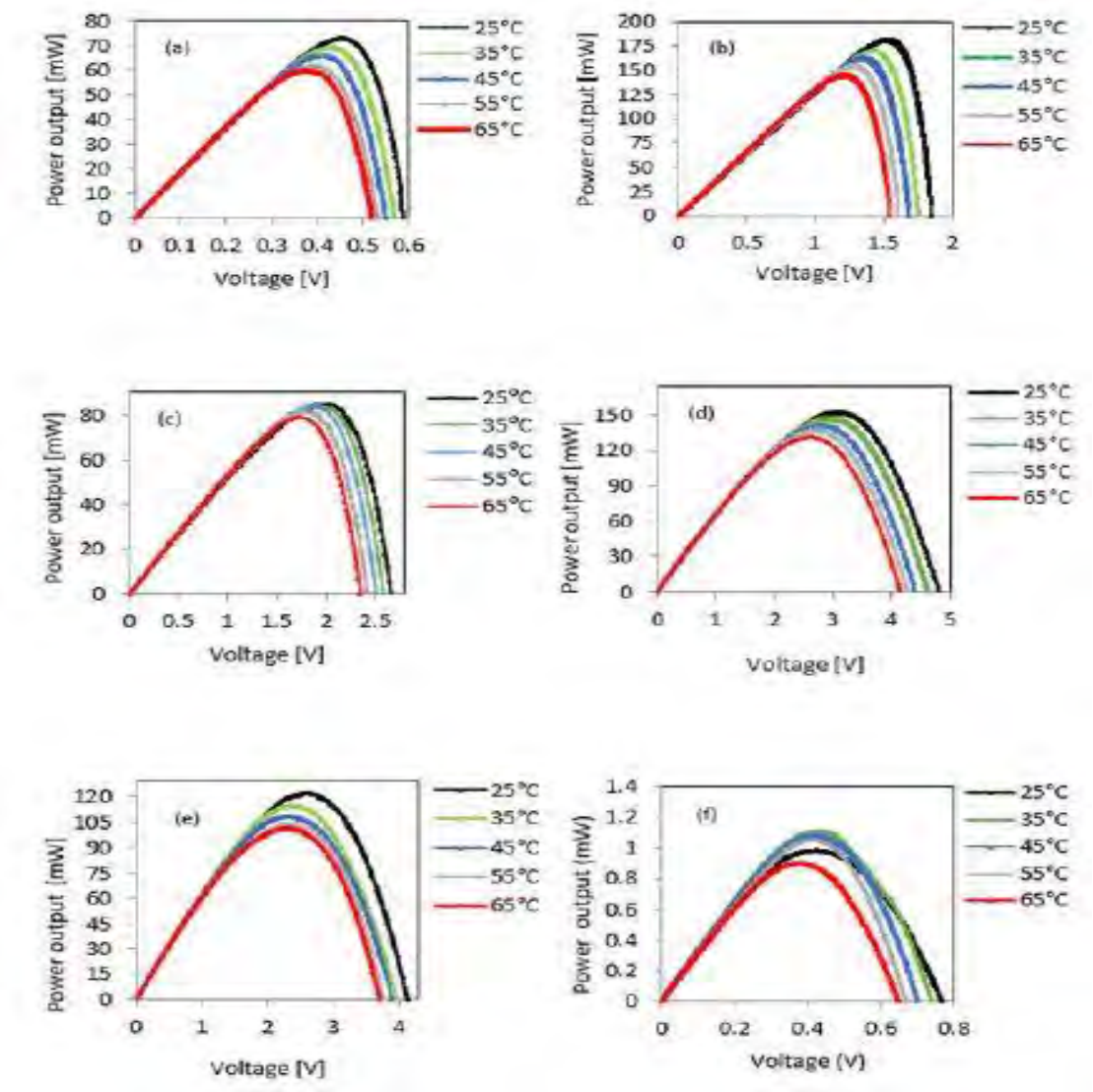

Fig 5.8: Output power vs voltage curves for (a) m-Si (b) p-Si (c) a-Si (d) CIS (e) CdTe and (f) DSC

The temperature dependence of the Pmax in a solar cell is usually measured so-called the temperature coefficient, which is defined by [**79**]

$$\frac{1}{P_{Max}}\frac{\Delta P}{\Delta T}$$

From the graph of m-Si,

P_{max}= 73 mW

$$\Delta P = (73 - 59.8) = 13.2\, mW$$

$$\frac{1}{73} \times \frac{13.2}{65 - 25} \times 100 = 0.45\ \%/K$$

It was found that the values determined from the experiment for m-Si (0.45 % / K) and p-Si (0.51 % / K) were in good agreement with the published data of the crystalline solar cells (0.65 %/K) [**79**]. Output power demonstration of six types of cell has shown in table 5.4.

Table 5.4 Output power demonstration of six PV cells at different temperature [**79**]

T in Degree	m-Si mW	p-Si mW	a-Si Mw	CIS mW	CdTe mW	DSC mW
25	73	181.5	84.4	150.5	121.5	1
35	69.5	170.1	84.1	147	113.7	1.1
45	65.5	161.5	82.6	140.6	108.1	1.1
55	62.2	153.4	82	137	103.2	1.1
65	59.8	143	79.6	131	101.3	0.9

The average rate of decrease in Pmax was calculated over three ranges of temperatures as presented in Table 5.5. The first range was (25°C- 45°C), where p-Si presented the quickest drop in Pmax. This indicates that p-Si is the worst type of solar cells for use in a PV/TEG hybrid system because of significant power loss at higher temperatures required by efficient operation by TEG.

Table 5.5: The drop in P_{max} for the six solar cells in three regions

T in Degree	m-Si	p-Si	a-Si	CIS	CdTe	DSC
25-45	-10.2%	-11%	-2.1%	-6.7%	-10.5%	+9.8%
45-65	-8.7%	-11.5%	-3.6%	-7.1%	-6.3%	-16.3%
25-65	-18.0%	-21.2%	-5.7%	-13.3%	-16.7%	-8.1%

The overall reductions in the investigated temperature range (25°C- 65°C) were calculated. It can be seen that the Pmax of the m-Si cells dropped significantly by 18 %. The p-Si device exhibited a higher drop in Pmax of 21.2 %. For CIS cells Pmax dropped by 13.3 % and the CdTe sample reduced by 16.7 %. The overall drop of Pmax in DSCs over 25°C- 65 °C is 8.1% due to a significant decrease (-16.3%) over the temperature range 45°C- 65°C, despite it increased by 9.8% over the temperature range 25°C-45°C. Finally the a-Si sample demonstrated the least temperature sensitivity of the samples tested (5.7 %).

The experimental results obtained from this work indicate that it is feasible to integrate either DSC or a-Si with TEG in a hybrid PV/TEG system. This will enable thermoelectric power generation using the waste heat from PV cells and the heat associated with light energy in the infrared region of the solar spectrum without causing a power reduction in the PV cells due to operating at an elevated temperature.

5.4 Optimization of TEG in the Hybrid System

For modelling the PV/TEG system, Selection of Thermoelectric generator is important. Bismuth telluride and its alloys are widely used as materials for thermoelectric refrigeration. They are also the best materials for use in thermoelectric generators when the temperature of the heat source is moderate.

5.4.1 Input Parameters of TEG

A total of 9 types of TEG modules were chosen to study the dependence of the maximum power output on the geometry of TEG modules. Each type of the module has the same number of N and A_{TE}, but the length of the thermoelements was varied along with ΔT to obtain the maximum power output (P_{max}).

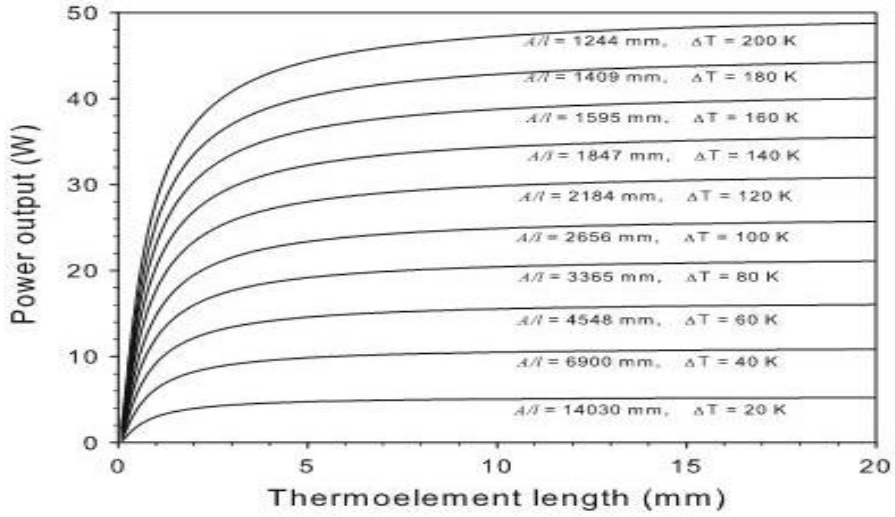

Figure 5.9: Power output vs thermo-element length for the system operating within an ambient atmosphere [**80**]

It can be seen from the figure 5.9 that the P_{TE} for a given type of module increases initially with an increase in L_{TE} until reaching the P_{max} at an optimal length and then the P_{TE} starts to decrease with a further increase in L_{TE}. This investigation shows that the integration of PV cell

with TEG module requires a trade-off between P_{TE} and that P_{PV}. It is necessary and vital to determine the optimal geometry of TEG module in order to obtain the improvement in a hybrid PV/TEG system. If this is not carefully done, the PV may lose more power than that are generated from the TEG. Also, the experimental results are in an agreement with theoretical calculation that predicted that the optimum geometry can be achieved using 62 elements with A_C of (0.8mm x 0.8mm) and L_{TE} of 2 mm. Geometrical factors have a significant effect on the power output and efficiency of both the PV cell and TEG module. Because the integration of TEG created a thermal resistance between PV cells and the heat sink, it will contribute to an increase in the operating temperature of PV cell. Using the wrong geometry will result in losing power from the PV cell and possibly wasting thermoelectric materials. The results demonstrate that a small-size module is preferred, rather than a larger size (i.e. in a similar size to PV cell), due to facilitating a higher power density with the added benefit of lower material consumption.

5.5 Hybrid Model Outline

A hybrid PV/TEG system is shown schematically in Figure 5.10. It consists of a PV cell connected to a TEG via a copper plate that serves as a thermal concentrator. The interfaces were filled with thermally conductive paste to ensure good heat transfer across these interfaces. The copper plate forms the hot side of the TEG, with the cold side of the TEG is attached to a heat exchanger with water circulating through it. The advantages of such a hybrid system are that the operating temperature of the PV cell will be reduced due to the transfer of heat into the TEG, and the TEG will generate additional power due to the temperature difference (ΔT) established across it. A schematic diagram of hybrid PV/TEG system has shown in figure (5.10)

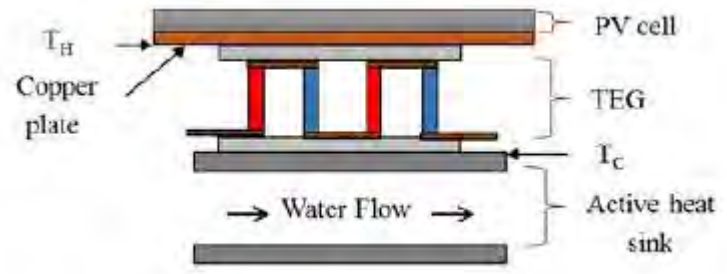

Figure 5.10: A schematic diagram of the hybrid PV and TEG system [**81]**

The rate of solar energy available to the PV cell is equal to the heat losses from the PV and electrical power generation, thus: **[78]**

$$[\alpha_c\beta_c G+\alpha_T\,(1-\beta_c)\,G)]A_{PV}=Q_c+Q_r+Q_k+P_{PV} \quad (5.8)$$

Where, τ_g is the transmissivity of the glass, β_c is the packing factor, α_c is the absorptivity of the PV cell, α_T is the absorptivity of the tedlar [84], G is the solar radiation intensity and A_{PV} is the device area of the PV cell. On the right side of Equation 5.8, Q_c denotes the convective heat loss from the surface of the cell, Q_r is the radiative heat loss, Q_k is the heat conducted from the PV cell to the TEG and P_{PV} is the electrical power generated by the PV cell [**82] [83**].

The heat loss from the PV cell to the ambient air due to convection and conduction is given by:

$$Q_c = U_t\, A_{PV}\,(T_{cell} - T_{amb}) \quad (5.9)$$

Where T_{cell} and T_{amb} represent the solar cell and ambient temperatures respectively. Ut is the heat transfer coefficient from the PV to the ambient air by convection and conduction [**78**]:

$$U_t = \left(\frac{L_g}{K_g} + \frac{1}{h_{cov}}\right)^{-1} \quad (5.10)$$

Where, L_g and k_g are the length and thermal conductivity of the glass respectively, h_{cov} is the convective heat transfer coefficient [87]. Radiative heat loss from the PV cell is described by:

$$Q_r = (T_{cell}^4 - T_{amb}^4) \quad (5.11)$$

Where, ε is the surface emissivity of the cell and σ is the Stefan-Boltzmann constant. Heat conducted from the PV cell into the TEG is given by:

$$Q_k = \frac{kA_{TE}N(T_{Cell}-T_c)}{L_{TE}} \quad (5.12)$$

Where, k is the thermal conductivity of the thermoelectric material, A_{TE} is the cross-sectional area of thermoelements, N is the number of thermoelements and L_{TE} is the length of thermoelements. ΔT is the temperature difference across the TEG.

In a real system, TEG has to operate in the closed-circuit operation in order to deliver the power to external load. Under such circumstances, the heat flow through the TEG consists both heat conduction and the Peltier heat. As a result, the ΔT in Eq. 5.11 should be replaced by **[80][84]**

$$\Delta T = (1+ZT_M)\,(T_{cell}-T_C) \quad (5.13)$$

Where, Z ($=\alpha^2/\rho.k$) is the thermoelectric figure of merit, α is the Seebeck coefficient, ρ is the electrical resistivity, TM is given as

$$T_M = \frac{(1+2s)T_h+T_C}{2(1+s)^2} \tag{5.14}$$

Where, s is the ratio of the load resistance to the internal resistance of the TEG module.

Using equation (5.13) to replace (T_{cell}-T_c) in equation (5.12), with s=1; as operating under the matched-load condition and assuming the hot side temperature of the TEG module is equal to the PV cell temperature, $T_{cell,}$ equation (5.12) can be written as:

$$Q_k = \frac{k.A_{TE}.N.\left\{1+\frac{z(3T_{cell}+T_C)}{8}\right\}.(T_{cell}-T_C)}{L_{TE}} \tag{5.15}$$

The power output of the TEG, with taking into account the electrical and thermal contact resistances, can be expressed as

$$P_{TE} = \frac{\alpha^2.A_{TE}N.(\Delta T_C)^2}{2.\rho(n+L_{TE})(1+\frac{2.r.L_C}{L_{TE}})^2} \tag{5.16}$$

Where, L_C is the thickness of the ceramic plates on the TEG. The variables n ad r are the electrical and thermal contact parameters, which correspond to the ratio of the bulk material electrical resistance and thermal conductivity to that of the contacts, respectively. [**85**] Figure 5.11 shows visually the N, L_{TE} and L_C parameters of a TEG module.

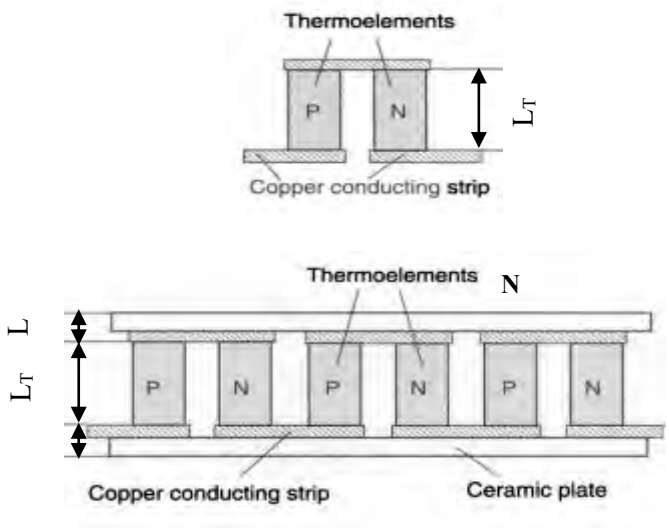

Figure 5.11 Basic configuration of a thermoelectric module [**85**]

From Equation (5.15) and Equation (5.16), the conversion efficiency of the TEG can be calculated by

$$\eta_{TE} = \frac{P_{TE}}{Q_k} \tag{5.17}$$

The power output, P_{PV} of the PV cell can be given as:

$$P_{PV} = \eta_{PV}\tau_g A_{PV} G \tag{5.18}$$

Where, η_{pv} denotes the efficiency of the PV cell. It varies with temperature and can be expressed as [**89**]

$$\eta_{PV} = \eta_0[1 - \beta_0(T_{cell} - 298)] \tag{5.19}$$

Where, η_0 is the efficiency of PV module at 25°C and β_0 is the temperature coefficient for silicon solar cells. As a result the total power output from the PV/TEG hybrid system is calculated as;

$$P_{Tot} = P_{PV} + P_{TE} \tag{5.20}$$

Consequently, the overall efficiency of the hybrid system, η_{tot} can be obtained as:

$$\eta_{tot} = \eta_{PV} + \eta_{TE}\frac{1}{1+(\frac{Q_C+Q_r+P_{PV}}{Q_k})} \tag{5.21}$$

Employing appropriate operating parameters for the hybrid PV/TEG system shown in Figure 5.9, the temperature of the PV cell and the temperature difference across the TEG can be calculated based on Equation (5.8) to (5.15). The power output and conversion efficiency of the system can be determined using Equation (5.16) to (5.21).

5.6 Validation of the System

5.6.1 Calculation

Calculation was performed to demonstrate the capability of the model for optimal design of hybrid PV/TEG system. Appendix 4 was used for the parameters to solve the equations.

Heat transfer coefficient U_t can be found from the equation (5.10),

$$U_t = \left(\frac{0.003}{1} + \frac{1}{5}\right)^{-1} = \mathbf{4.926}$$

The heat loss from the PV cell to the ambient air due to convection and conduction can be calculated using equation (5.9),

$$Q_c = 4.926 \times 1.6 \times 10^{-3}\,(318 - 298)$$
$$= 4.926 \times 1.6 \times 10^{-3} \times 20 = \mathbf{0.158}$$

Radiative heat loss from the PV cell can be calculated using equation (5.11),

$$Q_r = 0.88 \times 5.67 \times 10^{-8} \times 1.6 \times 10^{-3}(318^4 - 298^4)$$
$$= \mathbf{0.187}$$

To find heat conducted from the PV cell into the TEG, first we need to calculate the thermoelectric figure of merit,

$$Z = \frac{\alpha^2}{\rho . k}$$
$$= \frac{(170 \times 10^{-6})^2}{1 \times 10^{-5} \times 1.5} = \mathbf{1.93 \times 10^{-3}}$$

Now, heat conducted from the PV cell into the TEG can be found using the equation (5.15)

$$Q_k = \frac{1.5 \times 6.4 \times 10^{-7} \times 62 \left\{1 + \frac{1.93 \times 10^{-3}\left((3 \times 318) + 298\right)}{8}\right\}(318 - 298)}{0.002}$$
$$= \mathbf{0.775}$$

The power output of the TEG, P_{TE} can be calculated using equation (5.16),

$$P_{TE} = \frac{(170 \times 10^{-6})^2 \times 6.4 \times 10^{-7} \times 62 \times (318 - 298)^2}{2 \times 1 \times 10^{-5} \times (0.0001 + 0.002)\left(1 + \frac{2 \times 0.01 \times 0.002}{0.002}\right)^2}$$
$$= \mathbf{0.01\,W}$$

From equation (5.15) and (5.16), efficiency of TEG can be calculated as

$$\eta_{TE} = \frac{0.01}{0.775} = \mathbf{1.35}\%$$

Now efficiency of PV module can be calculated using equation (5.19), **[87]**

$$\eta_{PV} = 0.05[1 - 0.0011(318 - 298)]$$
$$= 0.049 \approx 0.05$$

The power output of PV cell can be found from the equation (5.18),

$$P_{PV} = 0.05 \times 0.95 \times 1.6 \times 10^{-3} \times 700$$
$$= \mathbf{0.053W}$$

Finally, the total power output form a single cell of PV/TEG hybrid system can be calculated from equation (5.20),

$$P_{tot} = 0.053 + 0.01$$
$$= \mathbf{0.063}\boldsymbol{W}$$

And overall efficiency of the system can be calculated from equation (5.21),

$$\eta_{tot} = 0.05 + (0.0135 \times 0.66)$$
$$= \mathbf{0.059} = \mathbf{5.9}\%$$

5.6.2 Field Implementation and Analysis

This section illustrates the possibility and procedure of a hybrid PV/TEG system across a land of 1 acre.

5.6.2.1 Cell, Module and Array

It is clear that PV/TEG hybrid system is more efficient then a single PV system. For better understanding about the feasibility of the system a mathematical research has been done. For the solar plant, an area of 1 acre or 4046.86m^2 was considered.

The basic element of a PV System is the photovoltaic (PV) cell, also called a Solar Cell. To increase its utility, a number of individual PV cells are interconnected together in a sealed, weatherproof package called a panel or module. For example, a 12 V module will have 36 cells connected in series and a 24 V module will have 72 PV Cells connected in series. To achieve

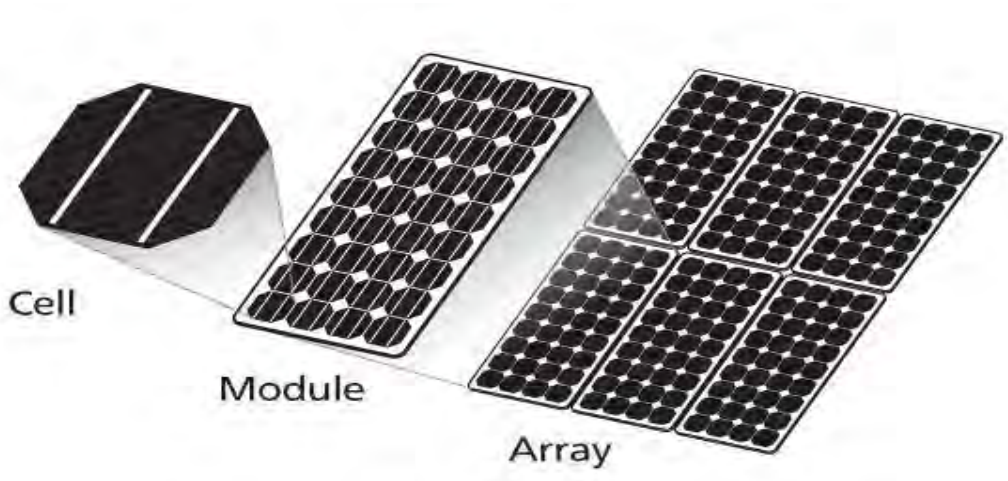

Figure 5.12 Photovoltaic cell, module and array

the desired voltage and current, modules are wired in series and parallel into what is called a PV Array. (See figure 5.12)

As per our previous calculation, each hybrid cell produces a output power of 0.063W. We are considering 12V modules, so each module will have 36 hybrid solar cells and output power of each module,

$$P_{Module} = 36 \times 0.063W$$
$$= 2.268W$$

Now a typical array consists of 6 modules. Thus total output power of an array,

$$P_{Array} = 2.268 \times 6$$
$$= 13.608W$$

5.6.2.2 Sizing and Shadow Spacing

A typical solar cell has an area of (40x40) mm^2 or $1.6x10^{-3}m^2$. So the total area of an array will be,

$$A_{Array} = (1.6 \times 216) \times 10^{-3}$$
$$= 0.3456\, m^2$$
$$= 0.589 \times 0.589\, m$$

Now while designing a solar array we need to consider shading along with the array sizes. Most of the locations for solar projects tend to get around 6 to 7 net sun-hours per day, so anything that obstructs that sunlight needs to be avoided at all costs. Shading just one corner of a module can cut production in half, so avoiding shade on the array is important. This is mainly an issue on ground mounts and some flat roof mounts, where rows of solar panels need to be optimally spaced to best use the available space as shown in figure (5.13).

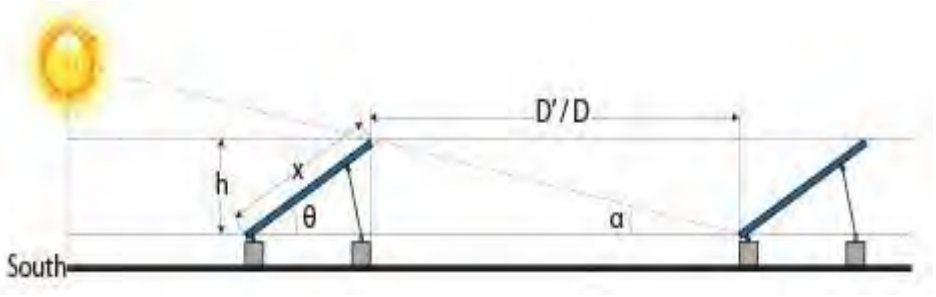

Figure 5.13 Side view of tilted array showing solar altitude angle [**88**]

The procedure for calculating shadow spacing starts with the sun's position in the sky. We need to obtain the minimum solar altitude angle α, which is the minimum angle the sun makes with the ground in our shade-free solar window. Next step is to get the suns azimuth angle, ψ. This is how far off true south the sun's position is (Figure 5.14) and will be needed to obtain the minimum allowable row spacing.

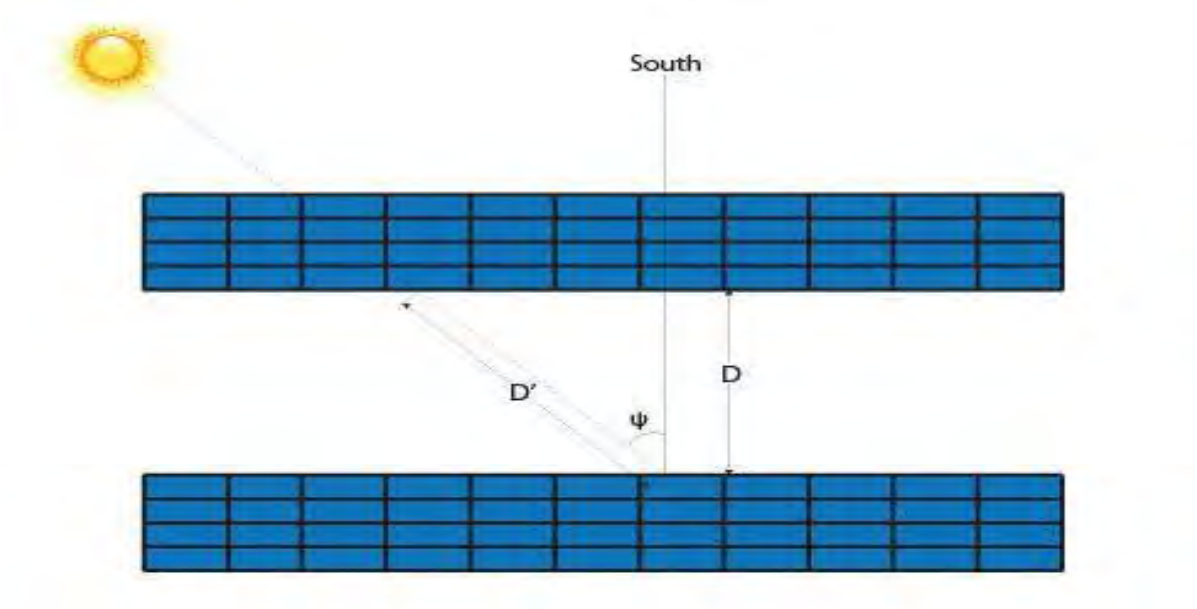

Figure 5.14: Top view of tilted array showing solar azimuth correction **[88]**

After finding the Solar Altitude and Azimuth angles, the calculations to determine row spacing can begin. For most ground and roof mounted systems where row spacing is a concern, the height (h) of the obstruction can be directly obtained from the dimensions of the solar panel and the array tilt. Alternately, it can be measured as the difference in height between the bottom edge of one row and the maximum height of the next row south of it (figure 5.13). Using this height, the maximum shadow distance can be obtained. The shadow distance is found through using simple trigonometry. The equation is:

$$D' = \frac{h}{\tan(\alpha)} \tag{5.22}$$

Where, height of the obstruction,

$$h = x * \sin(\theta) \tag{5.23}$$

x= titled module length=0.589m

θ= tilt angle

As we are designing this system from the perspective of Bangladesh, the solar altitude, azimuth angle and tilt angle should be considered with respect to Bangladesh. For finding solar altitude and azimuth angle, we have used a solar calculator called NOAA (see figure 5.15). It takes input as coordinates and time zone information. We also need to select e specific date for the operation; in our case 21st December because that is when the sun will be lowest in the sky. [**89**]

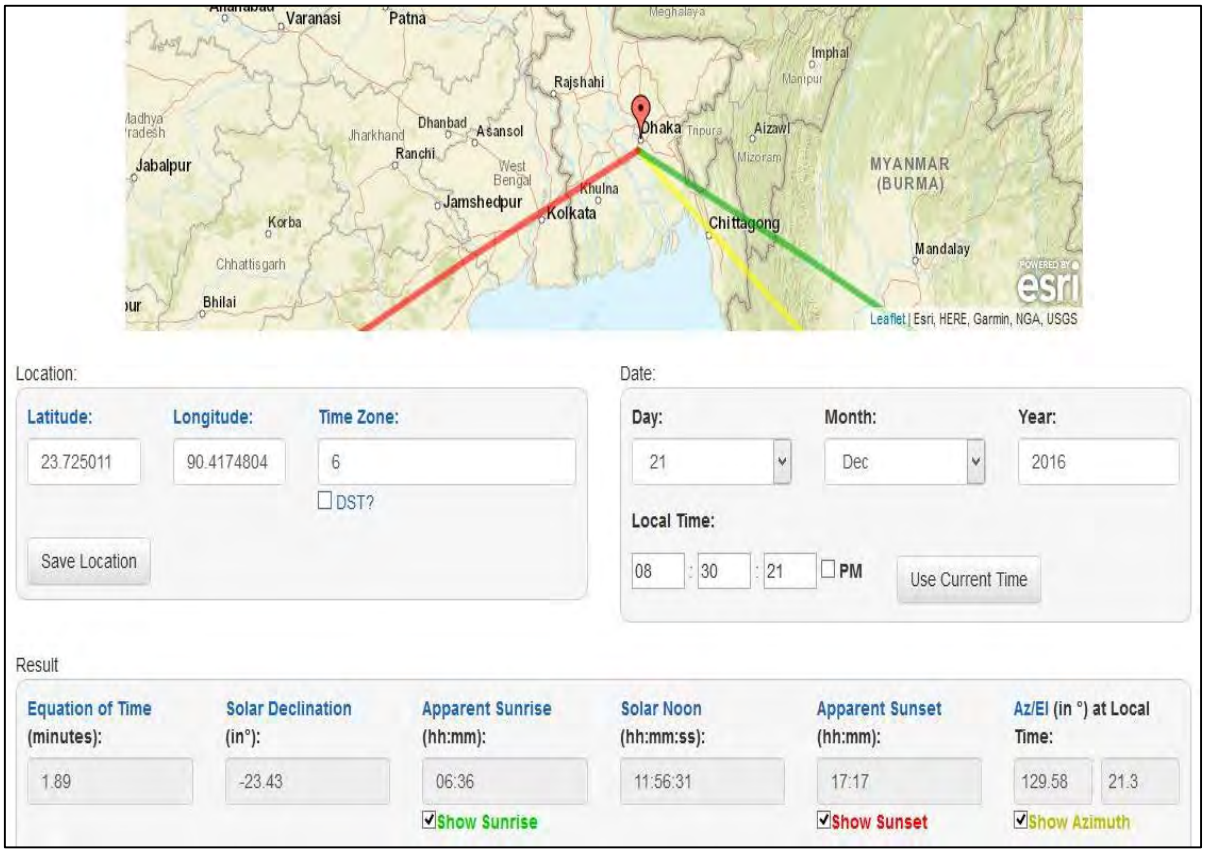

Figure 5.15 NOAA solar calculator showing relevant data [**88**]

Table 5.6 The input and output parameters of NOAA solar calculator

Input	Output
Longitude – 90.417 (Dhaka)	Azimuth angle, ψ=129.58 ^{0}
Latitude – 23.725 (Dhaka)	Solar altitude, α =21.3 ^{0}
Time zone- GMT +6.00	Apparent Sunrise = 06:36
Day- 21 Dec	Apparent Sunset = 17.17

We need the tilt angle to find out the height of the obstruction. As tilt angle varies every month, we need to consider the average value to find out our desired angle. The tilt angle variation graph for Bangladesh throughout the year is given in figure 5.16.

Figure 5.16 Optimum tilt for different months of the year [**89**]

The above data sheet gives the average tilt angle, θ= $\mathbf{25.42^0}$

From equation (5.23)

$$h = 0.589 \times \sin(25.42^0)$$
$$= \mathbf{0.25m}$$

Now we can calculate the maximum shadow length using equation (5.22).

$$D' = \frac{0.25}{\tan(21.3°)}$$
$$= \mathbf{0.64m}$$

So, maximum array row spacing,

$$D = D' \times \cos(180 - \psi) \quad (morning)$$
$$= 0.64 \times \cos(180° - 129.58°)$$
$$= \mathbf{0.41m}$$

Now the length of the array along with shadow spacing from north to south will be,

$$L_{N-S} = (0.589 + 0.41)$$
$$= 0.997 \approx 1m$$
$$L_{E-W} = 0.589m$$

Total area of the array along with the shadow spacing will be,

$$A_{array} = (0.997 \times 0.589)$$
$$= 0.587\ m^2$$

So the number of arrays we can set up in an area of 1 acre or 4046.86 m^2 will be,

$$N_{Array} = \frac{4046.86}{0.587}$$
$$= 6892.93 \approx \mathbf{6893}$$

Each array produces output power of 13.608W. So the total output power from an area of 1 acre can be obtained by multiplying the total number of arrays with the power output of each of them.

$$P_{PV+TEG} = (6893 \times 13.608)$$
$$= 93799.0029\ W$$
$$= \mathbf{93.80\ KW}$$

If only a single PV system is considered over a hybrid PV/TEG system, we will obtain output power as

$$P_{PV} = (0.053 \times 36 \times 6 \times 6893)$$
$$= 78911.064\ W$$
$$= \mathbf{78.91\ KW}$$

So we are getting additional (93.80-78.91) = **14.91 KW** of power from 1 acre of land for the hybrid system.

5.6.3 Grid Connected Hybrid System

The PV/TEG hybrid system is a Grid connected solar system which will always have a connection to the public electricity grid via a suitable inverter because a photovoltaic panel or array only deliver DC power. Some other instrument is also needed for the installation procedure.

5.6.3.1 Inverter

The inverter is the most important part of any grid connected system. The inverter extracts as much DC electricity as possible from the PV array and converts it into clean mains AC

electricity at the right voltage and frequency for feeding into the grid or for supplying domestic loads. It is important to choose the best quality inverter possible for maximising the efficiency during the conversion.

5.6.3.2 Electricity Meter

The electricity meter also called a Kilowatt hour (kWh) meter is used to record the flow of electricity to and from the grid. Two kWh meters can be used, one to indicate the electrical energy being consumed and the other to record the solar electricity being sent to the grid. A single bidirectional kWh meter can also be used to indicate the net amount of electricity taken from the grid

5.6.3.3 AC Breaker Panel and Fuses

The breaker panel or fuse box is the normal type of fuse box provided with a domestic electricity supply and installation with the exception of additional breakers for inverter and/or filter connections. A simplified structure of grid connected PV system is shown in figure 5.17.

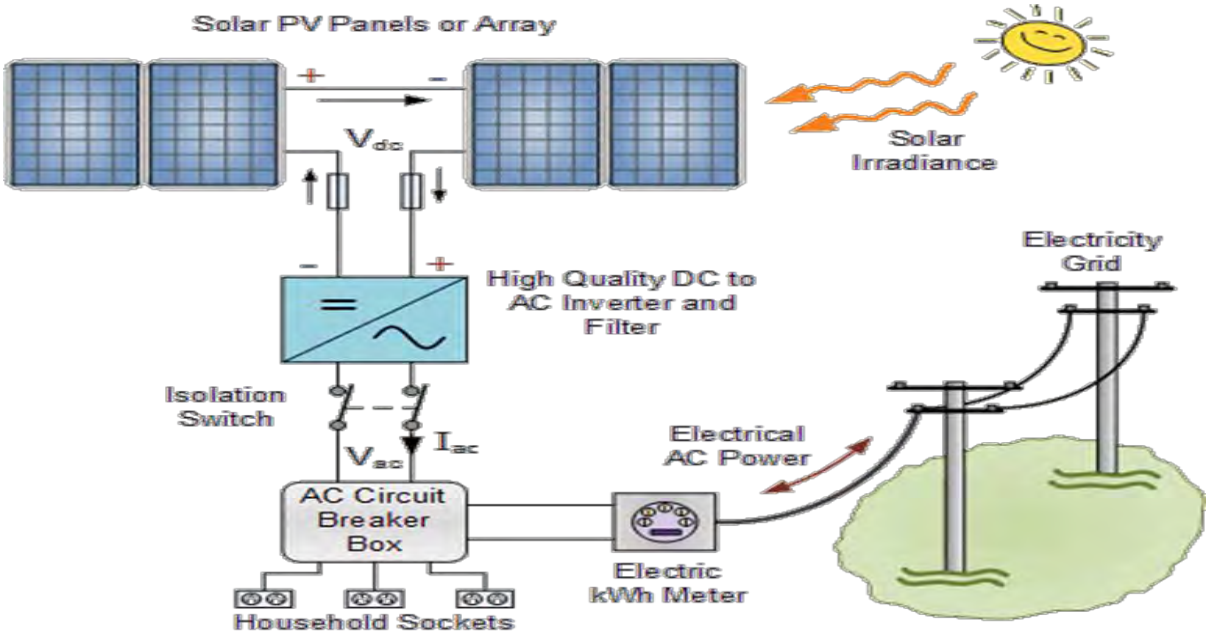

Figure 5.17: Simplified grid connected PV system

5.6.3.4 Safety Switches and Cabling

A photovoltaic array will always produce a voltage output in sunlight so it must be possible to disconnect it from the inverter for maintenance or testing. Isolator switches rated for the maximum DC voltage and current of the array and inverter safety switches must be provided separately with easy access to disconnect the system.

5.6.3.5 The Electricity Grid

Finally the electricity grid itself to connect too, because without the utility grid it is not a Grid Connected PV System.

A grid connected hybrid system is cost efficient in comparison to an off grid system because of not having batteries for store purposes. Thus less maintenance cost and greater efficiency can be achieved.

5.7 Cost Analysis

Amorphous silicon (a-Si) technology developed by Energy Photovoltaics, Inc. has significant cost advantages over traditional crystalline (c-Si) photovoltaic modules. Additionally, a-Si profits by a relative increment in power during the spring and summer months because of the warm tempering of metastable imperfections. A study result is demonstrated in the figure (**5.18**) where double junction a-Si PV module is leading in terms of yielding energy.

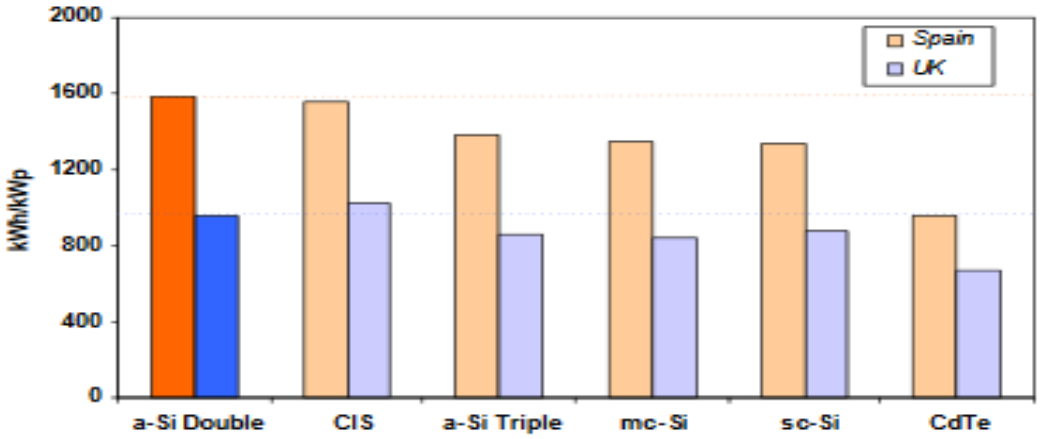

Figure 5.18: Annual energy yield in Spain and the UK for several PV technologies [**90**]

In the past, various cost analyses have been utilized to justify the selection of a-Si PV system over a p-Si system. Under the traditional evaluation of cost on a dollar per rated-Watt basis, systems using c-Si usually have a lower installed cost, especially for large arrays. A more appropriate measure of the economics, however, considers the levelized cost of energy generated from a PV system over its lifetime. A cost analysis that is based on energy generation and not on evaluated power is more appropriate since a PV system operator is compensated for the energy that is produced and not for the rated power of their system. To demonstrate this variance, two similar large-scale arrays are considered. One array is based on published data for a 1 MW c-Si system in Germany [**91**], and the other is a similarly designed, hypothetical array using the lowest cost commercially available a-Si modules, the EPV-40, manufactured by Energy Photovoltaics, Inc.

5.7.1 Total Installation Costs

Amorphous modules have a distinct cost advantage over crystalline modules in view of their low materials cost and unique low cost manufacturing process. In the current module market, EPV modules, at selling prices in the range of $2.80/Wp, are roughly 20% less expensive than average crystalline modules at $3.50/Wp. However, the lower efficiencies of thin film technologies result in the need for more modules and land area to deliver the same rated power as a crystalline PV system. This increases the wiring and structural mounting costs for thin film. Consequently, the higher balance of system and O&M cost offsets the savings in module cost. As a result, a crystalline PV system has a total installed cost advantage of roughly $0.50/W, which is about 10% lower than the cost of an EPV-based system (**see Table 5.7**).

The PV module cost is typically between a third and a half of the total capital cost of a PV system. Although accurate data on global average PV module prices are difficult to obtain and in reality there is a wide variation of prices, depending on the cost structure of the manufacturer, market features and module efficiency. However, an estimate for the global price of c-Si PV module in 2012 was around USD 1.05/W whereas the global price of a-Si PV module was around USD 0.8/W. Because of the recent development of manufacturing process, this had declined to around USD 0.6/W.

5.7.2 Generated Electricity Costs

Currently, a-Si systems, including those built with EPV modules, have a higher total installed cost. However, they consistently demonstrate that they will generate more electricity during their lifetimes across a range of climates. In Spain or an equivalent area, the lifetime energy yield is 15% higher. In the UK or similar climates, an EPV system is expected to produce 12% more electricity. **[90]**

Table 5.7 Cost comparisons for 1 MW EPV (a-Si) and c-Si PV systems **[92]**

System Elements	EPV per W	EPV 1.6 m^2 module, per W	EPV 1.6 m^2 HV module, per W	c-Si, per W
Modules	\$2.80	\$2.60	\$2.60	\$3.50
Balance of System	\$2.13	\$1.55	\$1.42	\$1.05
Mounting	\$1.38	\$0.88	\$0.88	\$0.53
DC Wiring	\$0.15	\$0.11	\$0.11	\$0.11
Inverter	\$0.51	\$0.51	\$0.38	\$0.38
Other (frenches, trenches)	\$0.08	\$0.05	\$0.05	\$0.04
Operation & Maintenece	\$0.40	\$0.40	\$0.40	\$0.30
Total Installed Cost	\$5.33	\$4.55	\$4.42	\$4.85
PV Electricity Cost				
UK	\$0.250/kWh	\$0.214/kWh	\$0.207/kWh	\$0.260/kWh
Spain	\$0.151/kWh	\$0.129/kWh	\$0.126/kWh	\$0.162/kWh

Consequently, a large 1MW EPV system currently would have a slight economic advantage over a crystalline system after the total installed costs and the lifetime energy production are accounted for. As Table 5.7 shows, by roughly doubling the current module size to 1.6m^2 and raising the maximum system voltage to 1000V, a 22% cost advantage can be obtained without any further technology improvements. In addition, significant cost reductions will be achieved by expanding production from the present capacity of a few MW/yr to 20-50 MW/yr and beyond. These advances will have the effect of lowering the installed cost/W of EPV a-Si relative to c-Si modules, while maintaining the energy performance advantage of the a-Si technology. Based on the potential of these improvements, it is fully expected that a system designed with the next generation of EPV a-Si modules will have an installed cost/W that is similar to present-day c-Si systems, and perhaps lower. With comparable installed costs/W, EPV-based systems are expected to see at least a 15-20% lifetime energy cost advantage relative to crystalline systems.

Although crystalline silicon PV is the prevailing technology choice today, amorphous silicon technology is very cost competitive. In spite of lower efficiencies and the need for more land area, EPV a-Si generates lower cost electricity. Moreover, the performance analysis makes a-Si a natural fit for architectural building integrated applications as well. These multiple benefits exhibits that a-Si is a compelling and economically advantageous alternative to conventional crystalline PV. **[92]**

5.8 Future Prospects

The following potential improvements and recommendation have been identified in terms of the simulation, experiments and design:

- The solar cells used in the experiment to study the influence of temperature had a low η_{PV}. This is mainly due to the fact that most of these solar cells (except CdTe and DSC) were commercial products. In order to evaluate their future prospects, the investigation should be performed using the solar cells with the highest efficiency.
- The current simulation assumed that the temperature of the cold side of thermoelectric generator is constant. The effect of using different coolants (such as Al_2O_3 nanofluid, TiO_2 nanofluid) instead of water should be theoretically studied in terms of the thermal power that could be generated by recycling the waste heat from the PV/TEG hybrid system.
- In this chapter, ΔT was considered around twenty degree for mathematical evaluation. In the hybrid system we can use solar concentrator to increase the hot side temperature of TEG and therefore increase the ΔT.
- The current hybrid system was fabricated by attaching the TEG to the backside of the a-Si. Heat sink compound was used to fill gaps between the a-Si and the TEG, which introduces potential reliability problems and additional thermal interfaces. Fabrication of the TEG directly on to the backside of the PV using integrated technology will eliminate many thermal interfaces and consequently minimize thermal resistance and improve the reliability.

5.9 Conclusion

Energy from the sun is by far the largest energy source available on the earth. The amount of solar energy reaching the surface of the earth annually (3.9×10^{24} J) is about ten thousand times more than the global primary energy demand and more than all available energy sources on the earth**. [93]** Thus conversion of this energy is a very promising renewable technology, but its wide-scale applications rely on further increases in efficiency and reductions in cost.

Bangladesh is lacking continuous supply of power from national grid connection especially in rural and remote areas. A new model of an efficient, reasonable hybrid system has been proposed in this chapter to overcome this problem. The main objective of this work was to design and investigate the feasibility and performance of a PV/TEG hybrid system. This objective has been achieved through systematic experimental investigation on the temperature coefficients of all available solar cells, development of theoretical model and mathematical validation. The hybrid system showed a significant improvement in the power output and efficiency due to enhanced thermal coupling between a-Si and TEG. The major achievements are summarised as follows:

- Six types of PV cells were studied under standard test condition. The experimental results showed that a-Si and DSC are preferable for integration with TEG. The a-Si showed the lowest drop in P_{max} and η_{PV} with increasing temperature.
- Using a TEG that has the same size as the PV cell will result in much smaller ΔT across the TEG. In addition, it also consumes more materials. Thus the results showed a small-size TEG is preferable over a larger one to establish larger ΔT.
- Theoretical calculations showed that not all types of PV cells are suitable for integration with TEG. A theoretical work was carried out to verify this result using two types of PV cells with different temperature coefficient, β_0. When integrated with a TEG using a p-Si that has large value of β_0, the PV cell loses significant amounts of power because of increased operating temperature. Although the TEG generated some power, the gain from the TEG is less than the loss in the PV, resulting an overall reduction in power output. However, when a-Si PV cell that has a small value of β_0 was integrated with a TEG, the power gained from the TEG overcompensate the loss from the PV and consequently overall increases in the P_{tot} and η_{tot} are obtained.

Chapter 6

Conclusion

6.1 Conclusion

This thesis attempts to come up with range of possibilities to overcome power deficits. Allocating renewable resources with the likes of solar energy and waste disposed that is being used as input into these methods, efficient generation of electricity has been calculated, schematics and design models have been proposed and effective costs has been evaluated relative to current market situation.

The thermoelectric generators have an unmatched potential for waste heat recovery system due to its unique properties such as compact size, non-movable parts, direct conversion method etc. These properties help enabling the proper design of the thermoelectric module for different systems that produce wasted heat. Hence, in the coolant and exhaust system of the diesel/gas generator, 7.62% of the total electrical output can be harvested from the wasted heat dissipated from the system. This harvested energy is DC and enough for compensating the auxiliary power (6-7%) required for the generator as well as other DC machines. This provides us the potential of 7.62% of power saving for all the reciprocating engine based power generation. Apart from the diesel and gas generators, TEM can be used in other systems such vehicle engines, steam turbine generators etc. where waste heat is dissipated.

Thermal plasma gasification which is superior in technology than conventional landfilling process has proven itself as a better alternative in terms of efficient power generation, land capacity and with less years of operation can reduce equivalent amount of GHG emissions. MSW produced in Dhaka City can generate about 100 MWh/day considering plant efficiency of 40% and 24 hours plant operation. Assuming MSW collection efficiency in Dhaka to be 60% the landfill gas (LFG) collection system can generate about 32 MWh/day on average which is 70% less efficient than the total electrical output from plasma gasification. The MSW processed by Alter NRG assumes to have a calorific value of 11.6 MJ/kg which is higher than typical calorific value of 8 MJ/kg used for calculations in Dhaka City and hence the projected power generation is assumed to be less. With just 10 years of operation thermal plasma gasification can reduce similar carbon content from atmosphere than LFG does from a usual landfilling that requires 21 years of operation.

In the field of solar thermal power generation system, dish-stirling technology is very striking because of its high efficiency and modular design. In Bangladesh, it can convert around 30% of incoming solar power to electricity. This is comparably higher than the power tower or parabolic trough designs or PV panel, which are around 15-16%. To observe the efficiency of dish-stirling system, total power generation at 1 acre of land is calculated. From the result it has been seen that this system can generate 150 KW of electricity. At the same amount of land PV panel (a-Si) can produce 78.91 KW of electricity, which is far less than Dish-Stirling system. In the same time it has been observed that installing dish-stirling system in a bigger range can also make this system more efficient and cost effective.

The power generation of Hybrid PV-TEG was investigated in this study. Experimental and theoretical results relating to solar-to-electrical and thermoelectric-to-electrical conversions using TEG and solar modules were shared. A total of 5.9% efficiency was calculated for the combined system whereas individual PV system offers 5% of power generation. A case study was performed across 1 acre of land. The result showed that combined PV-TEG system can produce 93.8 KW whereas individual PV system yields 78.91 KW. Although the cost of the TEG modules is still high, but the size of modules is considerably smaller than the solar modules which is an advantage as the projects have space limitations.

Even though there are not widely used evidences of conversion potential and practical applications of the discussed methods, more efforts should be devoted to material research, structure optimization and commercialization.

6.2 Future Works

There are plenty of scopes for improvements in near future which are needed to be addressed including achieving optimum efficiency in proportion to increasing demand by reducing temperature gradient in case of thermoelectric generator, efforts to minimise operating conditions like high temperature, cost management of installation, annual maintenance of torches and waste collection efficiency for plasma gasification, experimenting with different materials and optimizing procedures for dish-stirling systems etc.

The efficiency improvement is a must for better performance of TEGs in the near future. Although, the current efficiency is quite useful for numerous applications, further improvement of efficiency is needed. The enhanced efficiency can enable a TEG to operate in low

temperature gradient, so that, energy can be harvested even from a low amount of wasted heat. And since, thermoelectric generation technology appears to very useful in wasted heat recovery applications of the reciprocating engines, an embedded system can be developed where the engines/ generators will have the built in TEMs for wasted heat recovery purpose. This system can be manufactured by the generator manufacturing companies. Similar type of thermal systems can have built in TEM technology for improved efficiency.

The scope for application and implementation of thermal plasma gasification is huge but the level of commercialization is not adequate. One of them being the plant capacity, there are still no sign of power plants with more than 1000 TPD on average in real life due to optimum operating conditions then going too high. Fortunately concerns like collection of waste as feedstock on a regular basis for supply into the reactor is on a minimal level in Bangladesh but factors like efficiency improvements in areas unlike Dhaka where MSW generation is comparatively lower but demand for power is significant needs to be dealt with and with lower operating costs. Since fossil fuel poses greater risk of being extinct and with shortage of wastelands in Bangladesh sooner or later this proposition is more of a subtle approach.

It is a big challenge to commercialize dish-stirling technology. Companies like Schlaich Bergermann und Partner (SBP), Stirling Engine System (SES) and Sandia National Laboratories are working on it. To overcome the difficulties they are trying to innovate some new technics. To overcome the dependability of solar resource availability, thermal energy storage system and hybridization can play a vital role in future. Without storage component dish-stirling system and PV can work in the same way. That is way Sandia National Laboratories, National Renewable Energy Laboratory and the University of Connecticut are trying to introduce thermal storage system components for Dish-Stirling power generation. This will enable dish-stirling system to produce electricity in the evening and the night time. On the other hand, hybridization of receiver (both for a conventional fuel such as natural gas and for renewable energy source such as biogas) can also solve this problem. This technologies are also currently under observation. Similarly, if the durability of the system is increased by replacing the steel currently used for stirling engine casing and parts, it can make the system more effective. By doing these types of innovations it is expected that dish-stirling system will be more efficient and cost effective in the future.

The efficiency of PV-TEG hybrid system largely depends upon the TEG. It has been predicted that the vacuum system improves the P_{max} and η_{TE} of the TEG. This investigation could be

extended to involve PV cell and the PV/TEG hybrid system. Also, expanding the validation study to verify the theoretical results of the vacuum system should be considered. A specifically designed TEG with optimised geometry should be fabricated and used for the validation, rather than the commercially available modules, to obtain more accurate data. Moreover, improving the heat exchanger by using nanofluid as a coolant can be further investigated to evaluate its potential benefit. The performance of the hybrid system under higher solar illumination (> 5x) should also be evaluated by using high intensity concentrators such as parabolic mirrors and Fresnel lenses.

Reference

1. Ullah, M. H., Hoque, T., & Hasib, M. M. (2012). Current Status of Renewable Energy Sector in Bangladesh and a Proposed Grid Connected Hybrid Renewable Energy System. *INTERNATIONAL JOURNAL OF ADVANCED RENEWABLE ENERGY RESEARCH*, *1*(11), 618–627.
2. Taheruzzaman, M., & Janik, P. (2016). Electric Energy Access in Bangladesh. *TRANSACTIONS ON ENVIRONMENT AND ELECTRICAL ENGINEERING*, *vol 1, No 2*.
3. Velimir Jovanovic, Saeid Ghamaty and John C. Bass, 2012, New Thermoelectric Materials and Applications, Hi-Z Technology, Inc
4. John W. Fairbanks, "The 60 Percent Efficient Diesel Engine; Probable, Possible, or Just A Fantasy?", Diesel Engine mission Reduction Conference, Palmer House, Chicago, August 24, 2005
5. A Thermoelectric Generator That Runs on Exhaust Fumes, By Martin LaMonica (14 October, 2014), IEEE Spectrum, accessed on 21 March 2017. http://spectrum.ieee.org/energywise/green-tech/conservation/a-thermoelectric-generator-that-runs-on-exhaust-fumes
6. Ducharme, C. (2010). Technical and Economic Analysis of Plasma-Assisted Waste-to-Energy Processes, 1–79.
7. Mancini T, Heller P, Butler B, et al. Dish-Stirling Systems: An Overview of Development and Status. ASME. J. Sol. Energy Eng. 2003; 125(2):135-151.
8. Bangladesh Power Development Board, Renewable energy, BPDB Website, http://www.bpdb.gov.bd/bpdb/index.php?option=com_content&view=article&id=26&Itemid=24 (accessed on March 25, 2017)
9. M. Rafiee, A. Siadatan and E. Afjei, Improving the Hybrid Electric Vehicles Efficiency, Using Si0.7Ge0.3 and Bi2Te3 Thermoelectric Materials, 2012 4th International Conference on Intelligent and Advanced Systems (ICIAS2012)
10. Bangladesh Power Development Board, Key Statistics, (01 February, 2017), BPDB Website,

http://www.bpdb.gov.bd/bpdb/index.php?option=com_content&view=article&id=5&Itemid=6, accessed on March 25, 2017

11. Kam Yu Lee, 2015, Silicon Nanowire Arrays Based On-Chip Thermoelectric Generators, IEEE TRANSACTIONS ON COMPONENTS, PACKAGING AND MANUFACTURING TECHNOLOGY

12. Mark Hodes, Optimal Pallet Geometries for Thermoelectric Power Generation, IEEE TRANSACTIONS ON COMPONENTS AND PACKAGING TECHNOLOGIES, VOL. 33, NO. 2, JUNE 2010

13. Jihui Yang. Potential Applications of Thermoelectric Waste Heat Recovery in the Automotive Industry. IEEE 24th International Conference on Thermoelectrics, Clemson, South Carolina 2005.

14. K. Smith and M. Thornton, Feasibility of Thermoelectrics for Waste Heat Recovery in Hybrid Vehicles, Anaheim, California, December 2–5, 2007

15. Gregory P. Meisner," Thermoelectric Generator Development for Automotive Waste Heat Recovery", *16th DEER Conference Detroit*, Michigan, 29 Sep. 2010.

16. Cobble, M.H, "Calculation of generator performance", CRC, Handbook of Thermoelectrics, CRC Press, Inc., 1995

17. M. Takeiishi et a', "Thermal conductivity measurements of Bismuth Telluride thin films by using the 3 Omega method". The 27th Japan Symposium on Thermophysical Properties, Kyoto, 2006.

18. Tan, J., "Thermoelectric properties of bismuth telluride thin films deposited by radio frequency magnetron sputtering". *Proceedings of SPIE*. 5836. pp. 711, 2005.

19. T. Okutani, Y. Kabeya," thermoelectric n-type Si-Ge synthesized by unidirectional solidification in microgravity", *Proceedings of ITP2011 Interdisciplinary Transport Phenomena VII*, Dresden, Germany, 19-23, Sep. 2011

20. Wärtsilä 32 - Product Guide (n.d), Wartsila Website accessed on March 21, 2017, http://cdn.wartsila.com/docs/default-source/product-files/engines/ms-engine/product-guide-o-e-w32.pdf?sfvrsn=6

21. 2015 power plat solution, Wartsila (n.d), Wartsila Website accessed on March 21, 2017,

http://www.wartsila.com/docs/default-source/Power-Plants-documents/reference-documents/power-plants-solutions-catalogue/pps2015_lowres.pdf?sfvrsn=2

22. CATERPILLAR G3516 GAS GENERATOR SET, LOW ENERGY GAS CONTINUOUS 1030 ekW 1287 KVA, 50 Hz, 1500 rpm, 400 Volts http://www.stet.pt/dl/3516LD.pdf , accessed on March 21, 2017

23. Technical data Diesel Generator Set CAT 3512B-1500, (11 November, 2011), Avesco Website, accessed on March 21, 2017. http://www.avesco.ch/fileadmin/dateien/ESYS/Dokumente/Datenblaetter/2013_11_CAT/CAT_EN/CAT_3512B-1500_EN.pdf

24. ORION POWER MEGHNAGHAT LTD. (n.d), Orion-Group Website Accessed on March 24, http://www.orion-group.net/concern/23/48/project-details

25. ABB AG, Power Generation, Energy efficient design of auxiliary system in fossil fuel power plants (n.d) , ABB Website, Accessed on March 24, 2017, https://library.e.abb.com/public/5e627b842a63d389c1257b2f002c7e77/Energy%20Efficiency%20for%20Power%20Plant%20Auxiliaries-V2_0.pdf

26. Moushumi Zahur., *Solid Waste Management of Dhaka City: Public Private Community Partnership*. BRAC University Journal, Vol. IV, No. 2, 2007. PP. 93-97.

27. *Population and Housing Census 2011*, Dhaka Zilla: Government of the People's Republic of Bangladesh, Bangladesh Bureau of Statistics, Statistics and Informatics Division, Ministry of Planning, June 2012.

28. Faisal Ibney Hai, M. Ashraf Ali., *A Study on Solid Waste Management System of Dhaka City Corporation: Effect of Composting and Landfill Location*. UAP Journal of Civil and Environmental Engineering, Vol. 1, No. 1, 2005.

29. Kolb, T. and Seifert, H., "Thermal waste treatment: State of the art – a summary", in *Waste Management 2002: The future of waste management in Europe*, 7-8 October 2002, Strasbourg (France), Edited by VDI GVC (Düsseldorf, Germany).

30. Rushbrook P, Pugh M., *Solid waste landfills in middle and lower income countries. A technical guide to planning design and operation.* Washington DC: World Bank technical paper No.426, the World Bank, 1999.

31. Zurbrugg C., *Urban Solid Waste Management in Low-Income Countries of Asia: How to Cope with the Garbage Crisis*. Scientific Committee on Problems of the Environment (SCOPE), Urban Solid Waste Management Review Session, Durban, South Africa, November 2002.
32. Ndu, The M.Sc., Asi Eugene., *Bottom-Up Approach to Sustainable Solid Waste Management in African Countries*, Ph.D Thesis, Faculty of Environmental Sciences and Process Engineering, Brandenburg University of Technology, 2013.
33. Young, G. C. (2010). Introduction to Gasification/Pyrolysis and Combustion Technologies. In *MUNICIPAL SOLID WASTE TO ENERGY CONVERSION PROCESSES ECONOMIC, TECHNICAL, AND RENEWABLE COMPARISONS* (pp. 1–15). Canada: John Wiley & Sons,Inc.,Publication.
34. Alter NRG. (2013, March). Westinghouse Plasma Gasification Technology. *Summary of Qualifications*.
35. Determination of an Application for an Environmental Permit under the Environmental Permitting (England & Wales) Regulations 2010 **,** Permit Number-EPR/XP3336NN , The Applicant/Operator-Air Products Renewable Energy Limited
36. Ahmmad, R. M., & Haque, Dr. Saiful. (2014). Providing Electricity by Digester Types on Biogas Productions from Municipal Solid Waste in Dhaka City, Bangladesh. *International Journal of Energy, Information and Communications*, *5*(3), 13–22.
37. NwachinemeluChibuzor, A. F. (2013). Plasma Gasification for Waste Destruction and Power Generation in Nigeria. *International Journal of Engineering Research & Technology (IJERT)*, *2*(7), 1067–1079.
38. Islam, Nazmul (2016). Municipal Solid Waste to Energy Generation in Bangladesh: Possible Scenarios to Generate Renewable Electricity in Dhaka and Chittagong City. *Hindawi Publishing Corporation Journal of Renewable Energy*, 1–16.
39. http://www.alternrg.com
40. Byun, Y., Cho, M., Hwang, S.-M., & Chung, J. (2012). Thermal Plasma Gasification of Municipal Solid Waste (MSW), 183–210. Retrieved from http://dx.doi.org/10.5772/48537
41. Hai, F. I., & Ali, A. M. (2005). A Study on Solid Waste Management System of Dhaka City Corporation: Effect of Composting and Landfill Location. *UAP Journal of Civil and Environmental Engineering*, *1*(1), 18–26.

42. NZIHOU, J. F., Hamidou, S., Bouda, M., Koulidiati, J., & Segda, Gerard B. (2014). Using Dulong and Vandralek Formulas to Estimate the Calorific Heating Value of a Household Waste Model. *International Journal of Scientific & Engineering Research*, *5*(1), 1878–1883.
43. Westinghouse Plasma Gasification,Scaling Up to 100MW,*SGC International Conference on Gasification*,Malmo, Sweden,October 16, 2014.
44. "Bangladesh: Ensuring a Reliable and Quality Energy Supply" http://www.worldbank.org/en/results/2016/10/07/bangladesh-ensuring-a-reliable-and-quality-energy-supply?cid=EXT_WBSocialShare_EXT
45. "Solar Energy in Urban Bangladesh: An Untapped Potential" http://chethoughts.com/solar-energy-in-urban-bangladesh-an-untapped-potential/
46. EPRI Report, 1986, ''Performance of the Vanguard Solar Dish-Stirling Engine Module,'' Electric Power Research Institute, AP 4608, Project 2003-5.
47. Koshaim, B., 1986, ''Report: Fifty KW Solar Membrane Concentrator,'' The SOLERAS Program, Saudi Arabian National Center for Science and Technology.
48. Lopez, C., and Stone, K., 1993, ''Performance of the Southern California Edison Company Stirling Dish,'' SAND93-7098, Sandia National Laboratories, Albuquerque, NM.
49. Mancini T, "Solar-Electric Dish Stirling System Development".
50. Heller, P., Baumu¨ller, A., and Schiel, W., 2000, ''EuroDish—The Next Milestone to Decrease the Costs of Dish/Stirling System Towards Competitiveness,''*10th Int. Symp. on Solar Thermal Concentrating Technologies*.
51. Sufian, S. M. A., Sagar, K. A., Ullah, M. A., & Durjoy, D. (2014). Harvesting Electrical Power from Waste Heat Using Stirling Engine, 343–346.
52. "Stirling Engine" http://www.robertstirlingengine.com
53. Kongtragool, B., & Wongwises, S. (2003). A review of solar-powered Stirling engines and low temperature differential Stirling engines. *Renewable and Sustainable Energy Reviews*, *7*, 131–154.
54. Sufian, S. M. A., Sagar, K. A., Ullah, M. A., & Durjoy, D. (2014). Design of a Stirling Engine to Generate Green Energy in Rural Areas of Bangladesh, 27-32.
55. Pitz-Paal, R. (n.d.). HIGH TEMPERATURE SOLAR CONCENTRATORS. *SOLAR ENERGY CONVERSION AND PHOTOENERGY SYSTEMS.*
56. ProEcoPolyNet Fact Sheet "SOLO Stirling 161"

57. Igo, J., & Andraka, C. E. (2007). SOLAR DISH FIELD SYSTEM MODEL FOR SPACING OPTIMIZATION.
58. Johansson, T., Kelly, H., Reddy, A., Williams, R., & Burnham, L. (Eds.). (1993). Solar-Thermal Electric Technology. In *Renewable Energy Sources for Fuels and Electricity* (pp. 213–296). Washington, D.C.: Island Press.
59. Laing, D., Thaler, H., Lundström, L., Reinalter, W., Keck, T., & Brost, O. (1999). Development of Advanced Hybrid Heat Pipe Receivers in Dish/Stirling Systems for Decentralised Power Production.
60. A. R. Jha, *Solar Cell Technology and Applications*. CRC Press, Boca Raton & Francis Group, LLC, 2010.
61. H. Graßl, J. Kokott, M. Kulessa, J. Luther, F. Nuscheler, R. Sauerborn, H.-J. Schellnhuber, R. Schubert, and E.-D. Schulze, "World in Transition Towards Sustainable Energy Systems" Technical report, German Advisory Council on Global Change, 2003.
62. Fisac, M., Villasevil, F. X., & López, A. M. (2014). High-efficiency photovoltaic technology including thermoelectric generation. Journal of Power Sources, 252, 264–269.
63. Bjørk, R., & Nielsen, K. K. (2015). The performance of a combined solar photovoltaic (PV) and thermoelectric generator (TEG) system, *Vol 120*, 187–194.
64. G. Min, "Thermoelectric Module Design under a Given Thermal Input: Theory and Example," Electron. Mater, vol. 42, no. 7, pp. 2239–2242, 2013.
65. V. V. Tyagi, S. C. Kaushik, and S. K. Tyagi, "Advancement in solar photovoltaic/thermal (PV/T) hybrid collector technology," *Renew. Sustain. Energy Rev.*, vol. 16, no. 3, pp. 1383–1398, 2012.
66. T. Marnoto, K. Sopian, W. R. W. Daud, M. Algoul and A. Zaharim, "Mathematical Model for Determining the Performance Characteristics of Multi-Crystalline Photovoltaic Modules," in *Proc. of the 9th WSEAS Int. Conf. on Mathematical and Computational Methods in Science and Engineering, Trinidad and Tobago,November 5-7*, 2007, pp. 79–84.
67. E. Radziemska, "Performance Analysis of a Photovoltaic-Thermal Integrated System," *Int. J. Photoenergy*, pp. 1–6, 2009.
68. E. Radziemska, "The effect of temperature on the power drop in crystalline silicon solar cells," *Renew. Energy*, vol. 28, no. 1, pp. 1–12, Jan. 2003.
69. B. J. Brinkworth, B. M. Cross, R. H. Marshall, and H. Yang, "Thermal regulation of photovoltaic cladding," *Sol. Energy*, vol. 61, no. 3, pp. 169–178, 1997.

70. X. Zhao, X. Zhang, S. B. Riffat, and Y. Su, "Theoretical study of the performance of a novel PV/e roof module for heat pump operation," *Energy Convers. Manag.*, vol. 52, no. 1, pp. 603–614, Jan. 2011.
71. C. Rowe, D. M., *Handbook of Thermoelectric,* Boca Raton, FL, CRC Press, 1995.
72. T. M. Tritt, "Thermoelectric Materials: Principles, Structure, Properties, and Applications," *Encycl. Mater. Sci. Technol.*, pp. 1–11, 2002.
73. Yatim, Nadhrah. Md, "Development of 'Open - Short Circuit' Dimensionless Figure-of-Merit (ZT) Measurement Technique for Investigation of Thermoelements and Segmented Thermoelectric Structures," Ph.D, Cardiff University, 2012.
74. G. Min, D. M. Rowe, and K. Kontostavlakis, "Thermoelectric figure-of-merit under large temperature differences," *J. Phys. D Appl. Phys*, vol. 37, pp. 1301–1304, 2004.
75. C. Rowe. D. M., *Handbook of Thermoelectrics: Micro to Nano*. London: CRC Press. 2005.
76. W. G. J. H. M. Van Sark, "Feasibility of photovoltaic – Thermoelectric hybrid modules," *Appl. Energy*, vol. 88, no. 8, pp. 2785–2790, Aug. 2011.
77. Y.-Y. Wu, S.-Y. Wu, and L. Xiao, "Performance analysis of photovoltaic–thermoelectric hybrid system with and without glass cover," *Energy Convers. Manag.* vol. 93, pp. 151–159, Mar. 2015.
78. Y. Deng, W. Zhu, Y. Wang, and Y. Shi, "Enhanced performance of solar-driven photovoltaic–thermoelectric hybrid system in an integrated design," *Sol. Energy*, vol. 88, pp. 182–191, Feb. 2013.
79. H. Najafi and K. A. Woodbury, "Modeling and Analysis of a Combined Photovoltaic-Thermoelectric Power Generation System," *J. Sol. Energy Eng.*, vol. 135, no. 3, p. 031013, Apr. 2013.
80. E. Radziemska, "The effect of temperature on the power drop in crystalline silicon solar cells," *Renew. Energy*, vol. 28, no. 1, pp. 1–12, Jan. 2003.
81. Hashim, H., Bomphrey, J. J., & Min, G. (2016). Model for geometry optimisation of thermoelectric devices in a hybrid PV/TE system. *Renewable Energy*, *87*, 458-463.
82. F. Sarhaddi, S. Farahat, H. Ajam, and A. Behzadmehr, "Exergetic performance assessment of a solar photovoltaic thermal (PV/T) air collector," *Energy Build.*, vol. 42, no. 11, pp. 2184–2199, Nov. 2010.
83. A. S. Joshi and A. Tiwari, "Energy and exergy efficiencies of a hybrid photovoltaic–thermal (PV/T) air collector," *Renew. Energy*, vol. 32, no. 13, pp. 2223–2241, Oct. 2007.

84. X. Ju, Z. Wang, G. Flamant, P. Li, and W. Zhao, “Numerical analysis and optimization of a spectrum splitting concentration photovoltaic–thermoelectric hybrid system,” *Sol. Energy*, vol. 86, no. 6, pp. 1941–1954, Jun. 2012.
85. G. Min, “ZT Measurements under Large Temperature Differences,” *J. Electron. Mater,* vol. 39, no. 9, pp. 1782–1785, Mar. 2010.
86. G. Min, “TE Module Design Theories,” in *CRC Handbook of Thermoelectrics; Micro to Nano,* D.M. Rowe, Ed. Baca Ration: CRC Press, 2006, pp. 11.1–11.15.
87. D.L. Evans, “Simplified method for predicting photovoltaic array output,” *Sol. Energy*, vol. Volume 27, no. no. 6, pp. 555–560, 1981.
88. http://www.affordable-solar.com/learning-center/building-a-system/calculating-tilted-array-spacing/
89. Datta, D., Hossain, M. J., & Datta, B. K. (n.d.). OPTIMUM TILT FOR SOLAR COLLECTORS IN RAJSHAHI, BANGLADESH. *International Journal of Scientific & Enginee Ring Research*, *Volume 5*(Issue 7), 245–249.
90. C. Jardine and K. Lane, " PV-COMPARE: Relative Performance of Photovoltaic Technologies in Northern and Southern Europe," *Proceedings of the PV in Europe Conference,* October 2002, Rome, Italy, pp. 1057-1060.
91. M. Bachler and C. Bindel. “Cost Comparison of Large Scale Crystalline and Thin Film Systems.” *Proc. of the 20th European Photovoltaic Solar Energy Conference*, Barcelona 2005, pp. 3134-3138.
92. Jansen, K. W., Kadam, S. B., & Groelinger, J. F. (2006, May). The advantages of amorphous silicon photovoltaic modules in grid-tied systems. In *Photovoltaic Energy Conversion, Conference Record of the 2006 IEEE 4th World Conference on* (Vol. 2, pp. 2363-2366). IEEE.
93. V. Quaschning. Understanding Renewable Energy Systems. Earthscan Canada, 2005.

Appendix

Appendix 1

MATLAB code for Bi_2Te_3 efficiency calculation

```
clc;
close all;
clear all;
 % Bi2Te3 specifications
length = 1*10^(-3);
width  = 6*10^(-3);
height = 6*10^(-3);
area = height*width ;
for Th= 340:1:390   % high temperature range
Tl = 300           ; % low temperature
alpha = 287*10^(-6); % seebeck coefficient
sigma = 1.1*10^5 ;   % electrical conductivity
K1 = 1.2         ;   % thermal conductance
dT = (Th - Tl)     ;  % temperature difference
Zt = (alpha.^2*sigma*dT)/(K1) ; % figure of merit
rho = (1/sigma)  ;    % resistivity
R = (rho*length)/area; % internal resistance
RL = 1.323*R;        % lead resistance
Voc = dT*alpha;       % open circuit voltage
I = Voc/(R+RL);       % open circuit current
P = (I.^2)*RL    ;        % power from a single unit of Bi2Te3 TEG
K = K1*area/length    ; % thermal conductance of the dimension
Qh = alpha*I*Th + dT*K - 0.5*I^2*R; % heat at hot side of the TEG
Qc = Qh - P      ;       % heat at cold side of the TEG
Eff = (P/Qh)*100;      % efficiency
fprintf('Th= %d  P= %d  Eff= %d  \n', Th,P,Eff );  % printing individual values for Th, P & Eff
hold on ;
plot (Th,Eff, '--bs'), xlabel('temperature'), ylabel ('efficiency in %')
end
```

Appendix 2

MATLAB code for $Si_{0.7}Ge_{0.3}$ efficiency calculation

```
clc;
close all;
clear all;
 % Si0.7Ge0.3 specifications
length = 0.3*10^(-3);
Dmtr = 10*10^ (-3);
area = pi*(Dmtr/2).^2 ;
for Th = 600:2:700
Tl = 300          ; % low temperature
alpha = 326*10^(-6); % seebeck coefficient
sigma = 49079.75 ;   % electrical conductivity
K1 = 4.4          ;   % thermal conductance
dT = (Th - Tl)     ;  % temperature difference
Zt = (alpha. ^2*sigma*dT)/ (K1); % figure of merit
rho = (1/sigma)  ;    % resistivity
R = (rho*length)/area; % internal resistance
RL = 1.323*R;         % lead resistance
Voc = dT*alpha;       % open circuit voltage
I = Voc/(R+RL);       % open circuit current
P = (I. ^2)*RL    ;        % power from a single unit of Bi2Te3 TEG
K = K1*area/length    ; % thermal conductance of the dimension
Qh = alpha*I*Th + dT*K - 0.5*I^2*R; % heat at hot side of the TEG
Qc = Qh - P      ;       % heat at cold side of the TEG
Eff = (P/Qh)*100;      % efficiency
Thc = (Th - 273)   ;     % temperature in celsius
fprintf('Th= %d  P= %d  Eff= %d  \n', Th,P,Eff );  % printing individual values for Th, P & Eff
hold on ;
plot (Thc,Eff, '--ks'), xlabel('temperature'), ylabel ('efficiency in %')
end
```

Appendix 3

Matlab code for output power calculation as a function of pressure

```
B=0.13; %Beale number
Pm= [5:2:20]; %Helium gas pressure
f=25; %Operating Speed
Vp=160; %Displacement volume
Po=B*Pm*f*Vp; %Output Power
plot(Pm,Po);xlabel('Pressure(Mpa)'),ylabel('Pout (W)')
```

Appendix 4

Parameters used for simulation of Hybrid PV/TEG model

Parameter	Value	Unit
L_g	0.003	M
K_g	1	$W.m^{-1}K^{-1}$
h_{cov}	5	$W.m^{-2}K^{-1}$
A_{PV}	$(0.04)^2$	m^2
T_{amb}	298	K
T_{cell}	318	K
A_{TE}	$(0.8x10\text{-}3)^2$	m^2
N	62	--
L_{TE}	0.002	M
G	700	$W.m^{-2}$
E	0.88	--
β_c	1	--
β_0	0.0011	K^{-1}
K	1.5	$W.m^{-1}K^{-1}$
A	170	μVK^{-1}

P	1×10^{-5}	Ω.m
N	0.0001	M
R	0.01	--
τ_g	0.95	--